1-1-2011

Monitoring, diagnosis, and control for advanced anesthesia management

Zhibin Tan
Wayne State University,

Recommended Citation

MONITORING, DIAGNOSIS, AND CONTROL FOR ADVANCED ANESTHESIA MANAGEMENT

by

ZHIBIN TAN

DISSERTATION

Submitted to the Graduate School

of Wayne State University,

Detroit, Michigan

in partial fulfillment of the requirements

for the degree of

DOCTOR OF PHILOSOPHY

2011

MAJOR: ELECTRICAL ENGINEERING

Approved by:

_____

Adviser   Date

_____

_____

_____

ACKNOWLEDGEMENTS

TABLE OF CONTENTS

LIST OF TABLES

LIST OF FIGURES

CHAPTER 1: INTRODUCTION

This work is the summary of my research during the period of pursuing my Ph.D. from the year of 2006 to present. I have comprehensively investigated several problems of modern anesthisa management such as depth monitoring, automatical drug control, and modeling the patient dynamics for prediction, diagnosis and warning by using the technologies of signal processing, control theory, and system identification. All of the analysis were based on the cranial EEG signals or its derivatives. In addition, I also have taken an initial step on the problem of analyzing the impact of anesthesia and noise lesion on the neural activities of primary auditory cortex from a system point of view. In this case, the output of the objective system is the function of intracranial EEG signals recorded through the intrusive electrode. The intracranial EEG is less noise contaminated and contains more information of the brain than the cranial EEG does.

1.1   Objective and Motivation

My research aims to potientally improve the current technologies for building a more safe, reliable, efficient, and economical clinical enviroment for anesthesia patients.

Modern anesthsia managment is a comprehensive, complex, even the most critical issue and plays a very important role in healthcares. In the past decades, it has attracted much attention of the researchers to investigate this issue from several

aspects. There are two main tasks:

- Monitoring aneshtesia depth, which aims to measure the anesthesia paptient unconsiousness levels by monitoring a seires of indexes. The main problem of this issue is how to choose or derive a reliable and sensitive depth index suiting for any anesthesia drug and any patient.

- Modeling anesthesia patient responses, such as anesthesia depth, blood pressure and so on, to anesthesia drugs and operation procedures etc. Those models can be used for displaying, control, diagnosis, and prediction etc.

Characterizing, measuring, and continuously monitoring the depth of anesthesia has been pursued extensively and persistently for many decades since the observations of the physiologic effects of anesthetic agents by John Snow's description of the various stages of ether anesthesia in 1847 [1]. Accurate monitoring of the anesthesia depth helps to avoid overdose of anesthetic agent, prevent intraoperative awareness, assist the anesthesiologists in anesthesia decisions and management. Furthermore, monitoring of the anesthesia depth can guide more precise titration of anesthesia agents, and consequently can potentially reduce drug costs, expedite post-anesthesia recovery, and shorten hospital stay [9]. My first research goal is to investigate the problem of measuring anesthesia depth based on EEG signal processing. The EEG is the voltage difference between two different recording locations on the scalp and can be recorded by properly arranged electrodes [13]. The use of EEG processing rests on the observation that anesthesia medications have substantial effects on neu-

ronal synaptic activity which produces the EEG and this change appears to produce the characteristic central nervous system (CNS) effects identified as anesthesia. The origin of the EEG and its characteristic of safety and noninvasion place the EEG monitors in a better perspective.

The second topic of this work is multi-input-multiouput real-time anesthesia patient modeling for multi-objective prediction, diagnosis and control. Real-time anesthesia decisions are exemplified by general anesthesia for attaining an adequate anesthetic depth and ventilation control etc. One of the most critical requirements in this decision process is to predict the impact of the inputs (drug infusion rates, fluid flow rates, etc.) on the outcomes (consciousness levels, blood pressures, heart rates, etc.). This prediction capability can be used for control, display, warning, predictive diagnosis, decision analysis, outcome comparison, etc. The core function of this prediction capability is embedded in establishing a reliable model that relates the drug or procedure inputs to the outcomes. Furthermore, anesthesia drugs have impact on multiple outcomes on an anesthesia patient. Most typical outcomes include anesthesia depth, blood pressures, heart rates, etc. Traditional modeling, diagnosis, and control in anesthesia focus on a one-drug-one-output scenario [48, 86, 50, 51, 52, 57, 64]. For a comprehensive anesthesia managment, it becomes essential that the impact of anesthesia drugs on multiple outcomes be taken into consideration.

The third task of my research is to investigate the performance of feedback anesthesia drug control in wireless connected system. This research goal was based on the following two issues:

- Operation room in the future

  In an operation room, a wide range of medical devices are connected together or connected to patient through cables for measuring, monitoring and diagnosis. The cable clutter interferes with patient care, creats hazards for clinical staff and delays transport and positioning. To improve the clinical room efficiency and safty, it is reasonable to replace those cables with wireless connections.

- Automatic anesthesia control

  In medical point of view, to maintain an adequate depth of anesthesia without compromising patient's health, an anesthesiologist usually works as a multi-task feedback controller to roughly regulate the drugs titration while observing a variety of patient outcomes. Designing an automatic anesthesia controller aims to automatically regulate anesthesia levels by taking account on several physilogical measurments and then frees up anesthesiologists for more important tasks in operation.

However, when wireless communication channels is involved, it would introduce noises due to quantization, channel noises, and haveing limited communication bandwidth resources. As a results, it would impact the performance of, even distablize the close-loop control systems. So investigating how the wireless communication channels affect the close-loop systems, then avoiding the unstable status and even optimizing the system performance become more critical than ever.

The final project is modeling for the impact of anesthesia and noise lesion on the

neuron activities of auditory systems. This project is motivated by the purpose of investigating the impact of anestheisa and noise lesion on the auditory system from a system view point. In tradition, the response of primary auditory cortex nerons to outside stimuli was represented by the STRF (Spectra temperal receptive field) which aims to completely characterize and predict the acitvities of the auditory neurons to any acoutic stimuli from wideband noises to nature sounds. The system identification methods were widely applied for estimating the mapping functions of the systems. Usually, the mapping functions contain much nonlinearity that potentially increases the computation complexities. However, for special applications, it is reasonable to utilize a simple model structure even linear model to represent the auditory systems. In this research work, a model structure was presented and applied for analyzing the impact of anesthesia and noise lesion on the primary auditory cortex neuron activities. Several interesting findings were highlighted.

1.2 Literature Survey

1.2.1 Measuring Anesthesia Depth Based on EEG Signal Processing

In previous research works, several EEG based depth indexes and EEG signal processing methods for measuring depth have been developed and investigated [2, 28, 40, 24, 26, 30, 34, 36, 44, 41, 42, 45]. Rampil etc. reviewed main of these technologies and the corresponding clinical applications, including the bispectral index used in BIS system which is the product of Aspect Medical Systems Inc.[28]. All of the methods

6

can be classified into two categories: time-domain methods and frequency-domain methods. Only one time domain method, burst suppression quantitation [36], is in current used in monitoring systems. Frequency domain analysis, which is based on Fourier transform, is an important alternative approach to time domain methods. Almost all the currently available devices: BIS system, Entropy system, Narcotrend, Sedline, and Snap II, are based on the power spectrum analysis of EEG. The results from frequency domain analysis can be described by sole parameters such as median frequency, spectral edge frequency, relative band power, band power ratio etc. and combined parameters such as bispectral index and spectral entropy index used in BIS system and Datex-Ohmeda S/5TM Entropy Module respectively. Unfortunately, no sole indicators could server as a comprehensive descriptor of anesthesia depth [40]. The combination of several parameters showed a higher discriminating power than sole parameters. For example, the measuring indexes of widely used BIS system and Entropy system are the combination of several EEG parameters. BIS monitor uses different algorithm to calculate the BIS during the different stages of anesthesia, e.g., burst suppression, frequency power ratio as well as bispectral analysis. The Entropy Module measures the depth of anesthesia by calculating two spectral entropy indicators: state entropy and response entropy, and the difference of them. The detailed algorithm to obtain the bispectral index and spectral entropy index was presented in [28] and [41] while the combination of those individual parameters is unknown. In addition, some other analysis methods such as artificial neural networks, complexity and wavelet analysis also were reported and proved to be useful tools in

measuring depth of anesthesia [26, 30, 42, 45].

Although the goal of monitoring anesthesia was initially focused on avoiding the hazards of overdose, a greater interest has been added in the prevention of recall or awareness during operation [7, 8, 15, 44]. In one of the papers of John C. Drummond, it was stated that a valuable monitor is that the average value yielded by the device in two distinct states should be statistically different and the range of values seen in those two stage should not overlap, ideally, the index of the device should be 100 percent sensitive and specified to the different states, and the critical threshold values that distinguish depth of anesthesia states of interest should not be influenced by the choice of anesthesia agent or by patient physiology [8]. But neither technique completely meets the two preconditions for identifying the probable patient awareness. Although the BIS system yielded the best combination of sensitivity and specificity of any commercially available monitors, a significant limitation that the BIS thresholds is dependent on the anesthesia agents administered can not be eliminated. Furthermore, some publications reported that some values recorded during adequate surgical anesthesia were within the range of values seen in awake patients [29]. Hence, the Middle Latency Auditory Evoked Response (MLAER) emerged as a new technology to predict the awareness [8]. Christian Jeleazcov etc. [19] analyzed the discriminant power of EEG, acoustic evoked potentials (AEP) and somatosensory evoked potentials (SSEP) respectively and the discriminant power of their combinations, and suggested that future anesthesia monitor should consider the combined information simultaneously distributed on different electrophysiological measurements.

1.2.2 Anesthesia Modeling and Control

- Modeling in anesthesia

  The standard modeling paradigm used to describe the releationship between in-
  put drugs and patient responses is Pharmacokinetic-pharmacodynamic(PKPD)
  compartmental models. Pharmacokinetics concerns the dynamic process of drug
  distribution in the body, pharmacodynamics decribes the effects of the drug on
  the body. This model formed the basis of target-controlled infusion(TCI) system
  used extensively in the world excepted for North America. The most frequently
  used model is a three-compartment model described in [46]. Currently, most
  of the anesthesia controller design and monitoring are based on PKPD models
  [48, 86, 50, 51, 52, 64]. An alternative modeling way is physiological-based mod-
  els which try to eliminate the disadavantages of simple compartmental models.
  Decription and illustration of these models are detailed in [47]. Those models
  are population based and can only be indentified off line or partially update PD
  model parameters online [48, 50]. As the increasing emphasis on multi-objective
  anesthesia diagnosis, researchers are moving their attention to the problems of
  the MIMO modeling for anesthesia patient. The representive works can be seen
  from those published papers of C. Nunes, M. Mahfouf, and H. Lin[53, 54, 55, 71].
  In papers [53, 54],the neural-fuzzy paradigm was applied to model the patient
  dynamics and measure the anesthesia depth. Neural network is widely used
  in anesthesia monitoring and diagnosis [70]. Such a smart system can assist

anestheologists in diagnosis and making decisions. H. Lin et al. developed a multi-variable piecewise-linear model to relates all drugs, surgical stimuliations to patient outcomes such as heart rate, BIS index, and blood pressure. The basic idea is dividing the whole anesthesia procedure into two parts according to the BIS value, then the nonlinearity of patient dynamics can be approximately linearized. The advantages of this model is that it can describe the interaction between inputs and can be easily identified through existing multivatiable indentification methods. The obvious shortcomings are that it is time consuming and can not be realized in real time. In paper [71], an automatic MIMO drug delivery system named 'RAN' was reported. In this paper, the PKPD model related the input drugs to patient outcomes. In our previous research works, an information-oriented model structure (a special case of Wiener models), for patient anesthesia depth responses to propofol infusion as an SISO system was introduced in [60, 61, 62]. This simple model structure contains few parameters and can be easily indetified in real-time.

- Control in anesthesia

Closed-loop control of anesthesia has been a goal of many researchers since the middle 20th century. Before the availibility of reliable anesthesia monitors, Schwilden et al. [72] used the median frequency of EEG as an index of depth of hypnosis and a simple model-based adaptive scheme based on a two-compartment model to adjust propofol infusion. In the 1990s Machfouf and

Linkens [73] used a number of model-based predictive control techniques to control muscular relaxation and mean arterial pressure. With the emergence of BIS monitor in late 1990s, the interests in closed-loop control of depth of hypnosis was renewed. The most notable works are seen in [74, 86, 64, 51]. Model predictive control and PID control are the widely used strategies in anesthesia applications. Both strategies requrie complete decrisption of the pateint models. Another strategy is the fuzzy-logic based controller which does not use the mathematic models [54]. In recent years, the multi-task controller for anesthesia applications attracted more interests [71, 75]. As a promising control strategy for regulation of anesthesia patient outcomes, model predictive control has been applied to regulate two patient outcomes simultaneously [67]. Most of the effort in this area is focused on control strategy design. As the emergence of the new demands in current operation rooms, we need to consider using new or curent technologies to fulfill those coming challenges. Wireless connection of medical devices in operation room with special applications on anesthesia is an example. To my knowledge, no related research works have been made to discuss these problems.

1.2.3 Modeling for Auditory System

The problem of modeling for auditory systems was extensively investigated by researchers in the past two decades. Although the outputs of the conventional models, STRF (Spectro-Temporal Receptive Field) and computational models, were neural

activities such as spike trains, action potentials or firing probabilities, these models have distinct applications. STRF was introduced by Aertsen to describe the input-output relationships of auditory neurons in 1981 [76]. It was widely used for describing and predicting the auditory neuron activities under such a wide range of stimuli as the pure tones, wideband noise, and natural sounds and so on [77, 78]. The model classes of the STRF can be either linear or nonlinear, parametric or nonparametric. The estimation of the STRF was typically summaried by using the maximum a posteriori(MAP) estimation [79, 97]. The computational model consists of several functional blocks (pass-band filter bank, nonlinear functions, etc.), with each block representing a physiological function of the ear or transmission channels in the neural system. This method was based on the knowledge of the neurophysiology of the auditory system and used for describing the audio signal processing at the physiological and perceptual levels and designing hearing-aid devices and cochlear implants [80, 81]. Recently, a simple dynamic model was derived to represent variability and state-dependence of auditory neuron responses [82].

The central nerve system (CNS) activities are affected by anesthesia drugs. Several EEG signal processing based methods were introduced to quantify and continuously monitor the anesthesia depth [83, 84]. In addition, modeling the anestheisa dynamics with the anesthesia drugs as inputs and EEG based indexes (eg: BIS) as outputs were widely investigated for the purpose of automatic anesthesia control, outcomes prediction and diagnosis [85, 86, 87]. The anestheisa drugs are widley believed to affect the neuron activities of the auditory cortex. The auditory evoked

potentials were proved to be more efficient than the EEG in decribing the transition from conciousness to unconciousness state of patients [88]. Futhermore, the noise lesion on auditory cortex may cause the auditory systems can not work properly. To understand the impact of anesthesia drugs or noise lesion on auditory cortex neuron activities, many researchers studied neuron activities (spontaneous or acoustically evoked) among awaked and anesthetized animals [89, 90, 91, 92, 93]. Low frequency hearing loss was even found after spinal and general anesthesia [94]. Most of the analysis methods were limited in their scopes and in model structures. Mechanism of the propofol's effect on neural activities was described through a physiological model with parameters determined by large amount of testing experiments [95].

1.3 Potential Original Contributions

During the study period, I have completed several projects of modern anesthesia management. They are the following:

1. Monitoring anesthesia depth based on EEG signal processing.

2. MIMO anesthesia modeling and diagnosis.

3. Feedback anesthesia control in wireless networks.

4. Analysis of the imapct of anesthesia and noise lesion on primary auditory cortex from a system point of view.

There are several origianl contributions in my research work.

The first contribution: developed a new EEG parameter and analized the EEG channel locations. Our initial analysis results show that the developed new parameter is stronger in monitoring anesthesia depth, especially for detecting awareness of a patient during anesthesia. Furthermore, the results of channel locations analysis give a guidance for EEG sensor placement in the viewpoints of drug sensitivity and signal to noise ratio in the application of depth monitoring.

The second contribution is the introduction of multi-input-multi-output real-time modeling method for anestheisa prediction and decision making. Anesthesia management is actually a MIMO problem. Usually, anesthesiologists watch several vital patient responses such as blood pressure, heart rate, and BIS index etc., then manipulate anesthesia drugs tirations based on current inforamtion to maintain an adequate anesthesia level roughly. With the assistant of this real-time and individulized MIMO anesthesia patient model, anesthesiologists can make decisions based on both of current and future information and achieve enhanced anesthesia management.

The third contribution of this research work is the hardware implementation of the developed MIMO model through Labview graphical programing software. The implemented multi-objective predicting and diagnosing model is proposed to be able to work as an Anesthesia Management Assistant Equipment in clinical room.

The forth contribution is theoretical conclusions of the feedback anesthesia control problem in wireless connected system. When signal averaging is inserted in such a closed-loop system for noise reduction, it is observed that the averaging window will destabilize the closed-loop system if the window size excess the stability margin. In

this work, the analysis and calculation of stability margin against exponential window, as well as the optimal strategy for choosing averaging window sizes are introduced. Those findings formed one of the fundamental theoretical basis for wireless connected medical device systems in future operation rooms.

The fifth contribitution is the introduction of the modeling method for the analysis of the auditory system under anesthesia and after noise lesion. In this project, I developed an auditory system structure, analized the system parameters when the system under different conditions. Serveral interesting points were highlighted in this work.

CHAPTER 2: MONITORING ANESTHESIA DEPTH BASED ON EEG SIGNAL PROCESSING

2.1 Background and Problem Statement

General anesthetics is proved to interference with synaptic function in the CNS(central neural system). CNS produces all kinds of cortical activities such as cognition, memory, attentiveness etc. Due to the depression of CNS caused by anesthesia drugs, the loss of consciousness, lack of movement to incisional pain of the patient etc. are the general phenomenons occurred during anesthesia[27]. The term *depth of anesthesia* is rooted in the principles developed by Guedel in 1937 with ether anesthesia when he was training inexperienced personnel to give anestheisa in Second World War[14]. Guedel defined a series of stages and planes using changes in vital signs and cranial nerve reflexes as ether anesthesia deepened. These effects are related to the progressive effects of ether on the cortex and brainstem with lighter levels primarily affecting the cortex and deeper levels acting on the brainstem as well. Using these signs, the patient could be adjusted to a level of responsiveness associated with "surgical anesthesia".

One of the developement of modern anesthesiology is the ability to monitor the depth of anesthesia. The main method is focused on the search of a reliable index to discriminate the statistically significant difference in anesthesia. Among the current available technologies, none has the sensitivity and specificity to allow the clinician

to draw certain conclusions about the depth of anesthesia in individual patients for whom he or she treats. The developed technologies and monitor devices just serve as a trend indicator of anesthesia stages as the variation of drug dose.

2.1.1 Previous Monitering Techniques in Anesthesiology

Traditionally, some measurable indicators such as arterial blood pressure, ventilation, and heart rate are used as anesthesia depth indicators which can predicte anesthesia depth roughly[3].

Another more general monitoring approach is to consider general anesthesia as a mixture of three basic components and then focus anesthetic management on each component. Traditionally, the following three components have been considered[27].

- patient movement,

- analgesia or insensitivity to pain,

- unconciousness.

Classic assessment of sedation is provided by Observer Assessment of Awareness and Sedation Score(OAA/S score)(Table 2.1.1)[6]. However, once the response to physical stimuli or verbal is absent, the ability to assess the cortical activity is lost.

Clearly, an effective method should be developed to characterize the state of higher cortical functions, such as level of conscisousness, so that a reasonable threshold for keeping the patient adequately anesthetized and not overdosed could be achieved.

Table 1: Modified OAA/S scale used in associating subject behavior with EEG change

Expected response	Score
Responds readily to name spoken in normal stone	5(Alert)
Responds only after name is called loudly andor repeatedly	4
Lethargic response to name spoken in normal stone	3
Responds only after mild prodding or shaking	2
Responds only after painful trapezius squeeze	1
Does not respond to painful trapezius squeeze	0(Unconscious)

2.1.2 Use of EEG to Monitor the Anesthesia

Scince EEG is the product of synaptic activity on the pyramidal cells in the superficial cortex, it can be recorded by the properly arranged electrodes placed on the scalp. A large amount of evidence substantiates the alteration in synaptic activity as a primary mechanism of anesthetic agent action(the details were presented in reference [27]), the EEG may be useful in assessing the anesthesia drug effects on synaptic activity which occurs with higher cortical processing.

1. *Description of EEG* The EEG activity can be described by those descriptors such as waveform, repetition, amplitude, frequency, distribution, phase relation, timing, persistence and reactivity [13]. In anesthesia field, the most frequently used discriptor for EEG is frequency. In frequency domain, EEG signal is usually divided into 5 groups or frequency band(Table 1) [28]:

Table 2: Five EEG frequency bands

Band Designation	Delta or δ	Theta or θ	Alpha or α	Beta1 or β_1	Beta2 or β_2
frequency range	Under 3.5Hz	3.5Hz to 7Hz	7Hz to 13Hz	13Hz to 30Hz	30Hz to 50Hz

Alpha waves or α are usually seen in patients who are awake. They are generally

more prominent over the vertex(top of the head)in a relaxed state as with
meditation (especially with eyes closed). Beta1 waves or β_1 are usually seen in
the prefrontal regions and to increase during the initial stages of sedation, and
amnesia caused by some anesthesia drugs. Theta waves or θ (also known as slow
waves) are normally seen in sleep. Delta waves or δ are usually seen in deep
sleep and are abnormal in the awake adult. Both of θ and δ are seen due to the
influence of anesthesia. The high frequency band, Beta2 waves or β_2 is thought
to play a role in perception and processing of sensory information [10, 32]. This
high frequency band are usually contaminated by EMG (electromyography)
signals, a composite of all the muscle fiber action potentials occurring in the
muscle(s) underlying the skin. Both of β_2 wave and EMG signal are normally
seen in awake person and depressed significantly by anesthetics, so they are
usually used as important indicators to measure the anesthetics effects [28, 41].
The overlap of the frequency content of the EEG and EMG is depicted in
Figure 1 where the relative amplitude is also shown (Copied from Jensen [77]).
As shown, the facial muscle EMG overlaps with the EEG even to the α band.

2. *Effects of Anesthesia Agents on EEG* In general, EEG has basic patterns such
that a change from these rhythms suggests a physiologic perturbation or drug
effect. Most anesthetic drugs alter EEG by producing an initial excitatory
stage characterized by desynchronization and increased relative power of faster
frequency [22]. The fast β activity is most prominent in the frontal regions and
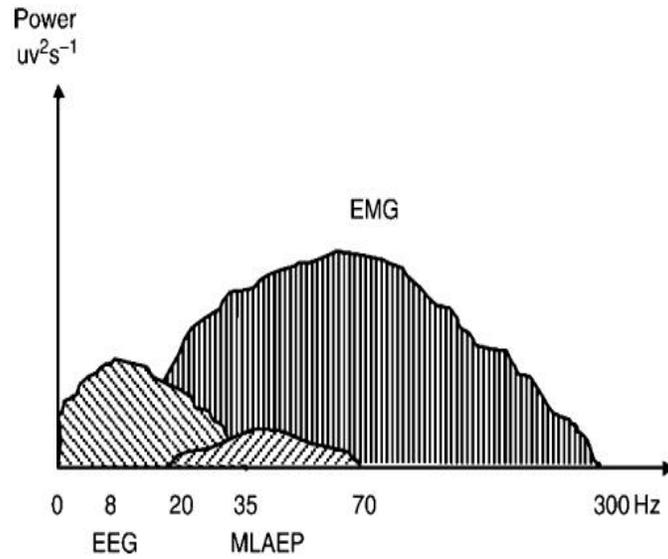
Figure 1: Power spectrum of the EEG, facial muscle EMG and midlatency auditory-evoked potentials(MLAEP).

moves posterior as the anesthetic drug effect increases. At the same time, a prominent area of EEG synchronization in the alpha range developes over the more posterior regions and moves to the frontal regions. As the increasing of anesthesia drug doses, the EEG will achieves burst surpression (where periods of EEG activity are interspersed with periods of flat EEG) [28].

The general pattern change during anesthesia is shown in Figure 2 [27]. First, frequency activity increases and then gradually decreases until electrocerebral silence occurs. Amplitude increases as the activity is synchronized into the $8 - 10$Hz range and then gradually decreases until the EEG is flat. Next the variability (or entropy) in the EEG decreases as the EEG becomes synchro-
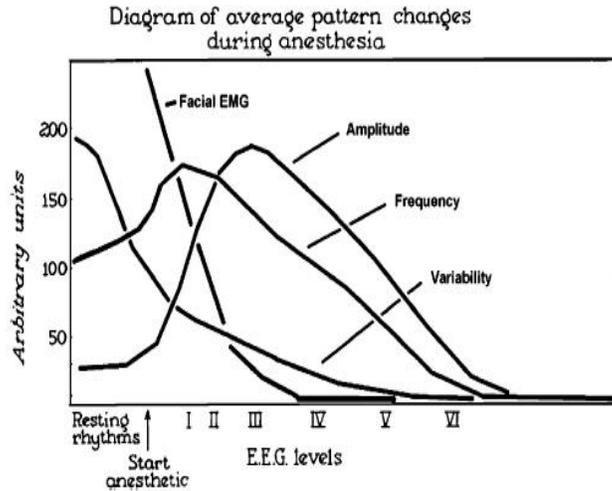
Figure 2: Changes of several EEG and EMG parameters as anesthesia is deepened

nized with the thalamic pacemaker. Finally, the EMG of the frontal muscles

disappears as the anesthesia deepens. Based on these observations the EEG

may be capable of reflecting a gradual change in anesthetic effect by using a

combination of EEG amplitude, frequency, variability, topography, and frontal

EMG.

With the central nervous system (CNS) being the target of anesthesia drugs, the

electroencephalogram (EEG) signal processing has been the focus for anesthesia depth

monitoring [13, 7]. A variety of methods based on EEG signals processing have been

developed [2, 28, 40, 42, 19, 24, 34, 45]. The goal of all these EEG processing methods

is to produce a scale quantitative EEG "index" that is clinically useful.

Currently, there are a few EEG based anesthesia depth monitors in the market,

such as the BIS monitor (Aspect Medical Systems, Inc.) and the Entropy Module

(GE Medical Systems, Inc.). Both monitors use frontal EEG signals and give an index from 0 to 100 continuously with '0' means brain dead and '100' means fully awake. The index is produced by weighted combination of several derived EEG parameters from both time domain and frequency domain. Although these machines improve the performance of anesthesia depth measurement much in certain level, their reliability in ICU applications remain to be enhanced, some cases of failure in predicting patient's status are reported in [15, 29]. As a result, investigation of such EEG parameters or processing methods that could serve as or produce a stronger depth indicator during some special situation such as recovery stage becomes a very important issue. Furthermore, in one aspect, frontal EEG locations are more convenient for signal collecting, on the other hand, these locations are more easily subjected to noise of eye movement and EMG which have detrimental imapct on the accuracy of depth measurement. So, it is necessary to compare the performance of the EEG indexes from different channel locations.

2.2   Evaluation of EEG β_2/θ-Ratio

2.2.1   EEG Signals Acquisition and Preprocessing

1. *Subjects and Anesthesia* All the EEG signal analysis results presented in this thesis are based on EEG recordings from 5 young healthy male volunteers. The study was conducted in the Receiving Hospital, Detroit, MI., and recieved institutional approval. All subjects were explained of the nature of the study

and consenting participants.

The BIS values and other physiological vital signs (blood pressures, heart rate, oxygen saturation, etc.) were continuously monitored during the entire process with BIS value used as a reference.

Propofol titration rates range from $170 - 200\mu g/km/min$. The data collection procedure was divided into four separated stages,which was showed in Figure 3(b):

(a) Awake stage (15 minutes): The subject was conscious and instructed to be calm and inactive. Facial and body movements were observed in this stage. No titration or injection of anesthesia drugs was administered. The EEG parameters in this stage served as a reference for the other stages. Other physiological vital signs were also recorded.

(b) Induction stage (15 minutes): Propofol titration starts at the beginning of the induction stage. During this stage, propofol titration rates were slightly adjusted to achieve a BIS value to the desired levels (between 30 and 50). Towards the end of this 15-minute period, the BIS values of all the subjects become stable. This stage was characterized by substantial changes of anesthesia depth towards its steady-state values. Occasional facial and body movements occurred.

(c) Maintenance stage (30 minutes): Propofol titration was continued 30 mins to the level that achieved the desired Bis level and depth of anesthesia. This

stage is characterized by relatively stable BIS values, no drug adjustment, and no body movements.

(d) Emergence stage (15 minutes or longer): This stage starts when propofol is stopped and the subject experiences a recovery process without any drugs. Due to differences in recovery speed, the duration varies. Body movements become gradually apparent in the recovery process.

2. *Equipments and EEG Channels* EEG signals from 16 channels were recorded by using the 16 channel Nolan Mindset-16 EEG data acquisition equipment(Nolan Computer Systems, L.L.C.). Each subject worn an electrode cap with electrodes arranged according to the international $10-20$ system, see Figure **??**. It uniformly covers the entire scalp and consists of 21 recording electrodes as well as one ground electrodes. The number of electrodes is enough for recording the EEGs in the whole scalp regions. Sometimes, the modified 10-20 system is used to increase the spatial resolution for special studies or to detect highly localized evoked potentials [13].

Every electrode is named by the position on the scalp where it locates, and depicted by a letter and subscript z for midline electrodes or number with odd number for left electrodes and even for the right. The electrodes in prefrontal are denoted by F_p, frontal by F, central by C, temporal by T, parietal by P, occipital by O, and auricular by A. Usually, there are no electrodes in the positions of F_z, P_z, and O_z, thus only 18 electrodes including two reference
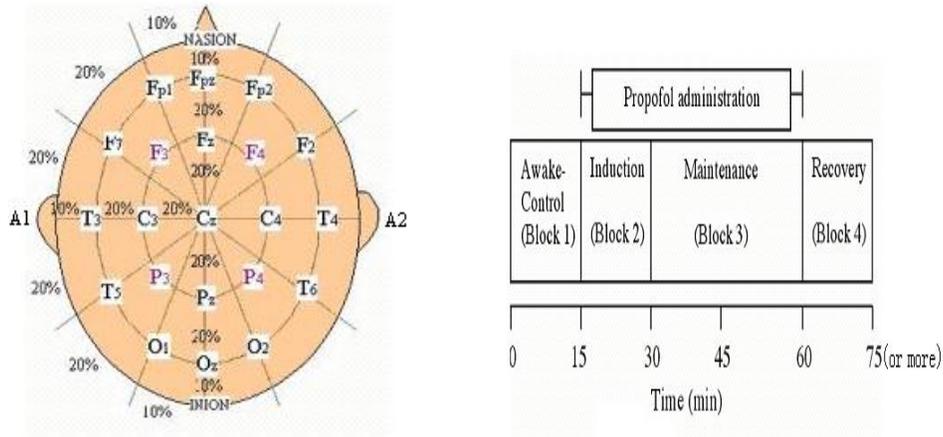
(a) Electrodes placement according to the $10 - 20$ system

(b) Propofol adminstration and time interval for each anesthesia stage

Figure 3: Electrodes placement and anesthesia stages division

electrodes (in reference montage) are used for EEG recording.

Actually, the recorded EEG is the potential difference between two recording electrodes, the absolute potential value at any individual electrode can never be known. How the two recording electrodes are combined for EEG recording (e.g. Which electrode is conected to inupt1 or input2 of the amplifer) is defined as *montage*. The are five basic kind of montages: bipolar, Laplacian, common reference, average reference and wieghted average reference. The difference between those montage are detailed in reference [13]. The common reference montage, simply, the reference montage, is used in all the experiments in this thesis.

3. *EEG signal preprocessing* The raw EEG signals were digitized at 256 Hz. Al-

though a low-pass filter with cutoff frequency 35 Hz was used in the Nolan Mindset-16, 60 Hz power line contamination was still visible in the recorded EEG signals. Scince the interested EEG signal frequency band is below 50Hz in monitoring anesthesia depth, the 60Hz power line contamintion can be easily removed by a low pass filter with cutoff frequency below 60Hz. While EEG signal is also easily contaminated by other artifacts such as eyemovement, body movement, ECG etc. ECG signals could be avoided by properly arrange reference electrodes. But the eyemovement is a high amplitude potential usually be recorded with EEG and locates in the interested EEG frequency band. Meanwhile, some artifacts, such as body movement and cabel movement, have large amplitude, which results in overflow of the recording equipment channels and invalid recording EEG signals. The eyemovement signal could be removed by some developed signal separation technologies, but the overflowed data points have to be discarded. In this thesis, what is going to be focused is the development and clinical application of various EEG parameters. For convenience, the original EEG data were manually cleared of highly visible artifacts (eye movements, body movements, equipment disturbance, cable movements, etc.), all the segments with those artifacts were discarded. Then, the remained artifactfree signals were seperated into 10 sencond (2560 data points) segments and a low pass filter with cutoff frequency of 47 Hz was designed to filter out the 60 Hz power line disturbances before the next data analysis step of the EEG signals. Each EEG parameters presented in the following chapters was calculated for

each preprocessed EEG segment and then the time trajectories of each parameter were obtained. For those EEG parameters based on EEG spectral analysis, the power spectrum of each EEG segment should be calculated first. The methods used in this thesis to estimated the power sepctrum is the following: the 10-second segment was divided into 4 50% overlapping subsegments of 4 seconds each, $[0, 4], [2, 6], [4, 8], [6, 10]$. The spectra of each subsegment was estimated by Welch's method [43] and the resulting spectra of the four subsegments were averaged to generate one spectra.

2.2.2 Methods

As presented in chapter 2, five frequency bands are frequently identified for the EEG signal: Delta band or δ ($0.5 - 3.5$ Hz), Theta band or θ ($3.5 - 7$ Hz), Alpha band or α ($7 - 13$ Hz), Beta-1 band or β_1 ($13 - 30$ Hz), and Beta-2 band or β_2 ($30 - 50$ Hz) [9, 27]. All five bands are influenced by anesthesia agents [27].

The relative β-ratio is one of the main parameters that are used jointly to produce the BIS index in the BIS Monitor. It is defined as $\log(P_{30-47}/P_{11-22})$ [28], where P_{x-y} denotes the sum of spectral power in the frequency band from x to y in Hz. It is well understood that the state of human awareness and alertness are associated with increased power in the higher frequency bands such as β and β_2 with an accompanied decreased power in the lower frequency bands (θ and δ bands). Consequently, it is a sensible choice of using power ratios of high power ranges to low power ranges as indicators of anesthesia depth.

However, sensitivity of band powers to awareness and alertness varies significantly. Author O. Dressler et al. introduces a measure of discriminating capability for awareness and alertness indications [7]. Figure 4 shows the re-mapped predicting probabilities, denoted by rP_k, of different frequency bins. The higher the rP_k, the better the discriminating power of the frequency band. It is reported that the best performance for discriminating the awareness and lacking of responsiveness was achieved by the high frequency band (> 26 Hz) and low frequency band (< 15 Hz) in EEG.
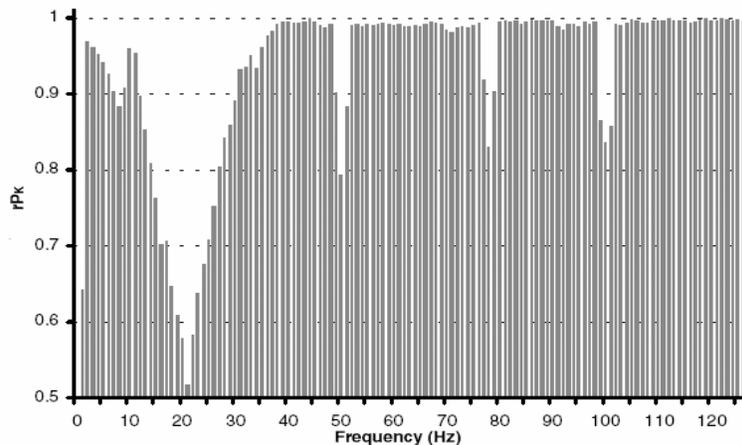
Figure 4: Remapped prediction probability of frequency bins from 1 to 128 Hz, copied from paper of O. Dressler et al. [7]

In particular, it is noticeable that the average rP_k value within θ band ($3.5 - 7$ Hz) is much higher than that of the band between 15 to 20 Hz, which is a major part of the band ($11 - 22$ Hz) used in the BIS monitor. Based on this observation, the aim of this study was to introduce a different band power ratio: the ratio of the β_2 and θ powers, which is defined as $\log(P_{30-47}/P_{3.5-7})$. This is termed as *the β_2/θ-ratio*.

There are several potential advantages to this method:

1. The β_2/θ-ratio have more sensitivity to changes in awareness and alertness as shown by Figure 4.

2. In the frequency band over 30 Hz, the EMG signal becomes more dominant than EEG signals in partially awake subjects. As presented before, the EMG signals can be a good indication of high awareness and alertness. As a result, in the two currently available anesthesia depth monitors, the BIS system (Aspect Medical Systems, Inc., Newton, MA) and Datex Entropy Module (Datex-Ohmeda Division, Instrumentarium Corporation, Helsinki, Finland), the frequency band dominated by EMG was used to enhance sensitivity to develop the depth indicators [28, 41].

   One adversary impact of this approach is that EMG frequencies can extend to the alpha band, which is covered in the relative β-ratio. This can reduce sensitivity since the EMG increases power concentration in both P_{30-47} and P_{11-22}. In contrast, the EMG has little effect in the θ range. As the θ power is used in the β_2/θ-ratio, this can become more effective than the relative β-ratio.

3. Both of the power in band β_1 and β_2 increase during the initial excitation state, so the ratio of these two band power conceals this special state. While the power of *theta* decreases at the initial excitation state, thus this state can be captured by β_2/θ-ratio.

2.2.3 Results

The trajectories of the β_2/θ-ratio and the relative β-ratio from the $F4$ EEG electrode for 5 patients are plotted in Figure 5, where a patient is only indexed by a code such as $S1$. While the awareness, induction, and maintenance stages had fixed lengths, the duration of the emergence stage was variable. The end of this stage for each subject is indicated by an arrow in the figures, indicating that the subject became fully awake at this time. The trajectories are divided by the four stages which are separated by vertical dotted lines and marked by letters 'awareness', 'induction', 'maintenance', and 'emergence'. As β and β_2 powers decrease and θ power increases when the anesthesia depth increases, both the relative β-ratio and the β_2/θ-ratio drop during induction and then rise during recovery. Due to symmetry of the left and right sides of EEG measurements, only the EEG data in the right side channels were analyzed. The only exception was when the data generated from the right side EEG signals became invalid due to noises and recording channel errors, in which case they were replaced by the corresponding signals from their symmetric channels on the left side.

The following results were derived from the data.

1. *Sensitivity of EEG Parameters to Anesthesia Depth Changes.* The trend of an indicator can be extracted from its trajectories by curve fitting. In this study, the approach of polynomial curving was used: For each anesthesia stage, a parameter's trajectory was represented by a second order polynomial which
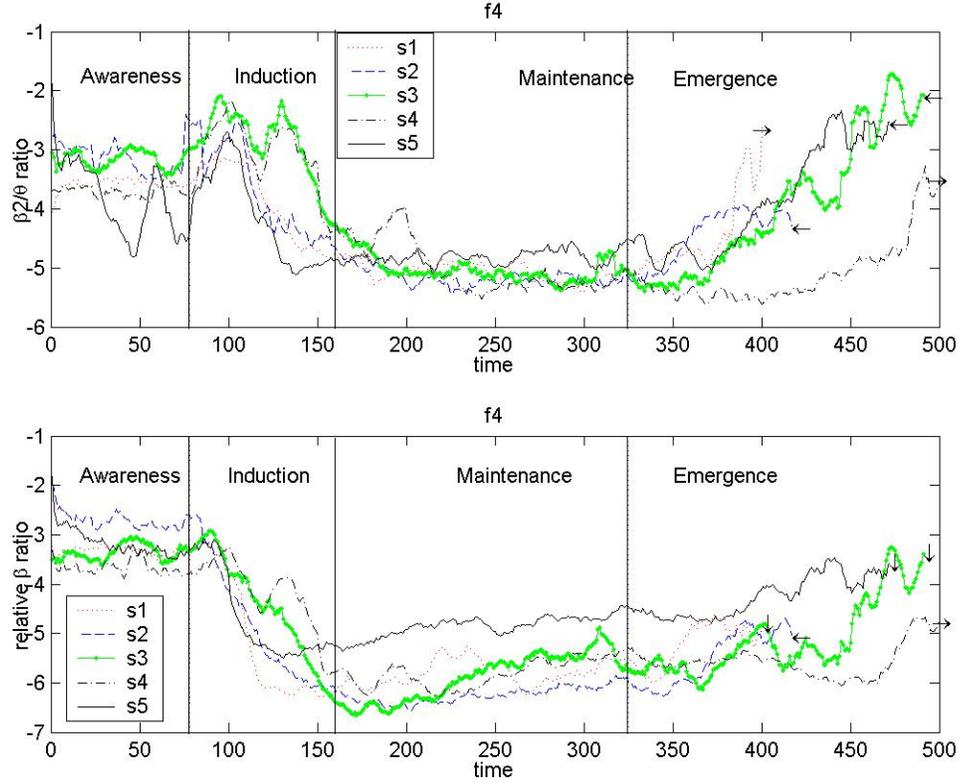
Figure 5: Relative β-ratio and β_2/θ-ratio of $F4$ channel

was obtained by optimal curve fitting.

The second polynomial curves of the β_2/θ-ratio and relative β-ratio in the emergence stage for the five subjects were showed in Figure 6. The larger slopes of the β_2/θ-ratio curves imply that it is more sensitive to the subject recovery than the relative β-ratio after the termination of anesthesia agents.

2. *Reliability of the Parameters.* One possible reliability test of an anesthesia depth indicator is its random deviations of its average trend. This can be represented by the sample variances of the parameter trajectories from its trend curve,
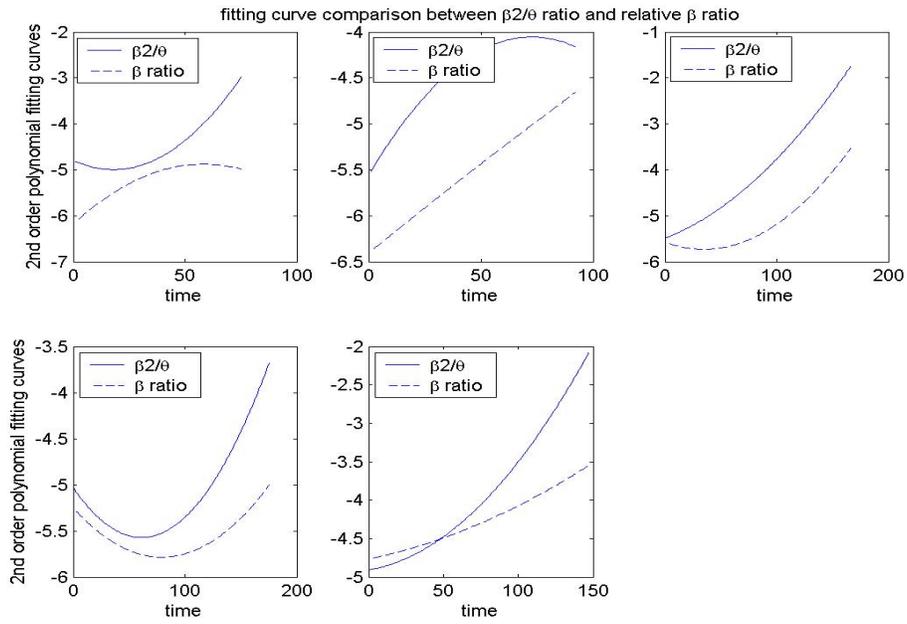
Figure 6: Comparison of 2nd order polynomial fitting curve between β_2/θ-ratio and relative β-ratio in emergence stage of all 5 subjects

and is precisely the curve fitting errors. Figure 7 illustrates the comparison of sample variances between β_2/θ-ratio and relative β-ratio in different stages. In control and induction stages, the sample variances of relative β-ratio is smaller than those of β_2/θ-ratio, while in maintenance and emergence stages,the case is reversed.
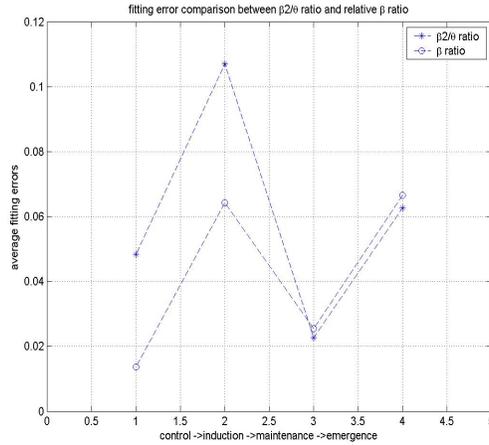
Figure 7: Comparison of 2nd order polynomial curve fitting errors between β_2/θ-ratio and relative β-ratio from control to emergence stage

2.3 Analysis of EEG Channel Locations

In this section, the analysis of EEG channel locations will be made from two aspects: sensitivity to anesthesia stage change and the noise resistance capability.

The sensitivity and reliability of EEG parameters are influenced significantly by the EEG signal channels. This can be seen by the following example. Figure 8 shows the β_2/θ-ratio and the β-ratio from the posterior channel $O1$. It is obvious that the same EEG parameter comes from $O1$ channel almost can not distinguish the

anesthesia stages although it works well during $F4$ channel. Frontal and posterior parts are separated by the central line on the cortex. It can be concluded that the EEG signals from the frontal part channels are far more sensitive to anesthesia depth changes than those from posterior part channels.
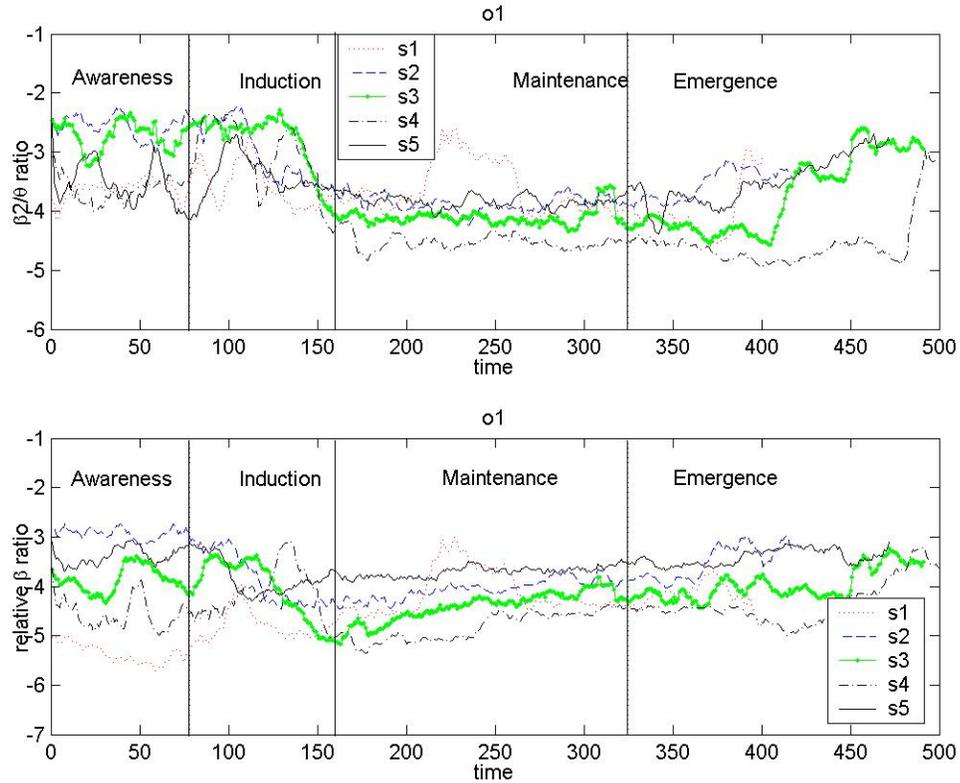
Figure 8: Relative β-ratio and β_2/θ-ratio of $O1$ channel

In addition, it is necessary to measure the noise resistance ability of different channels since it may be helpful in some cases, such as in ICU, the noise artifacts may severely affect the performance of those EEG indexes.

1. *Sensitivity of EEG Signals from Different Channels to Anesthesia Depth Varia-*

tions The sensitivity of EEG from frontal region to anesthesia agent is stronger than that of posterior region can be shown by the distinct EEG signal variances change range in different regions. Table 1 details the difference between the maximum and minimum values of the fitting curves of EEG variance trajectories in induction and emergence stage. The relative large values appeared in frontal channels.

Table 3: Averaged EEG signal variances change range of different channels during induction and emergence stages

	induction	emergence
Fp1	226.0929	129.1887
Fp2	213.4230	126.2557
F7	134.2772	75.8060
F3	102.6195	149.1918
F4	289.7570	153.2214
F8	208.3282	116.6764
T3	40.2689	16.5473
C3	120.9685	46.8462
C4	115.1856	47.8127
T4	52.4477	22.9725
T5	22.8496	15.9653
P3	61.2498	27.7901
P4	68.1277	27.6742
T6	39.1953	23.5402
O1	62.8832	26.3245
O2	54.8328	27.3487

2. *Noise Resistance of EEG Channels.* The amplitude of EEG signals is noticeably lower than noises. When an epoch of the EEG signal is contaminated by artifacts, the variance of this epoch will change markedly from the average of

recent previous ones. This is the artifact detection method used in Narcotrend monitor of anesthesia depth [4]. Figure 9 illustrated the variance changes caused by artifacts.
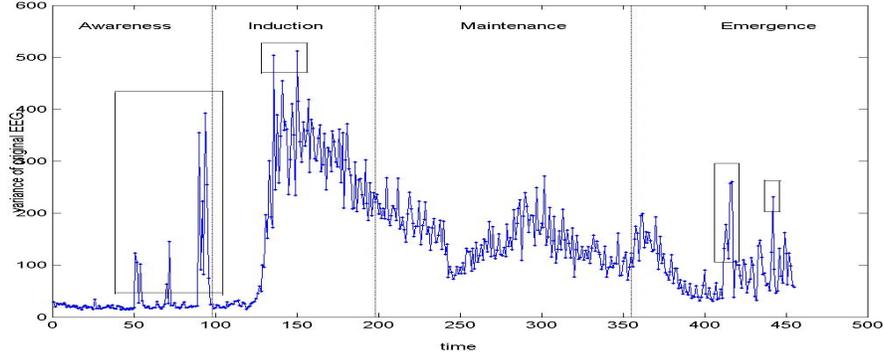
Figure 9: Variances of 10 seconds original EEG epochs from control stage to emergence stage in Fp1 channel. The variances of artifact contaminated epochs were included in some rectangular frames

To understand the noise resistance capability of different EEG recording channels, it was measured by the signal-to-noise ratio:

$$\text{SNR} = \frac{\text{Noise Free Signal Power}}{\text{Noise Power}}$$

The larger the SNR, the stronger the ability of the channel to resist noise. Table 8 details the averaged SNR of different channels from the control to emergence stages. In the control stage, the main artifact is eye movements. It is most obvious in the $Fp1$ and $Fp2$ channels, which results in the lowest SNRs in these two channels. In the maintenance stage, the SNRs in all channels are higher than other 3 stages because there are no facial or body movements of

the subjects. In the induction and emergence stages, the SNR in the $F4$ channel is the highest among all the channels. The SNRs are also relatively high in the $C3$, $C4$,and other frontal part channels.

Table 4: Averaged SNRs(dB) of different channels in different stages

	control	induction	maintenance	emergence
Fp1	6.4465	14.0269	31.9007	22.5068
Fp2	8.1891	14.4074	33.6381	19.1656
F7	10.3199	14.0059	30.4129	17.1422
F3	10.7433	13.7870	33.3786	23.5401
F4	14.5430	16.4383	31.3622	27.8633
F8	10.8283	15.8591	30.7116	18.0307
T3	13.7144	11.9399	29.0920	11.5183
C3	13.4724	14.0608	30.3207	18.4979
C4	16.0707	15.4230	31.4219	18.7303
T4	13.2940	13.2449	33.8836	12.4270
T5	15.9161	12.2889	29.0741	9.7702
P3	17.0888	13.8646	31.5286	15.6814
P4	19.6762	14.9575	31.4345	15.1456
T6	17.8059	13.0461	29.7781	11.7184
O1	16.9754	11.2980	29.0531	11.1733
O2	17.5309	12.0858	27.0983	11.0979

2.4   Conclusion and Discussion

2.4.1   Slection of EEG Parameters

The relative β-ratio and the β_2/θ-ratio can demonstrate different sensitivities in distinct anesthesia stages. In the induction stage, the relative β-ratio falls down faster than the β_2/θ-ratio. From Figure 5, a delay of the β_2/θ-ratio is observed in the induction stage. This shows that the relative β-ratio provides fast initial response to

drug inputs during the induction stage. But the β_2/θ-ratio can capture the initial excitation while relative β-ratio can not. In the emergence stage, the β_2/θ-ratio is more responsive to the depth changes during recovery than the β-ratio. This is evidence by Figure 6. These observations imply that that a better description of the anesthesia depth may be obtained by using the β_2/θ-ratio in the emergence stage and the relative β-ratio in the induction stage.

In terms of reliability,In the control and induction stages, the relative β-ratio has less random fluctuations than the β_2/θ-ratio(Figure 7). The trend is reversed during the maintenance and emergence stages. This observation points towards a possible combined utility of the two parameters: Using the relative β-ratio during the control and induction stages and shifting to the β_2/θ-ratio in the maintenance and emergence stages.

2.4.2   Slection of Channels

Figures 5 and 8 show the traces of the relative β-ratio and β_2/θ-ratio in the $F4$ and $O1$ channels respectively. The results demonstrate that both the relative β-ratio and β_2/θ-ratio can track anesthesia depth changes with substantial sensitivity when they are computed from the channel $F4$. The same parameters that are computed from the channel $O1$ do not provide sufficient discriminating capability. This phenomenon prevails to other frontal/central vs. posterior channels. This observation means that the posterior cortex EEG signals are less desirable for depth measurements in terms of the relative β-ratio and the β_2/θ-ratio.

The sensitivity to the anesthesia agent propofol is distinct between different cortical regions. For comparison of the sensitivities from different EEG channels, the EEG signal variance change ranges (the differences between the maximum and minimum values of the fitting curves of the artifact-free EEG signal variance traces) were calculated for induction and emergence stage and averaged for all the subjects. The larger the ranges are, the more sensitive the EEG parameters are to anesthesia agents. In Table 1, the largest ranges, both in induction and emergence stages, occur in the channel $F4$. This result renders the $F4$ channel EEG signals most sensitive to the influence of anesthesia agent. On the other hand, the parameters derived from the channels $Fp1, Fp2, F3, F7$, and $F8$, are sufficient to make them candidates for depth measurements. However, derived from the temporal, parietal and occipital regions are of little use. From the data derived in this study, it appeared that the EEG signals recorded from the frontal and central channels can best describe the brain activities during anesthesia.

The noise resistance capability is also distinct between different channels. An analysis of data from Table 8 reveals that in the control and induction stages, due to facial, eye, and body movements, the EEG signals suffer from large artifacts, represented by lower SNRs. Within the front and central channels (that provide substantial sensitivity for depth measurements), the $F4$ channel has a stronger SNR. This is not the case when in the maintenance stage as artifacts become very small, all channels dispaly similar SNRs. During the emergence stage, the front and central channels are relatively noise resistent with the $F4$ channel demonstrating a slightly

stronger SNR.

These analysis suggests that the non-frontal channels such as $F4$ may be a sound candidate for a better tradeoff between signal sensitivity to the depth changes and noise resistance capability. This may be especially useful in consideration the typical case studies of BIS reliability in ICU (Intensive Care Unit) settings where noise artifacts make the BIS index far less reliable than in deep anesthesia patients.

CHAPTER 3: MULTI-OUTCOME ANESTHESIA PATIENT MONITORING AND DIAGNOSIS

In this chapter, the problem of real-time multi-input-multi-output anesthesia modeling has been thoughly investigated from the aspects of the motivations, modeling methods, and the concepts and ideas of multi-outcome diagnosis. In addition, the model structure was also implemented in hardware level and applied in the operation rooms to assist the anesthesiologist in monitoring, diagnosing, and predicting outcomes in real time.

3.1 Data Acquisition for Anesthesia Modeling

The patient population age group is between 20 and 70 years old. These patients are undergoing upper extremity arteria-venous fistula placement or thrombectomy, under intravenous unconscious sedation. Anesthesia is administered by an experienced anesthesiologist or registered nurse anesthetist. The patient is seen, examined and evaluated in the pre-operative holding area by an anesthesiologist. The anesthesiologist makes sure that the patient is ready for the surgery. Labs are checked in the pre-operative holding area and 1 mg of Midazolam IV is administered to the patient, after receiving full consent for the surgery and the participation in this study. All risks and benefits are thoroughly explained to the patient while obtaining consent.

The patient is, then, taken to the operating room, placed on the OR table, started on face mask oxygen at a rate of 8 liters/min, hooked to the electrocardiogram mon-

itor, noninvasive blood pressure cuff is placed on the contralateral arm, and the cuff cycle is set to measure blood pressure every three minutes. A pulse oximeter is hooked on the patient's contralateral index.

The patient consciousness levels during anesthesia are measured by a BIS (bispectrum) monitor (Aspect Medical Devices, Inc.). It is one of the anesthesia monitors commercially available and widely used in operation rooms [56, 59]. The monitor provides continuously an index in the range of $[0, 100]$ such that the lower the index value, the deeper the anesthesia state. Hence, an index value 0 will indicate "brain dead" and 100 will be "awake." A bi-spectral (BIS) electrode is placed on the patient's forehead before administering anesthesia to the patient. The electrode is connected to the BIS monitor, which in turn is connected to a special computer system to allow continuous recording and saving of the BIS values. The computer's software is a monitoring system designed by the Department of Electrical and Computer Engineering at Wayne State University. The system performs prediction of BIS values for the specific patient by generating patient models in real time using response data from the patient under anesthesia, see Figures 28 and 29.

Figure 10: Computer data acquisition system
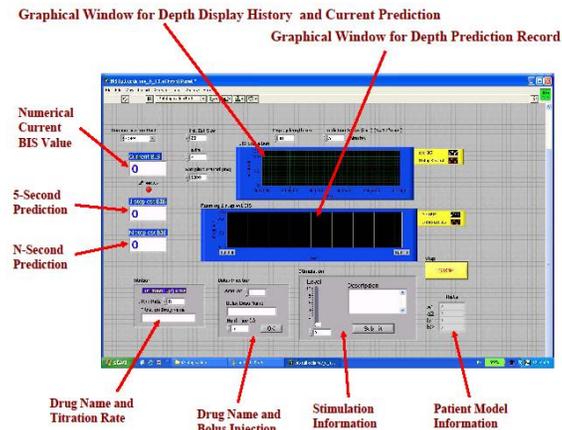
Figure 11: Front panel of the system

A baseline BIS value of at least 90 is recorded before the administration of anesthesia. The patient is given 1-2 mcg/kg of bolus IV Fentanyl at the beginning of the surgery and 1 mcg/kg bolus during the surgery, as needed. The patient is started on intravenous propofol pump at a rate of 50 mcg/kg/min and titrated as needed during the surgery. All measured heart rates, blood pressures and pulse oximetry values are entered and saved manually into the computer every three minutes and following any bolus administration. The propofol rate, any changes made to the propofol rate, and any propofol or Fentanyl bolus given are transmitted to the computer monitoring system automatically and continuously at the sampling rate of 1 Hz (one sample per second). Towards the end of the procedure, and after making sure no more surgical stimuli are applied to the patient, all anesthetics are turned off and the patient is awakened with the BIS value of more than 75. The patient is then taken to the recovery room on oxygen tank for a period of two hours of observation.

3.2   Motivations for Muliti-Outcome Real-time and Indeividulized Modeling

The Anesthesia modeling problem can be figured out as a multi-input-multi-output nonlinear system indentification problem in Figure 12.
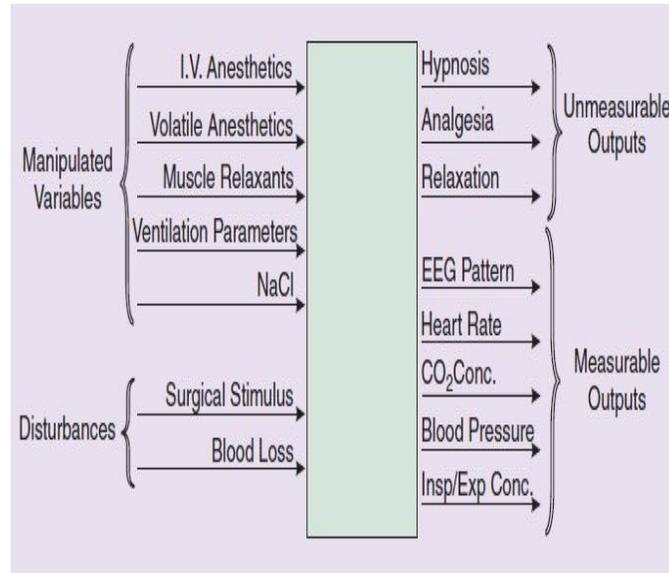
Figure 12: Input/Output representation of anesthesia problem

We also can see that from Figure 13 which shows a typical recording of a patient's response to propofol and fentanyl titration and bolus injections. For this patient, the anesthesia drugs not only reduce the patient BIS values to a lower level, but also depress the blood pressure and make the heart rate fluctuate. For monitoring, diagnosis, and control, it becomes essential that the impact of anesthesia drugs on both anesthesia depth and blood pressures be taken into consideration.
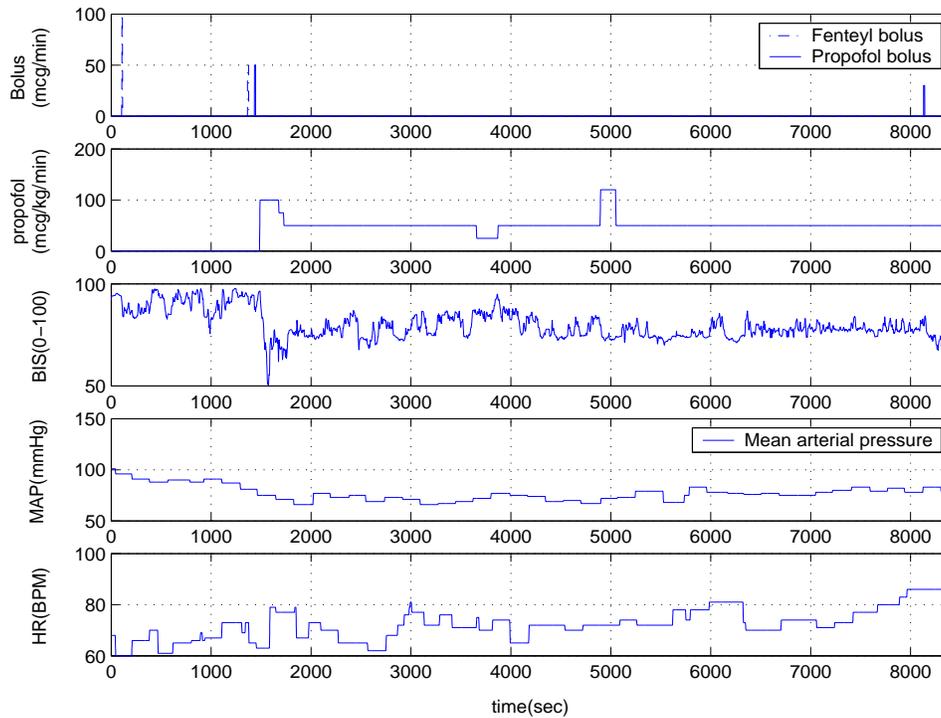
Figure 13: Drug inputs influence many patient outcomes

3.2.1 Individualized and Time Varying Patient Dynamics

Each patient responses to drug inputs with very different dynamics. Figure 14 is another patient's response to the same types of anesthesia drugs as in Figure 13. In comparison to Figure 13, this patient demonstrates slower response after drug changes or bolus injections, lower sensitivity near steady state, and more heart rate variations during the process. For example, this patient's BIS index reaches the steady state value of 75 after 750 seconds, in comparison to the steady state BIS value of 60 after around 1600 seconds in the patient data in Figure 13. Similar disparity also shows in blood pressures. In Figure 14, the blood pressure drops to the value around 90 mmHg in comparison to the value of 65 mmHg in Figure 13. Consequently, to improve

accuracy in anesthesia management, it is necessary to obtain individualized patient models.
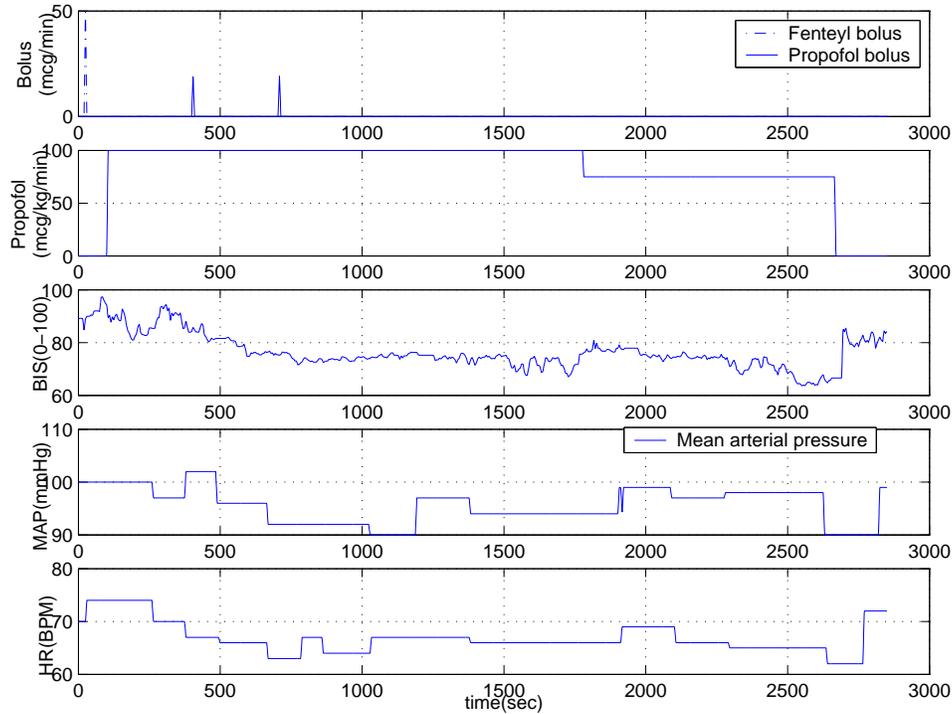
Figure 14: Different patients demonstrate different dynamics

Even for the same patient, responses to the same drugs change with time and surgical stages, and patient conditions. The patient in Figure 15 initially has a more sensitive response in BIS values to propofol infusion, see the BIS trajectory in the first 100 seconds in which the BIS value drops from 100 to 65 after the propofol rate is increased to 75 mcg/kg/min. However, late in the time interval of $240 - 310$ seconds, the BIS values become higher, around 75, even though the same rate of propofol is administered.
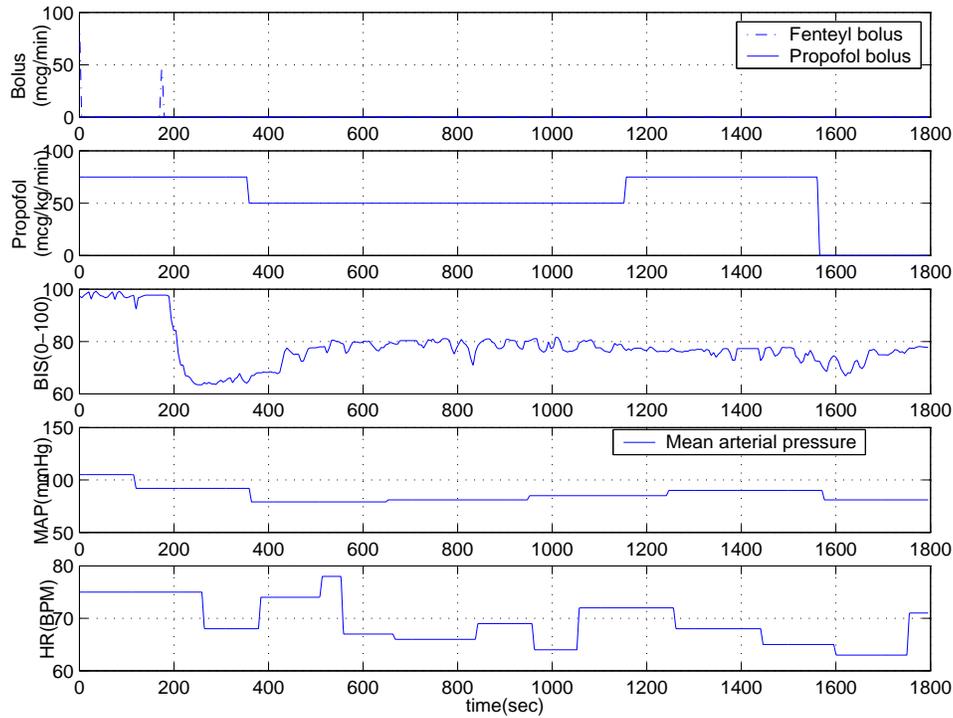
Figure 15: Patient dynamics change with time

3.2.2 Multiple Drugs and Multi-Objective Anesthesia Administration

Our case studies involve both propofol and fentanyl. Both drugs impact multiple outcomes, although to a different degree. For instance, fentanyl has direct influence on blood pressure while it has no obvious influence on BIS values. In the time interval of 0-200 seconds, the initial injection of fentanyl bolus depressed the blood pressure from 110 to 90, while there are no obvious changes on BIS values. The propofol controls both anesthesia depth and blood pressure significantly. During time interval of 350-1000 seconds, both of BIS value and blood pressure are climbing up as the propofol titration rate is decreased. These are seen in Figure 15.

Anesthesia management must consider all essential patient outcomes. For in-

stance, if one focuses only on the anesthesia depth, propofol will be increased when the BIS is too high. However, if this occurs when a patient's blood pressures are low and if the patient's blood pressures respond to propofol sensitively, a much more cautious control action will be preferred since aggressive propofol increase may drive blood pressures to an alarming level. Consequently, a multi-objective control strategy can potentially deliver a better anesthesia management. Some researchers have investigated the problems of multi-variable feedback control with applications in anesthesia [54, 55, 66, 67]. As a promising control strategy for regulation of anesthesia patient outcomes, model predictive control has been applied to regulate two patient outcomes simultaneously [67]. Most of the previous work has concentrated on population based models.

To understand the importance of the multi-objective anesthesia modeling and control, we make a comparison of control actions between the regulation of two patient outcomes (BIS and blood pressure) and the regulation of one patient outcome only. Figure 16 illustrates the simulation results which are produced by the MATLAB function "scmpc" in the model predictive control toolbox. Those data used for simulation are collected real-time patient data in operating rooms. We can see that the control actions (the propofol titration rate) are very different in the two cases.

The above discussions indicate that for enhanced anesthesia monitoring and control, it is necessary and beneficial to consider a patient as a multi-input-multi-output dynamic system whose characteristics change substantially among different patients and over different time intervals.
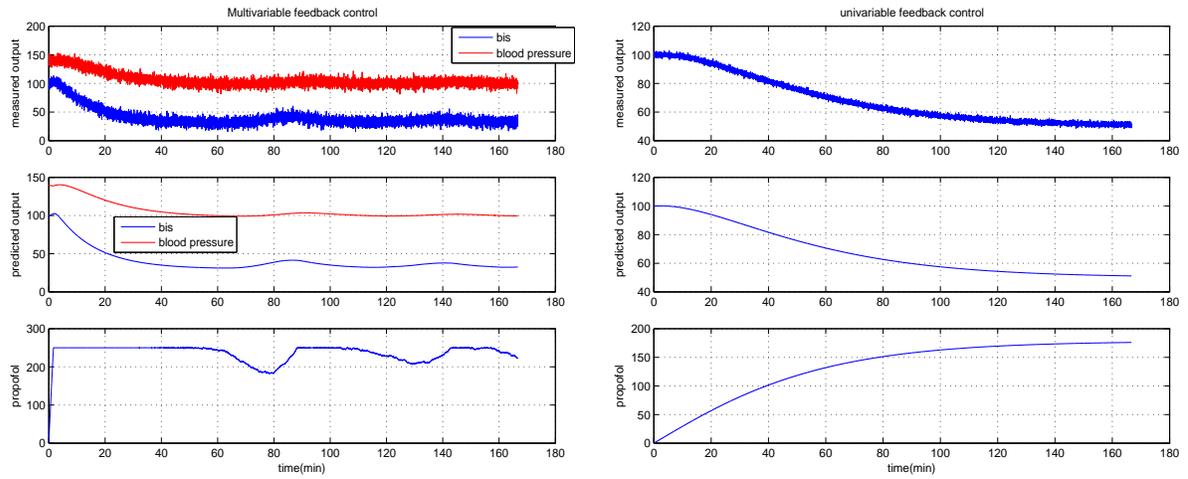
(a) Propofol control based on combined performance criterion on BIS and blood pressures

(b) Propofol control based on BIS only

Figure 16: Anesthesia managements differ when multiple outcomes are considered

3.3   MIMO Anesthesia Modeling and Diagnosis

3.3.1   Wiener Model Structure in Anesthesia Application

For the purpose of real-time prediction, diagnosis, and control, it is necessary to use a simple model structure without sacrificing much accuracy. A basic information-oriented model structure (a special case of Wiener models), for patient anesthesia depth responses to propofol infusion as an SISO system was introduced in [60, 61, 62]. This model can also be applied to relate other patient outcomes, such as blood pressure and heart rate, to input drugs. Its basic idea is summarized below.

The anesthesia drug propofol is administered by an infusion pump. The patient anesthesia depth is measured by BIS monitor. The dynamics of a patient's BIS response to a drug infusion can be divided into several blocks. The response from

the titration command to the drug infusion at the needle point is the infusion pump dynamics and can be represented by a transfer function $G_i(s)$. Similarly, the BIS monitor dynamics can be represented by a transfer function $G_m(s)$.

The patient dynamics is a nonlinear system. Although the actual physiological and pathological features of the patient require models of high complexity, for prediction or control purposes it is not only convenient but essential to use simple models as long as they are sufficiently rich to represent the most important properties of the patient response. Understanding the information used by anesthesiologists in infusion control, we characterize the patient response to propofol titration with three basic components: (1) Initial time delay τ_p after drug infusion: During this time interval after a change of the infusion rate, the BIS value does not change due to time required for drugs to reach the target tissues, to complete volume distribution. (2) Dynamic reaction: This reflects how fast the BIS value will change once it starts to respond, and is modeled by a transfer function $G_p(s)$. (3) A nonlinear static function for sensitivity of the patient to a drug dosage at steady state: This is represented by a function or a look-up table f. The meaning of these system blocks is illustrated in Figure 17. Combined with infusion pump and monitor models, this model structure for titration response is a special case of the Wiener models shown in Figure 18.

To establish patient models for monitoring and control, clinical data were collected. One of these data sets is used in this paper. The anesthesia process lasted about 76 minutes, starting from the initial drug administration and continuing until last dose of administration. Propofol was used in both titration and bolus. Fentanyl
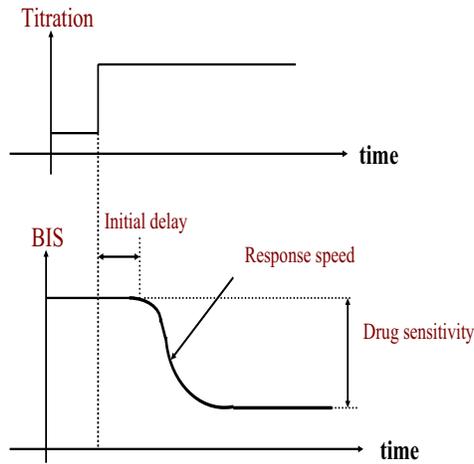
Figure 17: Simplified patient model structure

Wiener Model Structure
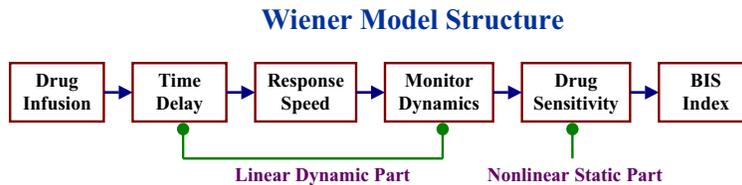
Figure 18: Wiener model structure

was injected in small bolus amount three times, two at the initial surgical preparation and one near incision. Analysis shows that the impact of Fentanyl on the BIS values is minimal. As a result, it is treated as a disturbance and not explicitly modeled in this example. The drug infusion was controlled manually by an experienced anesthesiologist. The trajectories of titration (in mcg/sec) and bolus injection (converted to mcg/sec) during the entire surgical procedure were recorded, which are shown together with the corresponding BIS values in Figure 20. The patient was given bolus injection twice to induce anesthesia, first at $t = 3$ minute with 20 mcg and then at $t = 5$ minute with 20 mcg. The surgical procedures were manually recorded. Three

major types of stimulation were identified: (1) During the initial drug administration (the first 6 minutes), due to set-up stimulation and patient nervousness. (2) Incision at $t = 45$ minute for about 5 minutes duration. (3) Closing near the end of the surgery at $t = 60$ minute.

The data from the first 30 minutes and in the interval where the bolus and stimulation impact is minimal (between $t = 10$ to $t = 30$ minutes)are used to determine model parameters and function forms. By optimized data fitting (least-squares) [58], we derive the estimated parameter values. For this data case, the patient sensitivity function shown in Figure 19 is close to a linear function. Under a sampling interval $T = 1$ second, which is the standard data transfer interval for the BIS monitor, the combined linear dynamics was estimated. The patient model with propofol infusion rate as the input and BIS measurement as the output was identified as

$$P(z) = \frac{0.01872z^2 - 0.08813z + 0.09016}{z^5 - 1.159z^4 + 0.7501z^3 - 0.5989z^2 + 0.2984z - 0.2678} \tag{3.1}$$

with sampling interval $T = 1$ second.
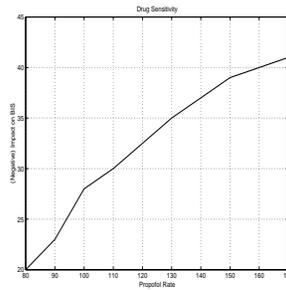
Figure 19: Drug sensitivity function (Titration)

The actual BIS response is then compared to the model response over the entire surgical procedure. Comparison results are demonstrated in Figure 20. Here, the

inputs of titration and bolus are the recorded real-time data. The model output represents the patient response very well. In particular, the model captures the key trends and magnitudes of the BIS variations in the surgical procedure. This indicates that the model structure contains sufficient freedom in representing the main features of the patient response.
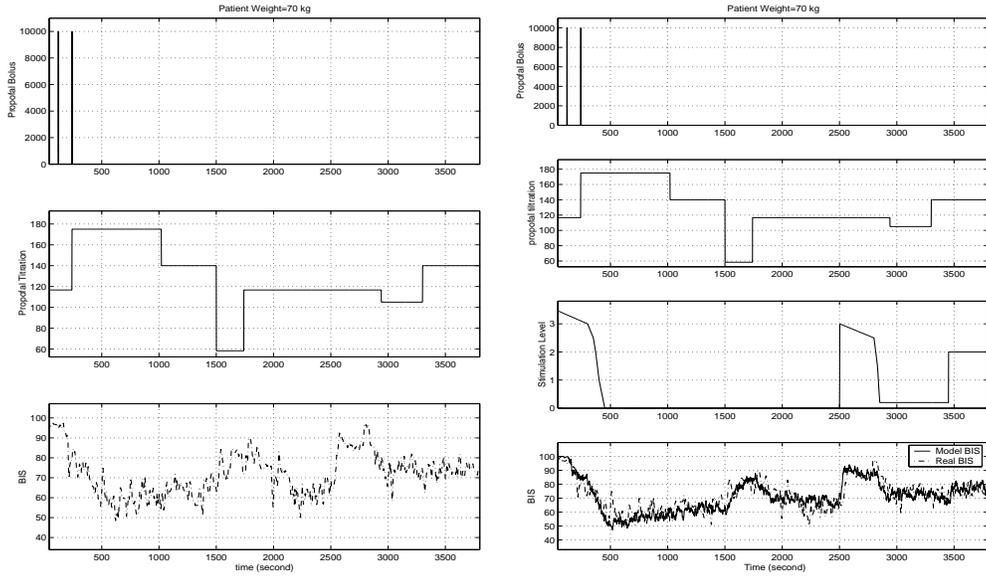
(a) Actual patient responses   (b) Patient model responses

Figure 20: Actual and model responses

The linear patient dynamics can be approximated by a simple system. The plant in this case is identified as a 5th order difference equation in (3.1). The system can be well approximated by a continuous-time system that consists of a pure time delay and a first-order dynamics, sampled with sampling interval $T = 1$ second. Let a continuous-time system be

$$P(s) = e^{-5s} \frac{0.93}{73s + 1}. \tag{3.2}$$

The step responses of the original system and the simplified system $P(s)$ are shown in Figure 21. Since this model contains only three parameters, it is much easier to be identified in real time.
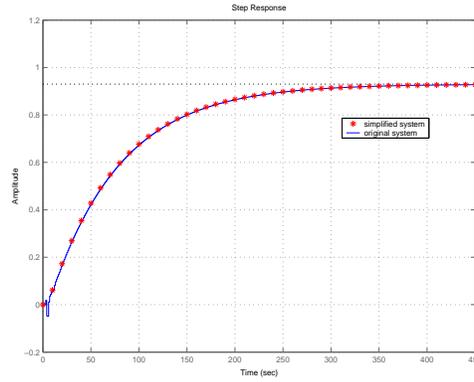
Figure 21: Step responses of the original system and the simplified system

It is also possible to use a simplified nonlinear function which has only three parameter r, α, b to represent the sensitivity function f:

$$y = r \left[u \pm \left(\frac{erf\left(\alpha u\right)}{erf\left(\alpha b\right)} - u \right) \right].$$

This function can be linear or nonlinear which is determined by the sign of $\pm$. Figure 22 shows an example of this function.

3.3.2 Extendsion to MIMO Anesthesia Modeling

Although in principle the SISO wiener model struture can be employed in MIMO models, by considering an m-input and n-output system as a collection of $m \times n$ subsystems, each of which represents one input and one outcome relationship. For example, if two drugs (propofol and fentanyl) are present and three outcomes (depth,
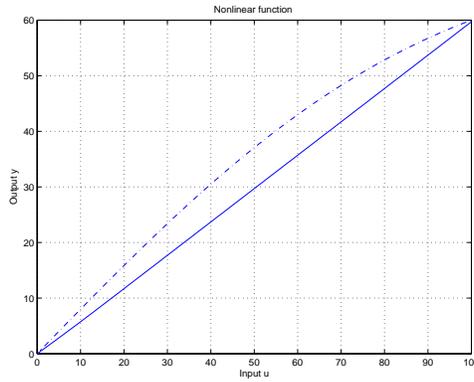
Figure 22: The sensitivity function is simplified by a nonlinear function which has three parameters: r, α, b. The sign of $\pm$ determines the function's shape.

blood pressures, and heart rates) are considered, we may view this as a collection of 6 subsystems, including propofol-to-depth, propofol-to-BP, propofol-to-HR, fentanyl-to-depth, fentanyl-to-BP, fentanyl-to-HR subsystems. This approach, however, involves many model parameters and encounters high system complexity in modeling processes. For example, if each submodel contains only L parameters, the over system will have $6L$ parameters that must be updated in real time, which is a substantial complexity in this application.

Modifications to the above approach are made to reduce modeling complexity by the following combination method. Since both propofol and fentanyl go through similar propagation and metabolism to influence blood pressure and heart rate, it is reasonable to use the same time delay and same dynamic response speed for both models. They, however, demonstrate very different sensitivity [65]. As a result, it is reasonable to use only one scaling factor to represent the difference between propofol and fentanyl in their impact on the blood pressure and heart rate. Furthermore,

fentanyl does not have influence on BIS index [65]. This method reduces significantly the number of model parameters. For example, if each model contains L parameters, in the case of two drugs and three outcomes, this method will reduce the number of parameters from $6L$ to $3L + 3$. For this application, we have $L = 11$ (8 parameters for the 5th order linear system and 3 for the nonlinear part) for the initial model structure; or $L = 6$ (6 parameters for the simplified delay system and 3 for the nonlinear part) after simplification. The above method of combining submodels can reduce model complexity from $6L = 66$ to $3L+3 = 36$ for the initial model structure; or from $6L = 36$ to $3L + 3 = 21$ for simplified delay systems. These complexity reductions are substantial in making real-time MIMO modeling a feasible option in anesthesia applications which are not data rich.

3.3.3 Multi-Objective Anesthesia Predictive Diagnosis

Here, we consider a special case that involves two outcomes: the anesthesia depth y_B and and mean blood pressure y_P. The continuous control is provided by propofol titration whose rate is denoted by u. Propofol or fentanyl bolus injections can be used when necessary to assist. Also, blood pressures may also be reduced by vasodilation agents or other means if necessary.

From a system viewpoint, we have a system with two types of control inputs: one main control variable u that is continuously managed, and another pulse types of control v that is used only when it is necessary. The system has two outputs y_B and y_P. The basic strategy is to use u to achieve control objectives as much as possible.

When u alone cannot achieve certain control objectives, v can be used to assist u to reach the goal.

This paper is focused on predictive diagnosis: (1) Given the current input u, what will be the outcomes in the near future? (2) If the input is changed to a new value, what will be the impact of this change? (3) If we want the outcomes to settle at a new level, will it be possible to achieve it with assistance from v?

The basic ideas and analysis are detailed in following. We first consider a patient whose BIS response to propofol titration rate u (mcg/kg/min) is modeled by

$$x_B = e^{-\tau_B s} \frac{K_B}{T_B s + 1} U(s); \quad y_B = 100 - f_B(x_B(t)) + d_B$$

where τ_B is the initial delay, K_B is the drug sensitivity, T_B represents the response speed of the patient, f_B is a nonlinear sensitivity function, and d_B is an external disturbance to the BIS value; and whose mean blood pressure response to propofol titration is represented by the simplified delay model

$$x_P = e^{-\tau_P s} \frac{K_P}{T_P s + 1} U(s); \quad y_P = 110 - f_P(x_P(t)) + d_P$$

where those parameters have the same meanings as in the BIS model.

We will use $w(t) = [y_B(t), y_P(t)]$ to represent the outputs. In real implementations of our prediction algorithms, the patient models will be generated in real-time, using actual input-output data. Here, for methodology description we use the above models to show how outcome prediction is performed.

Outcome Prediction

Suppose that the output vector $w(t)$ is initially at an equilibrium point with $w(t_0) = [y_B(t_0), y_P(t_0)]$ and input $u(t_0) = u_0$. When $u(t)$ is increased from u_0 to $u_0 + \Delta$, we may observe the outcome $w(t)$ starts to change due to this input jump. Outcome prediction shows how $w(t)$ will change in the near future and where it will settle to a new equilibrium. When the patient model is available, outcome prediction can be calculated from the model as follows.

From $x_B = e^{-\tau_B s} \frac{K_B}{T_B s + 1} U(s)$, we can derive the response $\widetilde{x}_B(t)$ to Δ jump at t_0 to be: $\widetilde{x}_B(t) = 0$, $t - t_0 \leq \tau_B$, and $\widetilde{x}_B(t) = K_B(1 - e^{-(t - t_0 - \tau_B)/T_B})\Delta$, $t - t_0 > \tau_B$. As a result, for $t > t_0$, we have

$$x_B(t) = x_B(t_0) + \widetilde{x}_B(t)$$

and

$$y_B(t) = 100 - f_B(x_B(t)) = 100 - f_B(x_B(t_0) + \widetilde{x}_B(t))$$

Furthermore, $y_B(t)$ will settle at the new equilibrium value $100 - f_B(x_B(t_0) + K_B\Delta)$. Following the same analysis, we have also

$$\widetilde{x}_P(t) = \begin{cases} 0, & t - t_0 \leq \tau_P \\ \\ K_P(1 - e^{-(t - t_0 - \tau_P)/T_P})\Delta, & t - t_0 > \tau_P. \end{cases}$$

As a result, for $t > t_0$, we have

$$x_P(t) = x_P(t_0) + \widetilde{x}_P(t)$$

and

$$y_P(t) = 110 - f_P(x_P(t)) = 110 - f_P(x_P(t_0) + \widetilde{x}_P(t))$$

and $y_P(t)$ will settle at the new equilibrium value $110 - f_P(x_P(t_0) + K_P\Delta)$.

The models will used in the following capacity to assist an anesthesiology to make decisions in anesthesia administration.

- **Drug Impact Prediction:** Drug impact prediction is an extension of outcome prediction. The outcome prediction provides the future outcome trajectories when one drug decision is made and implemented. Drug impact prediction is an assessment of future outcomes when several drug decisions are being considered. This prediction capability will allow an anesthesiologist to evaluate and decide the optimal choices.

- **Reachable Sets:** Suppose that the output vector $w(t)$ is initially at an equilibrium point $w(t_0) = w_0$. The question here is to determine if the propofol titration control alone is sufficient to achieve a designated target w_f. If the answer is affirmative, then assistance from v is not needed. Otherwise, v must be used such that after applying a bolus injection v, w_f becomes reachable. The reachable set of the outputs under one drug actions will exhaust all possible values of that drug and determine the set of the outputs that can be reached. If the desired outputs are outside of this reachable set, the second drug, in our case it is either the fentanyl bolus or propofol bolus, must be used so that the new reachable set will contain the desired output values.

3.3.4 Results

To demonstrate our ideas presented in the previous sections, clinical data were collected and analyzed, as detailed in Section 3.3.3. One of the case data sets, shown in Figure 13, is used here. The three inputs include propofol titration, propofol bolus injection, fentanyl bolus injection. The two outputs are the BIS index and MAP. Since fentanyl bolus has very small impact on the BIS index, we neglect the submodel from the fentanyl bolus to the BIS index. As a result, there are a total of 5 submodels: propofol titration to BIS and MAP, propofol bolus to BIS and MAP, and fentanyl bolus to MAP.

The patient data are used to identify these models, with the identified model listed below.

1. **BIS to propofol titration:** $x_B(s) = e^{-3s}\frac{0.0163}{46s+1}U(s)$,

$$y_B(t) = 100 - 9 * (x_B(t) - (erf(0.4 * x_B(t)) - x_B(t)))$$

2. **BIS to propofol bolus:** $y_B(s) = 100 - e^{-15s}\frac{200}{2000s+1}U(s)$

3. **MAP to propofol titration:** $y_P(s) = 110 - e^{-250s}\frac{0.1}{200s+1}U(s)$

4. **MAP to propofol bolus:** $y_P(s) = 110 - e^{-25s}\frac{42}{4000s+1}U(s)$

5. **MAP to fentanyl bolus:** $y_P(s) = 110 - e^{-100s}\frac{80}{4000s+1}U(s)$

Figure 23 illustrates the identified model outputs with the real patient outcomes. The models capture the main trends of the BIS and MAP quite well. We should emphasize that this is achieved with a very low model complexity. This trend information

will be similar to what an anesthesiologist usually requires in making anesthesia drug
administration decisions.
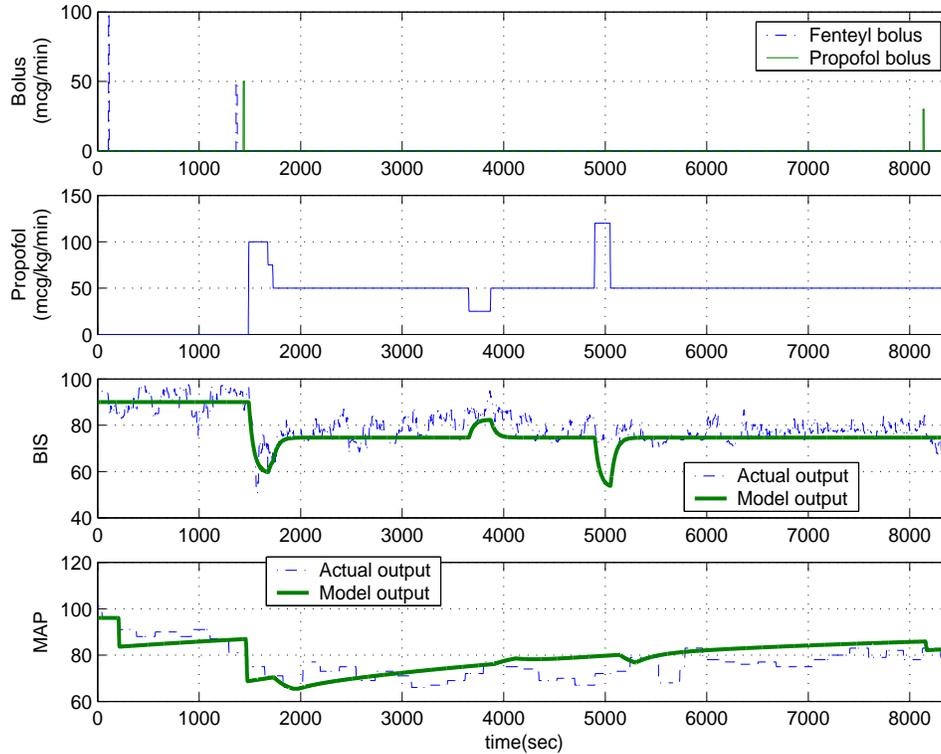
Figure 23: Multi-input-multi-output patient model

The models can be used for drug impact prediction. For example, suppose the
propofol rate is increased by 30 mcg/min at $t_0 = 80$ second. Figure 24 shows how this
drug infusion rate change will affect the BIS value and MAP. In any time instant, to
provide decision assistance to an anesthesiologist, different drug infusion strategies
can be considered and their impact on the outputs can be plotted to evaluate and
compare consequences of such actions in the near future. For example, to understand
drug impacts prediction of increasing propofol rates by $10, 20, 30, 40, 50$, we may plot
all these cases simultaneously. These impact predictions are plotted in Figure 25.
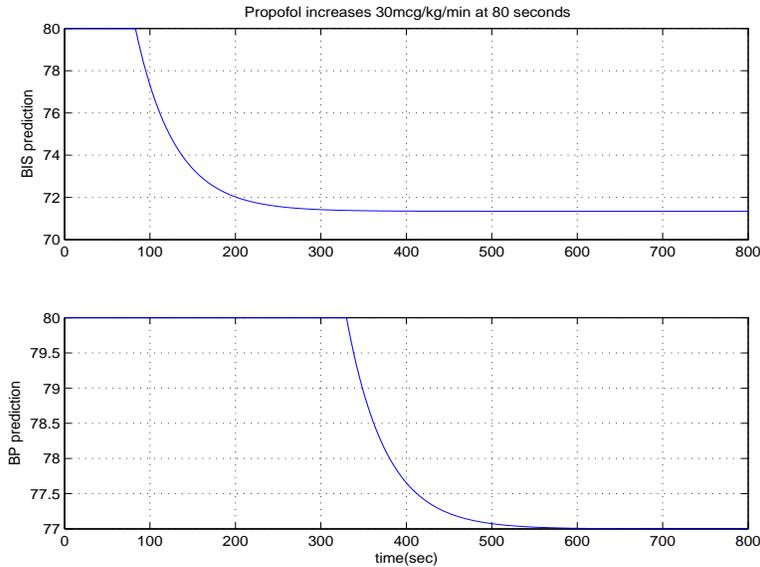
Figure 24: Outcome predictions

To study the reachable sets, suppose at a given time the BIS index is 70 and the MAP is 80 mmHg. Figure 26 shows all potential patient steady-state outcome sets when various drugs are administrated. From Figure 26, we can see that different designated targets can be achieved through administrating different drugs. For Example, if we want to depress the patient blood pressure without changing BIS values, then only fentanyl bolus is needed. But, if we want to push the BIS value to a low level of 60 without much effect on blood pressures (mean arterial pressure of 80 mmHg is usually the desired level during anesthesia), then it will be better to use propofol bolus than propofol titration. This is reflected in the reachable set of propofol bolus that has less impact on the MAP. We should also point out that one may also use propofol bolus with a reduced propofol titration to actually keeps MAP unchanged.
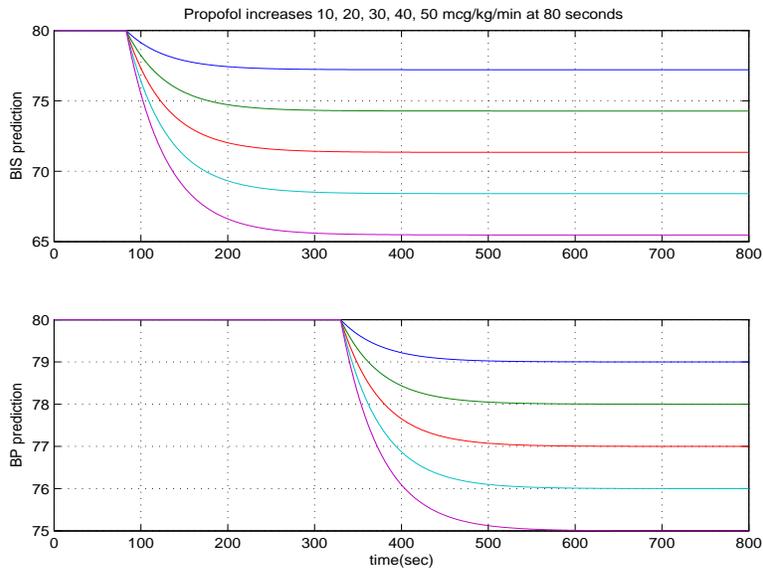
Figure 25: Drug impact prediction

3.4   Device Development for Anesthesia Depth Predication

In this section, the introduced model structure 3.3.1 was implemented in device

level to benifit anesthesia patients management. With this device, anesthesiologists

can monitor the futu   S at the same time.

Here, the technical de   n device were demon-
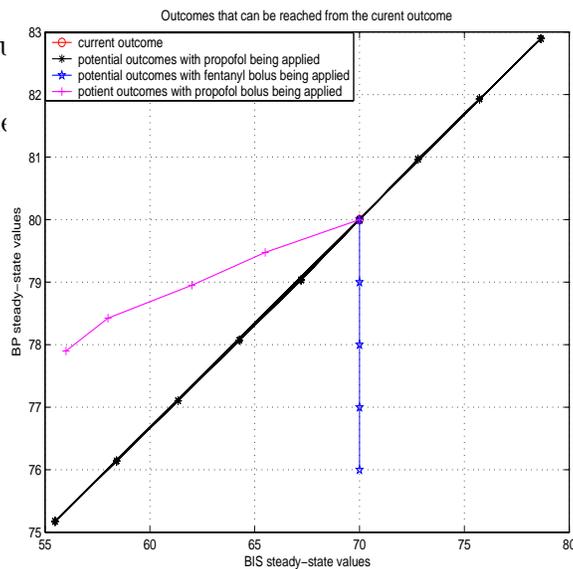
Figure 26: Reachable outcomes from the current outcome with different drugs inputs

strated. With this device, the model parameters is indentified online through a embeded method in [62]. This device has been tested in operation room for real-time anesthesia depth prediction.

3.4.1 Implementation Diagram and Hardware Setup

The complete BIS prediction system diagram is shown in Figure 27. This system is composed of four components: BIS sensor, BIS monitor, RS232 to USB converter and a Laptop.
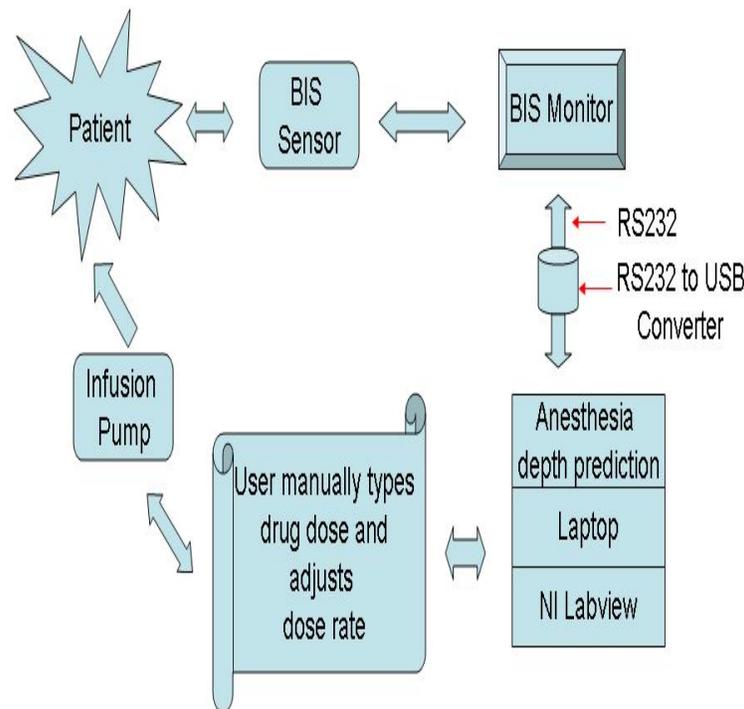
Figure 27: BIS prediction system diagram

The hardware setup is shown in Figure 28.

A BIS sensor is attached on the forehead of an anesthesia patient, then in turn

Figure 28: BIS prediction system hardware setup

connected with a BIS monitor. EEG signals were collected and send to BIS monitor for processing and producing BIS index. BIS data is transmitted to the laptop through a RS232 to USB standard converter which connects the RS232 output port of BIS monitor with the Laptop. Other input data including drug titration rate, bolus, and stimulations are manually typed into the frontal panel of the software. The indentification and prediction algorithm is implemented through Labview graphical programing language(Version 7.1, Natioanl Instrument Inc.) and run on a IBM laptop.

3.4.2 Requirement Analysis and Development Tool (IDE) Selection

In this software implemetation, our software need to do the following tasks simutaniously in real time: 1) communication with BIS monitor and DAQ to get data; 2) Process data and do model-based prediction; 3) Output and display result on user interface. More over, this project has urgent time requirement which leave us quite

short time for development. Based on these reasons, we choose National Instruments (NI) LabVIEW as our software development tool. The NI LabVIEW has several advantages which matches our development requirements:

- Fast implementation

- Excellent hardware support for NI hardware, standard interfaces, and third-party hardwares which will make our software has good extendability for integrating/fusion data from and control signal to other devices (such as drug pump, other medical devices,etc) in the future.

- Simple implementation of user interface development

In this project, we spent just two weeks to complete this simple version and tested it. The total development (two versions development, debugging, and validation in clinic room) time is two months. In the following two sections, we will describe the software in more details.

3.4.3 User Interface

Figure 29 and Figure 30 show the user interfaces of the simple version and the complete version of our anesthesia depth prediction software respectively.

In the user interface of the complete version, three more display windows including EEG signal, as well as heart and lung sound signal display windows are added for comprehensive diagnosing purpose.
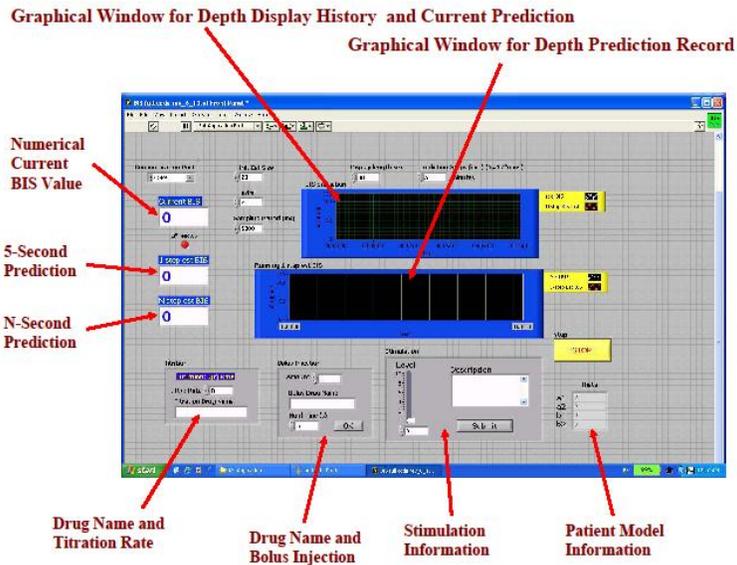
Figure 29: Front panel of the simple version system
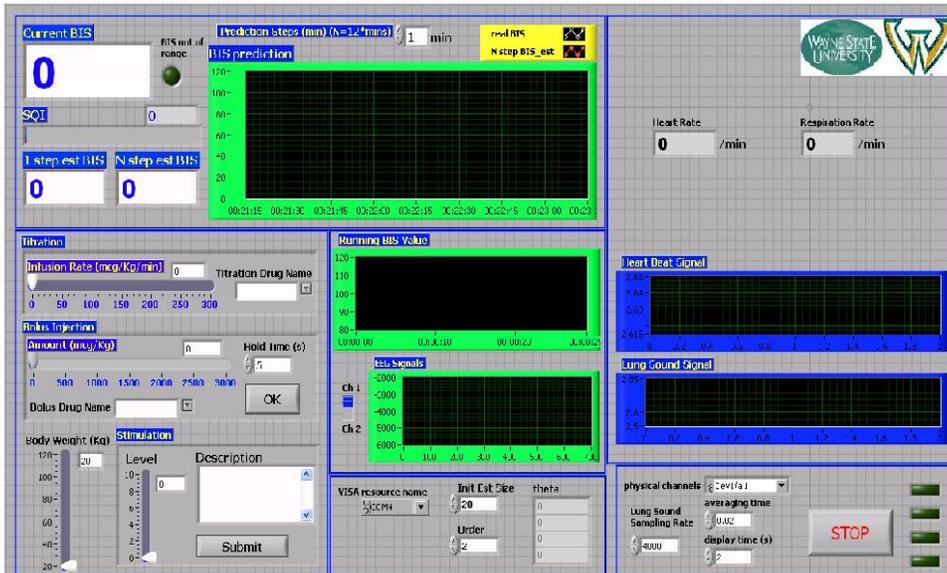
Figure 30: Front panel of the complete version system

3.4.4 Code Implementation

Since NI LabVIEW is a graphical programming languange and the code execution is data-flow driven (another example is Mathworks Simulink) and the code is straitforwad for viewing and reading. Figure 31 and Figure 32 illustrates our code implementation for the simple and complete version respectively.
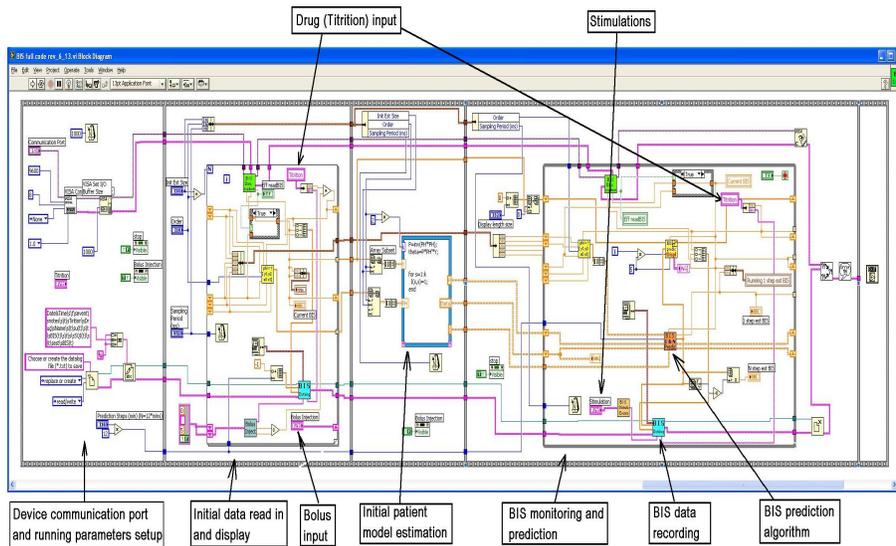
Figure 31: Block diagram of the simple version system

From the program block diagram, we can see this code is running sequencially.

1. The first section is communication port setup and running parameters initialization. The commnication port setup let user select the COM port they are using to connect with the BIS monitor. And setup the communication protocal and data transfer rate. The runnig parameters initialization includes setting the prediction steps and sampling rate, as well as data recording settings.

Figure 32: Block diagram of the complete version system

2. The second section is initial data logging. This initial data (usually 20 sample points) are used for the inital patient model estimation in section 3.

3. Initial patient model estimation.

4. The last and the major section is the BIS prediction section. After estimation of the initial patient model, we can run the BIS prediction. In this block diagram, the BIS prediction algorithm is represented by a subVI, which is implemented in MATLAB and embbed into the LabVIEW execution. Thanks to the Matlab script functionality of LabVIEW, which makes it possible to implement complex algorithms in Matlab and use them in LabVIEW. This let the user can combine

the advantages of both tools.

3.4.5 Results

This system has been studied on five patients at the Detroit Medical Center with varying age, body mass index, coexisting disease and drug responses. This case report shows the 60 second BIS prediction of one of the patient.

Propofol is used as the sole anesthetic drug throughout the procedure. Anesthesia was provided manually by an anesthesia resident and lasted about 76 minutes starting from the initial drug administration until the last dose of administration. A prototype of the Anesthesia Depth Prediction System (ADPS) is used for anesthesia depth prediction. BIS monitor measurements are sent to the ADPS in real time, which are then used to generate the patient model.

Figure 33 illustrates all the predicted BIS values at a time point. Here all BIS values in the future 300 seconds are predicted. The comparison between real BIS and predicted BIS in front of 60 seconds is shown in Figure 34. We can see from this figure that the predicted BIS catches the variation of the real BIS very well.

3.5 Conclusions

This chapter investigates the problem of real-time monitoring, diagnosing, and predicting multiple outcomes of anesthesia patients. For the enhanced anesthesia management, it is essential to view the anesthesia patient dynamics as a multi-input (multi drugs) and multi-output (multi outcomes) system. For predictive diagnosis and
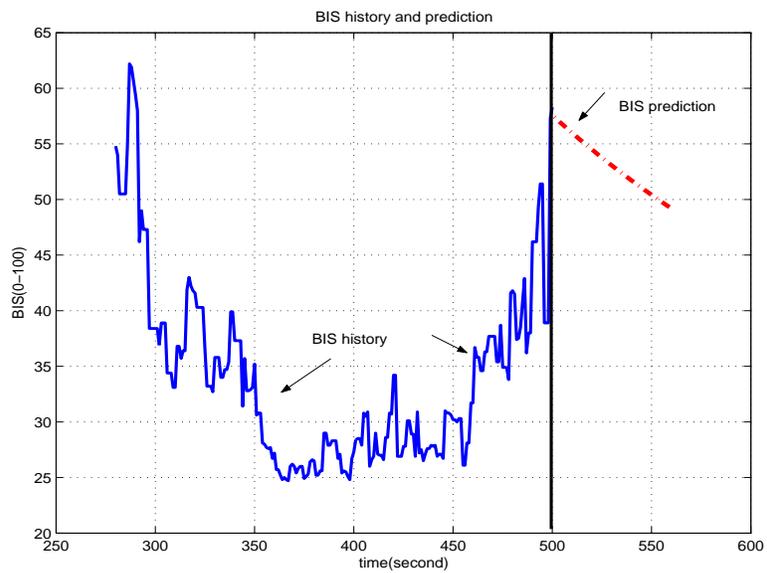
Figure 33: BIS prediction
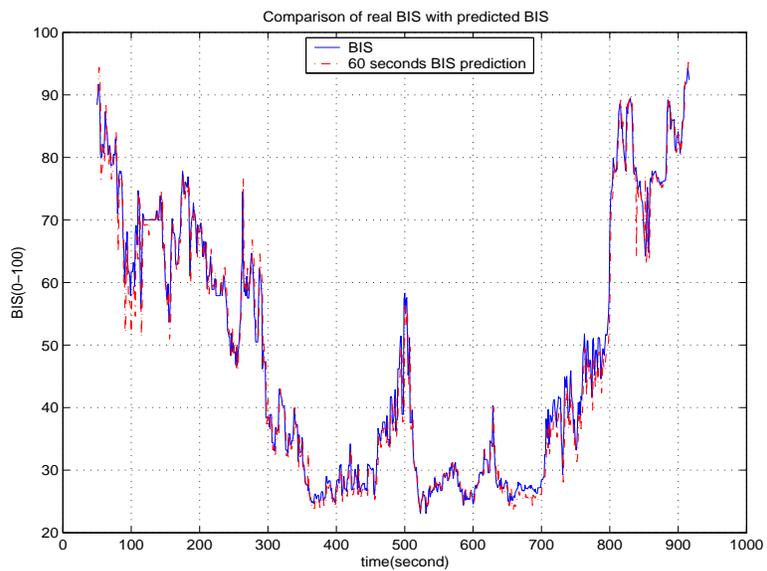
Figure 34: Comparison between real BIS and predicted BIS

decision assistance, a simplified Wiener model structure is introduced and studied for

its suitability in representing the patient responses to drug infusion. Furthermore, a

method of consolidating submodels is introduced which can significantly reduce the

total number of MIMO system parameters. The identified models are shown to have significant utility in anesthesia decision assistance, by developing outcome impact analysis and reachable sets. In addition, we discussed the development of BIS prediction system with details in hardware setup and software implementation. Labview programing languange is a wonderful tool for medical device implementation because of its characteristics of graphical programing and friendly user interface design. This developed BIS prediction system is tested in operation room and our results show that this system is competent for anesthesia depth predition. As we presented before, anesthesia problem is actually a multi-input-multi-output problem, MIMO modeling and multi-outcome diagnosis are necessary for enhenced the anesthesia management. In future work, I will consider to upgrade this system to a MIMO identification and prediction system.

CHAPTER 4: ANESTHESIA CONTROL IN WIRELESS CONNECTED SYSTEMS

In this chapter, I investigated the impact of noise and signal averaging on patient control in anesthesia applications, especially in networked control system settings such as wireless connected systems, sensor networks, local area networks, or tele-medicine over a wide area network.

4.1   Problem Statement

While anesthesia patient vital signs such as anesthesia depth index, blood pressure, heart rate etc. are trasmitted through a noisy wireless channel in a wide area, those trasmitted signals will be corrupted by the transmission noise. To improve the accuracy of the received signals, it is necessary to reduce the noise effect as much as possible. It is well understood that within most algorithms that reduce effects of random noises on signals and systems, some types of signal averaging are used [69, 68]. This is mainly because the laws of large numbers and central limit theorems provide a foundation for noise reduction. The rationale is that when averaging is applied, noises diminish in an appropriate sense. This fundamental understanding leads to algorithms in filtering, signal reconstruction, state estimation, parameter estimation, system identification, and stochastic control. On the other hand, signal averaging introduces dynamic delays. While feedback control is intended, such delays will have detrimental effects on closed-loop systems, even destabilizing the system.

Consequently, signal averaging encounters a fundamental performance limitation in feedback systems. Performance and stability analysis are needed for this closed-loop system with averaging filter. To explain this phenomenon, we analyze stability margins under signal averaging and derive some optimal strategies for selecting window sizes. We will use a typical anesthesia control problem to understand impact of communication channels and utility of signal averaging on anesthesia monitoring and control.

4.2 Signal Averaging and Control Performance

4.2.1 Signal averaging

There are different window functions for signal averaging, such as uniform windows, exponential windows, etc. They are different only in their forms, but most conclusions for system analysis or error bounds are usually valid for all window types. As a result, we shall use the exponential windows to carry out our analysis. A signal averaging by exponential decaying weighting of rate $0 < \alpha < 1$ is

$$h_k = (1 - \alpha) \sum_{i=-\infty}^{k} \alpha^{k-i} x_i \tag{4.3}$$

whose transfer function is

$$F_\alpha(z) = \frac{(1 - \alpha)z}{z - \alpha}. \tag{4.4}$$

4.2.2 Open-Loop Systems and Closed-Loop Systems

In wireless-based monitoring and diagnosis applications, the system is running in open-loop. In this case quantization errors and communication noises can be grouped as an additive noise to the patient output y. When signal averaging is applied to reduce noise effects, the resulting system can be represented by the block diagram in Figure 35.
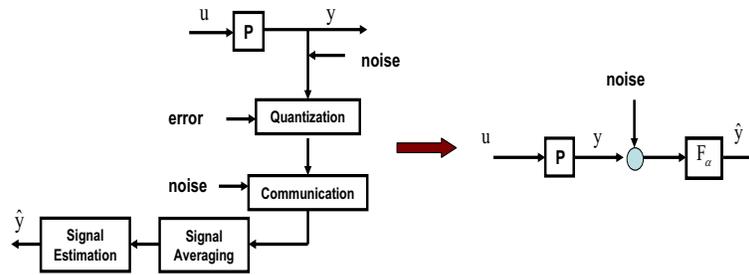
Figure 35: Signal filtering in open-loop systems

Figure 36 illustrates impact of filtering on open loop systems. In open loop applications, filtering will not de-stabilize the system. Consequently, one may choose a window of long horizon to reduce the effects of noise. It is apparent that the longer the averaging window, the less the noise effect on the signal. However, it is also observed that signal averaging slows down system's response to the input. In other words, filtering introduces a dynamic delay. This delay has very important implication in the closed-loop applications.

On the other hand, if feedback control for anesthesia management decisions are intended, signal filtering becomes part of a closed-loop system. When signal averaging is applied, the averaging filter F_α is inserted into the system, resulting in a modified
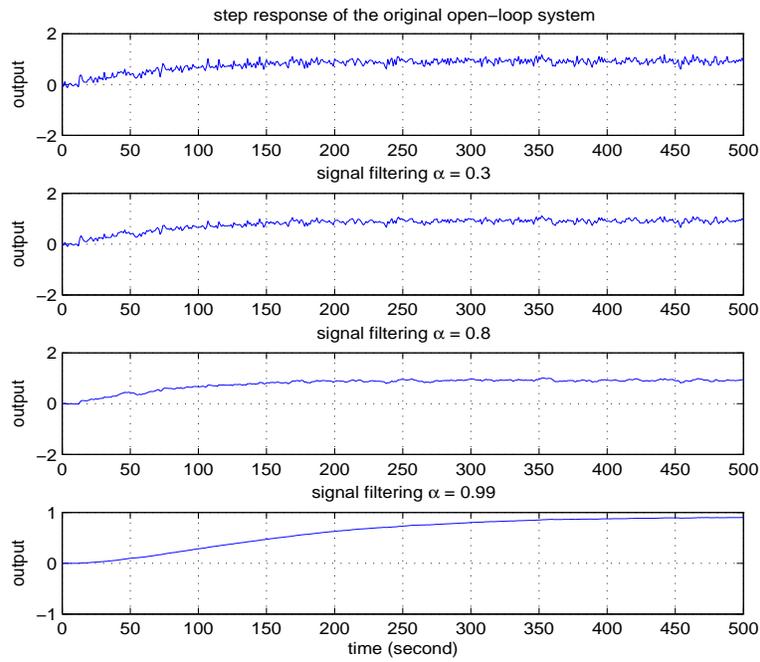
Figure 36: Effects of signal averaging on open-loop systems

closed-loop system shown in Figure 37.
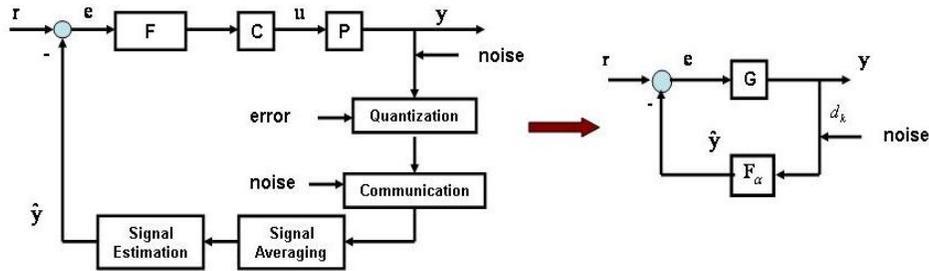
Figure 37: System modules and their equivalent representation

The close-loop system equations are:

$$y_k = Ge_k, \quad e_k = r_k - F_\alpha(y_k + d_k). \tag{4.5}$$

Then

$$y_k = Gr_k - GF_\alpha y_k - GF_\alpha d_k,$$

and

$$y_k = H_r r_k + H_\alpha d_k \qquad (4.6)$$

where,

$$H_r = \frac{G}{1 + F_\alpha G}; \quad H_\alpha = \frac{-F_\alpha G}{1 + F_\alpha G}. \qquad (4.7)$$

Figure 38 illustrates impact of filtering on closed loop systems. Although signal filtering can reduce the noise effect of the signal, it introduces a dynamic delay which has detrimental effects on the closed-loop system. The plots confirm that when filtering window is long the filter can destabilize the closed-loop system. Even when the filtering window size is small, its effectiveness is not very obvious. This example suggests that in closed-loop applications, signal filtering has limited effectiveness. This understanding will be used to introduce new methods to reduce noise effects in such applications.

4.3 Analysis of Stability and Performance

4.3.1 Feedback Robustness against Signal Averaging

Definition 1 *The stability margin against exponential averaging, abbreviated as α-margin and denoted by $\alpha_{max}(G)$, is the largest $0 \leq \alpha \leq 1$ such that for all $0 \leq \alpha < \alpha_{max}(G)$, the close-loop system (4.6) is stable and the system is unstable if $\alpha > \alpha_{max}(G)$. If the close-loop system is stable for all α, we denote $\alpha_{max}(G) = 1$.*
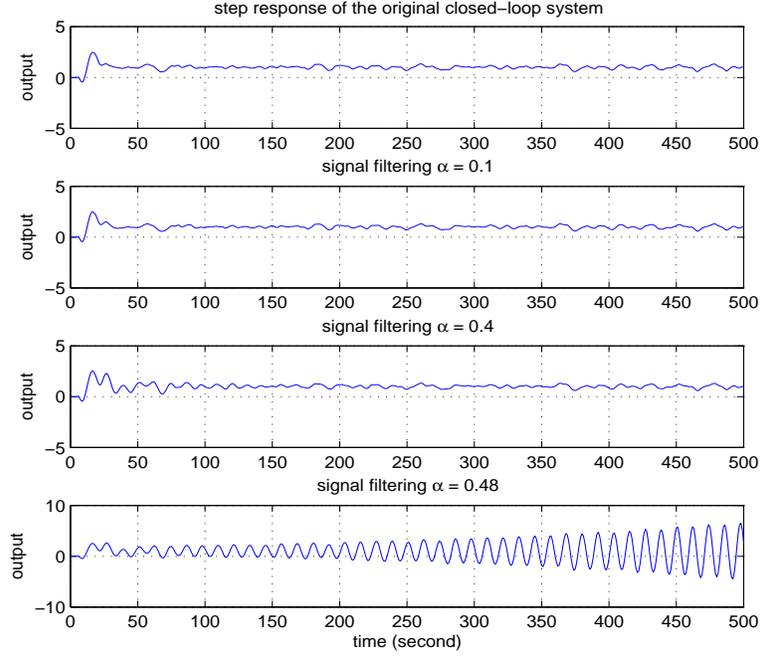
Figure 38: Effects of signal averaging on closed-loop systems

4.3.2 Discrete and Continuous Time Averaging

Suppose that the input to the filter is a noise corrupted constant

$$x_k = \theta + d_k.$$

An exponential window of rate $0 < \alpha < 1$ is applied to this signal and its output is

$$h_k = (1 - \alpha) \sum_{i=-\infty}^{k} \alpha^{k-i} x_i = \theta + (1 - \alpha) \sum_{i=-\infty}^{k} \alpha^{k-i} d_i = \theta + \varepsilon_k,$$

where

$$\varepsilon_k = (1 - \alpha) \sum_{i=-\infty}^{k} \alpha^{k-i} d_i.$$

If d_i is i.i.d. (independent and identically distributed) with $E d_i = 0$ and $E d_i^2 = \sigma^2$, then $E \varepsilon_k^2 = 0$ and

$$E \varepsilon_k^2 = \frac{1 - \alpha}{1 + \alpha} \sigma^2.$$

Consequently, using h_k as an estimate of θ can reduce errors by $\frac{1-\alpha}{1+\alpha}$. We will call α as the decaying rate. Convergence (in the mean square sense) is achieved when $\alpha \to 1$:

$\lim_{\alpha \to 1} E\varepsilon_k^2 = 0$.

Consider an exponential filter

$$F(s) = \frac{1}{\lambda s + 1} \tag{4.8}$$

whose impulse response is

$$f(t) = \frac{1}{\lambda} e^{-t/\lambda}, \ t \geq 0. \tag{4.9}$$

Note that

$$\int_0^\infty f(t)dt = 1.$$

Now,the input-output relationship of this filter is

$$y(t) \ = \int_{-\infty}^t f(t - \tau)x(\tau)d\tau$$

$$= \frac{1}{\lambda} \int_{-\infty}^t e^{-(t-\tau)/\lambda}x(\tau)d\tau.$$

When the signals are sampled with sampling interval T, we denote $x_k = x(kT)$ and $y_k = y(kT)$. If α is related to λ and T by $\alpha = e^{-T/\lambda}$, we have

$$\lim_{T \to 0} \frac{T}{\lambda(1 - \alpha)} = 1.$$

For small T, $y(t)$ is approximated by

$$y_k = y(kT)$$

$$= \frac{1}{\lambda} \int_{-\infty}^{t} e^{-(t-\tau)/\lambda} x(\tau) d\tau$$

$$\approx \frac{T}{\lambda} \sum_{i=-\infty}^{k} (e^{-T/\lambda})^{k-i} x_i$$

$$= \frac{T}{\lambda(1-\alpha)} (1-\alpha) \sum_{i=-\infty}^{k} \alpha^{k-i} x_i$$

$$\approx (1-\alpha) \sum_{i=-\infty}^{k} \alpha^{k-i} x_i.$$

In other words, for system analysis, we may approximate the discrete-time filter in (4.3) by its continuous-time counterpart in (4.8). These relationships between discrete-time averaging and continuous time averaging will be used to derive stability margins.

4.3.3 Stability Margin Against Exponential Averaging

The relationship between α and λ will allow us to focus on stability analysis in continuous time systems and then transform the results to the discrete-time filters. This is stated in the following theorem.

Theorem 2 *If the exponential stability margin in the continuous-time domain is* λ_{max}, *then*

$$\lim_{T \to 0} \frac{T}{-\ln \alpha_{max}} = \lambda_{max}.$$

Proof: This follows from the relationship

$$\alpha = e^{-T/\lambda}.$$

$\square$

We now concentrate on calculation of λ_{max}.

Definition 3 *The stability margin against exponential averaging for the continuous-time closed-loop system, abbreviated as continuous exponential A-margin and denoted by $\lambda_{max}(G)$, is the smallest $\lambda > 0$ under which the closed-loop system becomes unstable. If the closed-loop system remains stable for all $\lambda > 0$, we denote $\lambda_{max}(G) = \infty$.*

Suppose $G(s) = N(s)/D(s)$ where $n(s)$ and $d(s)$ are polynomial functions of s and coprime (that is, $N(s)$ and $D(s)$ do not have common zeros). Then λ_{max} is the largest $\lambda > 0$ before the closed-loop system becomes unstable. Consider the characteristic equation of the closed-loop system

$$1 + F_\lambda(s)G(s) = 1 + \frac{1}{\lambda s + 1}\frac{N(s)}{D(s)} = 0$$

or

$$\lambda s D(s) + D(s) + N(s) = 0 \tag{4.10}$$

which leads to

$$1 + \lambda\frac{sD(s)}{D(s) + N(s)} = 0. \tag{4.11}$$

This expression leads to the following conclusion.

Theorem 4 *The exponential A-margin $\lambda_{max}(G)$ of $G(s)$ is the gain margin of*

$$H(s) = \frac{sD(s)}{D(s) + N(s)}. \tag{4.12}$$

We make several interesting observations from (4.11). First,from (4.10), λ_{max} may be calculated by using the Routh-Hurwitz test. Second, (4.11) is in a standard form for using root locus technique. So, we may plot the root locus of the system (4.12) (it is an improper system) and detect the λ value that reaches marginal stability, which will be λ_{max}. The root locus plot starts at the poles of system (4.12) which are precisely the poles of the closed-loop system without the averaging filter. Since the closed-loop system is stable, for small λ the closed-loop system with the filter will remain stable. The root locus plot moves towards the zeros of system (4.12) which are the poles of the open-loop system. Hence, if the open-loop system is unstable, the exponential A-margin is always finite.

Example 5 Suppose $G(s) = (s + 2)/(s - 1)$. Then,

$$H(s) = \frac{sD(s)}{D(s) + N(s)} = \frac{s^2 - s}{2s + 1}.$$

The gain margin can be obtained by using the Matlab function "margin" (which gives $\lambda_{max} = 2$) or by plotting the bode plot as shown in Figure 39 which gives $\lambda_{max} = 6.02$ dB $= 2$. Alternatively, from

$$(2s + 1) + \lambda(s^2 - s) = \lambda s^2 + (2 - \lambda)s + 1 = 0,$$

we can calculate $\lambda_{max} = 2$ by the Routh-Hurwitz method.
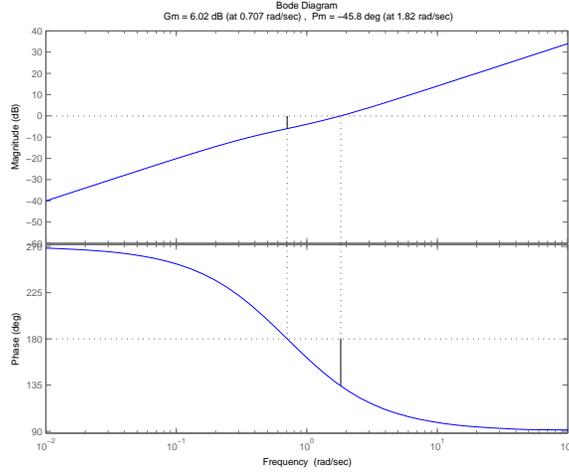
Figure 39: Using bode plots to obtain the gain margin.

4.3.4 Performance Analysis

Within the A-margin, what is the benefit of signal averaging? On one hand, signal averaging can reduce noise effect. On the other hand, averaging introduces delays and reduces closed-loop system performance. Consequently, an optimal choice of averaging becomes an issue.

Similarly, the continuous time close-loop system equations are:

$$y = \frac{G}{1 + F_\lambda G} r - \frac{F_\lambda G}{1 + F_\lambda G} d \tag{4.13}$$

Here,we denote

$$H_\lambda = \frac{-F_\lambda G}{1 + F_\lambda G} \tag{4.14}$$

If d is a white noise, noise attenuation aims to reduce the L^2 norm of H_λ. Naturally, for optimal noise reduction, we should select

$$\eta = \inf_{0 < \lambda < \lambda_{max}} \|H_\lambda\|_2 \,. \tag{4.15}$$

Example 6 For the system in Example 5, when λ takes values $0, 0.1, \ldots, 0.9$, the corresponding H^2 norms for the closed-loop system H_λ are

λ	0	0.1	0.2	0.3	0.4	0.5	0.6	0.7	0.8	0.9
η	6.22	7.00	7.87	9.00	10.49	12.59	15.73	20.96	31.44	62.85

The monotone increase of the L^2 norms indicates that for this system, averaging cannot reduce noise impact on the output. As a result, there should be no averaging for this system.

Example 7 For another example, consider a system

$$G(s) = \frac{s^2 + 2s - 1}{s^2 - s + 4}$$

The closed-loop system's characteristic equation is

$$\lambda s D(s) + D(s) + N(s) = \lambda s^3 + (2 - \lambda)s^2 + (1 + 4\lambda)s + 3 = 0.$$

It can be calculated by the Routh-Hurwitz method that $\lambda_{max} = 1.366$. The H^2 norm of H_λ as a function of λ is plotted in Figure 40. The optimal averaging occurs at $\lambda = 0.59$ with the norm $\|H_{0.59}\|_2 = 2.5263$.

From the relationship $\alpha = e^{-T/\lambda}$, for small sampling interval T,

$$\alpha = e^{-T/\lambda} = e^{-T/0.59} = e^{-1.7T}$$

is the optimal rate for averaging in the discrete-time domain. For example, if $T = 0.01$, we obtain $\alpha = 0.983$.
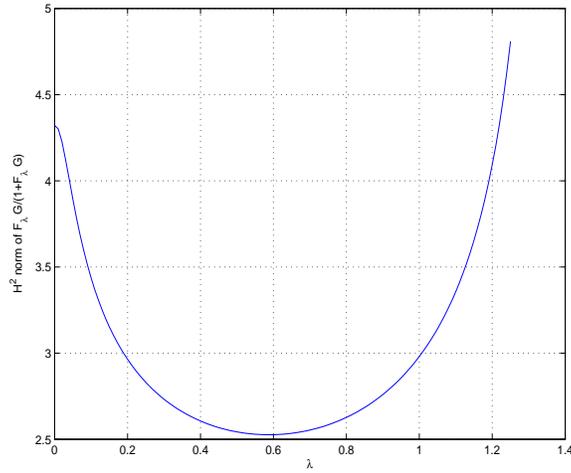
Figure 40: Optimal averaging rate

4.3.5 Fast Sampling for Disturbance Attenuation

Although the optimal L^2 performance η in (4.15) cannot be improved for the continuous-time system, noise attenuation in the sampled system can be further improved.

We first establish a relationship between the L^2 norm of the continuous-time system and the l^2 norm of its sampled system. Suppose that the disturbance sequence d_k passes through a ZOH of interval T to become $d(t)$. The continuous-time system H is stable with impulse response $g(t)$. Then,

$$y(t) = \int_0^t h(t - \tau)d(\tau)d\tau.$$

Suppose d_k is a pulse sequence, $d_0 = 1$, and $d_k = 0$, $k \neq 0$. Then, $d(t) = 1$, $0 \leq t < T$, and $d(t) = 0$, otherwise. Under this input

$$y(t) = \int_0^T h(t - \tau)d\tau.$$

Hence, the sampled values of $y(t)$, which form the pulse response of the sampled system, become

$$y_k = y(KT) = \int_0^T h(kT - \tau)d\tau.$$

For small T this can be approximated by

$$y_k = Tg(kT).$$

We note that for small T,

$$\|H\|_2^2 = \int_0^\infty h^2(t)dt \approx T\sum_{k=0}^\infty h^2(kT).$$

Consequently, if we use $\widetilde{H}$ and $\widetilde{h}_k$ to denote the sampled system and its pulse response of the continuous-time system H, we have $\widetilde{h}_k = Th(kT)$ and

$$\|\widetilde{H}\|_2^2 = \|\widetilde{h}_k\|_2^2 = T^2 \sum_{k=0}^\infty h^2(kT) = T\|H\|_2^2$$

From

$$y_k = \sum_{i=0}^k \widetilde{h}_{k-i}d_i$$

if d_k is i.i.d., mean zero and variance σ^2, then

$$\sigma_k^2 \;=\; Ey_k^2$$

$$= \sum_{i=0}^{k} \sum_{j=0}^{k} \widetilde{h}_{k-i} E d_i d_j \widetilde{h}_{k-j}$$

$$= \sigma^2 \sum_{i=0}^{k} \widetilde{h}_{k-i}^2$$

$$\leq \sigma^2 \|\widetilde{h}_k\|_2^2$$

$$= \sigma^2 T \|H\|_2^2$$

In fact,

$$\sigma_{max}^2 = \sup_k \sigma_k^2 \approx \sigma^2 T \|H\|_2^2.$$

If $\|H\|_2^2$ is optimized, then $\|H\|_2^2 = \eta^2$ as in (4.15). Consequently, the noise reduction

ratio can be expressed as

$$\widetilde{\eta}^2 = T\eta^2. \tag{4.16}$$

This is a relationship between noise reduction in the sampled system and the optimal

L^2 norm of the continuous-time system. This analysis concludes that using faster

sampling (smaller T) can reduce the noise effects.

4.4 Results

Consider the identified patient model in section 3.3.1 with BIS as model output and propofol titration rate as input:

$$P(z) = \frac{0.01872z^2 - 0.08813z + 0.09016}{z^5 - 1.159z^4 + 0.7501z^3 - 0.5989z^2 + 0.2984z - 0.2678}$$

The sampling rate of BIS machine is $T = 1$ second.

Usually to eliminate steady-state error in tracking control, an integrator is inserted into the system

$$C(z) = \frac{1}{z - 1}.$$

A stabilizing feedback controller is then designed for the patient model (3.1) by using a full-order observer and pole placement design, leading to

$$F(z) = \frac{1.234z^5 + 0.6298z^4 - 3.644z^3 + 3.67z^2 - 1.981z + 0.2479}{z^6 - 2.341z^5 + 2.284z^4 - 0.7252z^3 - 0.4057z^2 + 0.5714z - 0.08343}.$$

These system components result in a combined open-loop system

$$G(z) = F(z)C(z)P(z). \tag{4.17}$$

It can be derived as

$$G(z) = \frac{N(z)}{D(z)}$$

with

$$N(z) = 0.02311z^7 - 0.09699z^6 - 0.01243z^5 + 0.4466z^4 - 0.689z^3$$

$$+0.5101z^2 - 0.2005z + 0.02235$$

and

$$D(z) = z^{12} - 4.5z^{11} + 9.248z^{10} - 11.48z^9 + 9.576z^8 - 5.684z^7 + 2.528z^6 - 0.7518z^5$$

$$-0.2721z^4 + 0.6608z^3 - 0.507z^2 + 0.2003z - 0.02234.$$

The open loop system is unstable.

When an exponential weighted filter is inserted for signal averaging, the closed-loop system's stability concerns have already been depicted in Figure 38. The closed-loop system's H^2 norm, which defines the system's ability in noise attenuation, is shown in Figure 41.
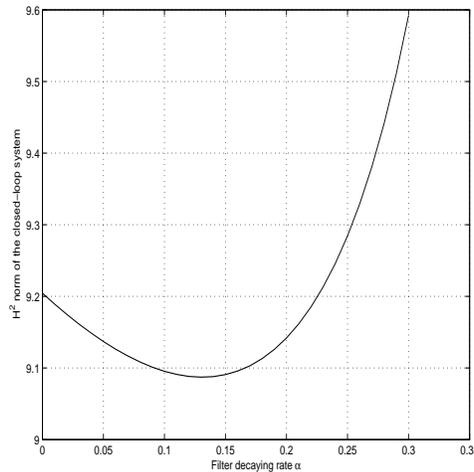
Figure 41: Closed-loop system performance vs. filter decaying rates

When $T = 1$, the optimal filter decaying rate is $\alpha_{opt} = 0.1300$ with the corresponding H^2 norm 9.0872. The closed-loop system's step response is simulated when the filter is optimally selected and shown in Figure 42.

To relate this to re-sampling, we note that the above model is derived with the sampling interval $T = 1$ second. From the relationship, $\alpha_{opt} = e^{-T/\lambda_{opt}} = e^{-1/\lambda_{opt}}$,
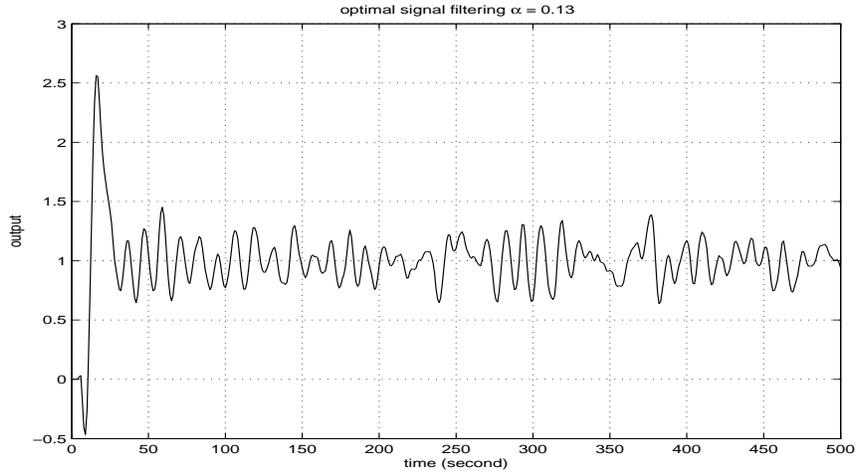
Figure 42: Step response of the close-loop system when the filter is optimally selected, and sampling interval $T = 1$

we obtain $\lambda_{opt} = 0.49$. This leads to the optimal choice of decaying rate when the sampling interval T is reduced from 1 as

$$\alpha = e^{-T/\lambda_{opt}} = e^{-T/0.49} = e^{-2.04T}.$$

When re-sampling is performed with $T \ll 1$, the H^2 norm of the closed-loop system will be reduced to $9.0872\,T$ as established in (4.16). For reduced sampling intervals, improvements of noise attenuation are illustrated in Figure 43.

4.5   Conclusions

The impact of communication channels on feedback control in anesthesia applications in wireless based systems was investigated in this paper. Such systems involve communication channels which are corrupted by noises and have limited bandwidth resources. Signal averaging is the fundamental method in dealing with stochastic
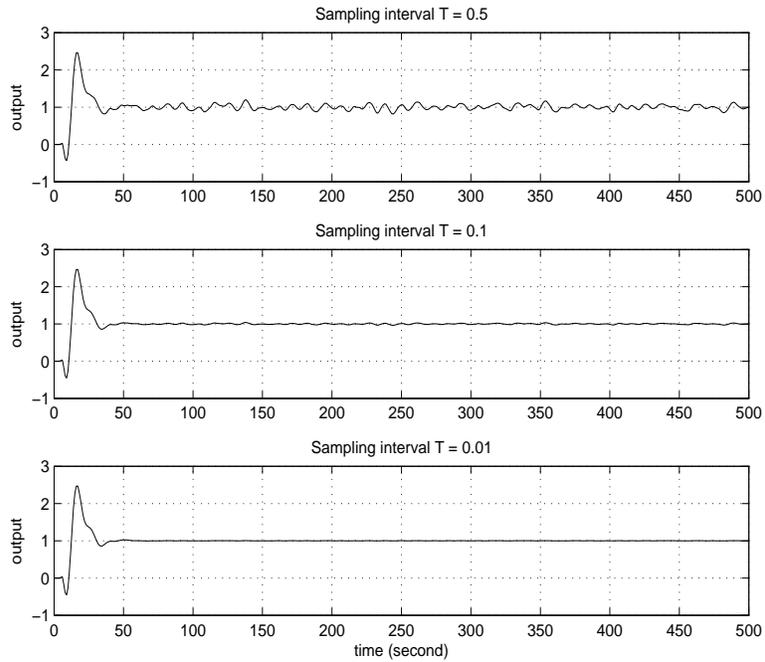
Figure 43: The closed-loop system performance for reduced sampling intervals

noises and errors. It is used effectively in reducing noise effects when only remote monitoring and diagnosis are involved. However, the case is different when feedback is intended.

Our results show that the decaying rate of the averaging window has significant impact on the performance of the close-loop system. When α is larger than some value, the close-loop system becomes unstable. A concept of stability margins against exponential averaging is introduced. Its calculation can be performed by either the Routh-Hurwitz method or the root-locus method on a modified system. Furthermore, the strategy for choosing the optimal decaying rate is derived. Our results conclude that fast sampling must be used for improving noise reduction after optimal filter design. The analysis and design method is applied to anesthesia patient control

problems.

Our analysis is conducted on the basis of the linear systems. Actually, anesthesia patient models contain nonlinearity. Our future work will consider analysis of nonlinear systems.

CHAPTER 5: MODELING FOR THE IMPACT OF ANESTHESIA AND NOISE LESION ON THE PRIMARY AUDITORY CORTEX

5.1 Problem Statement

This work was motivated by the goal of characterizing the impact of anesthesia on the auditory system and diagnosing hearing damage from a system's viewpoint. In this chapter, we derived a comprehensive mathematical model and the auditory system was modeled as a black-box input-output system. Two model structures were employed to capture distinct neural activities: an ARX (Auto-Regression with External Input) model for the auditory system under external stimuli and an ARMA (Auto-Regression and Moving Average) model for the spontaneous activities of the neurons in primary auditory cortex. The models provide a quantitative characterization of anesthesia's impacts and diagnosis of hearing loss on auditory transmission channels. It was shown that impact of anesthesia dosage levels and hearing damage can be characterized by some distinct model parameters such as the time constant, delay time, model bandwidth, and weighting coefficients. To demonstrate these features, in this study different dosages of anesthesia were related to model parameters to quatify their impact on the auditory system. This modeling approach offers several advantages. They can be potentially used to understand mechanisms of auditory signal transmissions and their dependence on anesthesia drugs. Also, model param-

eter changes under different conditions can be used to analyze the impact of drugs, stimulations, and physiological conditions on the auditory system. As such, they may be used as a tool for diagnosis. The derived models can provide a quantitative characterization of such impacts. In addition, rats with hearing damage demonstrated different neural responses in comparison to normal control groups. By comparing the models of healthy and damaged auditory systems, it is possible to reveal how hearing damage affects the neural activity recorded from different channels in the auditory cortex. Finally, model analysis may provide some insights on remedies to correct adverse effects of anesthesia drugs or hearing loss.

5.2 Materials

5.2.1 Surgery and Animal Preparation

The data were collected from five long-Evans rats. The subjects were anesthetized with isoflurane (gas). To understand the impact of anesthesia on the auditory system, two dosages were used: a low dose of concentration 1.25-1.5%, which is about 1.25-1.5 times of the minimum alveolar anesthesia concentration (MAC)for rats;[1] and a high dose of concentration 2.5-3.0%. The anesthesia was maintained over the entire period of the experiments. To investigate the effect of noise stimuli and impact of noise lesion, different experiments were designed for those rats. Table 5 listed all available rat data sets under various conditions.

---

[1] The MAC is the lowest anesthesia dosage for preventing purposeful movement in response to supramaximal noxious stimulation in 50% of animals. The MAC is about 0.98 for the rat

Table 5: Experiment arrangement and available data sets of five long-Evans rats. 'A' indicates that the data set is available, 'NA' means that the data were either not collected or unreliable.

Rat No.	Stimulus interval: 10sec	Stimulus interval: 5sec	noise lesion
Impl25	A	NA	A
Impl26	A	A	A
Impl29	A	NA	A
Impl30	A	A	NA
ABI017	NA	A	NA

5.2.2 Establishing ABR (Auditory brainstem response) thresholds before and after noise exposure

While the animal was under anesthesia, ABR thresholds were obtained by evaluating hearing conditions. Following sound calibration, 3 subdermal platinum electrodes were inserted. The active electrode was inserted in the vertex, the return electrode inserted below the left pinna, and the ground electrode placed into the contralateral temporal muscle. Tone bursts of 10 ms duration were delivered to an electrostatic speaker at $4, 8, 10, 16, 20, 24$, and 30 KHz (2.5 ms rise/fall, 0 ms plateau). The stimuli were generated by RX6 Multifunction Processor and SigGenRP software (TDT System 3). Calibration of tone bursts was achieved using SigCalRP software. ABR signals were amplified, band-filtered (300 Hz - 3 KHz) and notch-filtered (60 Hz), and averaged 300 times.

5.2.3 Surgical preparation

Following anesthesia, the head of each animal was fixed on a stereotaxic appa-
ratus (Kopf Model 1350). For sound delivery, a pair of custom-made hollow earbars
was used. The animal's body temperature was maintained at $37\,^{\circ}$C by a thermostat-
controlled blanket. Surgery was performed to expose the right auditory cortex (AC)
for placement of an array. To expose the right AC, a 3×4 mm^2 craniotomy was per-
formed at 4 mm lateral and 5 mm posterior to the bregma. The auditory core and belt
regions were identified by stereotaxic coordinates, vascular landmarks (the anterior
and posterior dorsoventral vessels) and physiological response properties to tone and
noise bursts. After taking photographs to record the surgical view, a 4×4, 16-channel
microwire electrode array was dipped in 3% Di-I solution (1,1'-dioctadecyl-3,3,3',3'-
tetramethylindocarbocyanine perchlorate, Invitrogen) prepared with DMSO to label
the track of electrode insertions. Then, the array was implanted in the AC and a
silver wire for grounding was connected to one of the pedestal screws. The array was
lowered $0.8 - 0.9$ mm from the AC surface, which corresponded to the pyramidal cell
layer. Each array consisted of 16 polyimide insulated platinum/iridium microwires
that were arranged in 4 rows with 4 wires in each row (diameter $= 50\ \mu m$; electrode
spacing $= 500\ \mu m$; row spacing $= 500\ \mu m$; impedance $=$0.2-0.5 $M\Omega$). The array cov-
ered the area of about 1.5×1.5 mm^2, and were implanted in an area that contained
both auditory core and belt regions.

5.2.4 Acoustic Stimuli and Data Recording

Sound stimuli were calibrated and presented to the left ear contralateral to the surgically exposed AC. The sample rate for audio output was 100 KHz with 16-bit resolution. Tone and broadband Gaussian noise bursts (1-32 kHz) were 50 ms in duration. Tones were ramped on and off with 2 ms rise/fall times, and noise bursts had 0.5 ms rise/fall times. The level of stimuli was 80 dB SPL.

Single- and multi-unit activity was recorded from the right AC. Neural signals were pre-amplified and bandpass filtered (300-10,000 Hz). Spontaneous activity was recorded for 10 min. Then stimulus-driven activity, in response to noise bursts (50 ms duration, burst/sec, 80 dB SPL) was recorded. The measured neural spike waveforms were processed to derive the neural firing rate trajectories over time.

5.3 Methods

5.3.1 Model Structure Selection

In this study, two parallel subsystems were introduced in the proposed auditory system models: one was an ARX (Auto-Regression with External Input) model structure representing the auditory system under external stimuli as the input and the neuron firing rate as the output, see the auditory system model in Figure 44. The output of this subsystem represented the firing rate in response to acoustic stimuli. The neuronal firing rate was a commonly-used variable to characterize neural activities. It contained essential information on neurons activities and was the core

of computational neuro-sciences [96]. The other subsystem was an ARMA (Auto-Regression and Moving Average) model structure which represented the spontaneous activities (no inputs) of the neurons in primary auditory cortex. The main reason for the model structure is that ARX is a general dynamic system model for an input/output system. By varying its delay time and model order this model structure is highly capable to describe a wide variety of physical systems. Here, the response of neural activity to external stimuli can be viewed as an input/output system. In contrast, neural spontaneous activities represent self-excited signal generation. ARMA models describe a self-excited signal as the output of a dynamic system driven by a standard white noise stimulation. In other words, it can be suitably used to describe internal activities of a physical system.

In a neural system these two activities coexist. Naturally, a combination of these two models become appropriate. By combining these two models, the total measured firing rate was a weighted sum of the two models. The weighting parameter $\gamma = \frac{y_{(arma)}}{y_{(base)}}$ in Figure 44 was a function of anesthesia levels and noise stimulus intervals. In this paper, the base activity is defined as the neural activity under the deep anesthesia($2.5 - 3\%$). As a result, $\gamma = 1$ when the anethesia is at $2.5 - 3\%$ concentration. The output of ARMA model, $y_{arma}(t)$ is normalized at anesthesia base level and the base value of $y_{arma}(t)$, is defined as: $y_{base}(t) = y_{arma}(t) \mid_{DeepAnesthesia}$, which is different among animals and corresponding to the doseage of drugs. As a result, the contribution of ARMA model to the measured firing rate should be $y_{arma}(t) = \gamma * y_{base}(t)$.
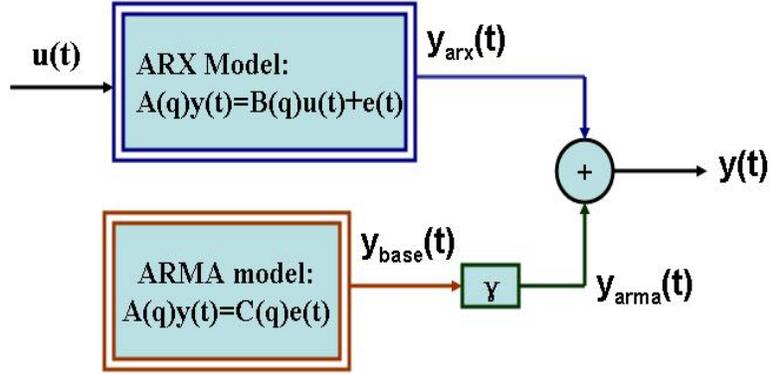
Figure 44: Diagram of the auditory system model

1. ARX Model for Stimulation Responses

The ARX model has noise burst u_k as the input and firing rate y_k as the output. The structure of the ARX model of order n_a is:

$$A(q)y_k = B(q)u_k + e_k$$

where $A(q) = 1 + a_1 q^{-1} + a_2 q^{-2} + \ldots\ldots + a_{n_a} q^{-n_a}$, $B(q) = b_1 q^{-1-n_k} + b_2 q^{-2-n_k} + \ldots\ldots + b_{n_b} q^{-n_b-n_k}$. Here, q^{-m} is the m-step delay operator: $q^{-m} y_k = y_{k-m}$. $n_b - 1$ is the number of zeros of the system, n_k is the delay, and e_k is an additive i.i.d. (independent and identically distributed) noise with mean zero and a finite unknown variance. This model structure means that the current output y_k at time $t = k\tau$ is related to previous sampled inputs at $k - n_b$, also related to previous outputs up to the time of $t - n_a$. This model can be completely described by parameters $\theta = [a_1, a_2, \ldots a_{n_a}, b_1, \ldots, b_{n_b}]^T$.

2. ARMA Model for Spontaneous Activities

When animals were not stimulated, the spontaneous activities may be viewed as a time-series generated from a noise stimulation of standard Gaussian distribution with mean zero and variance one. It can be expressed as an ARMA model structure:

$$A(q)y_k = C(q)e_k$$

where $A(q) = 1 + a_1 q^{-1} + a_2 q^{-2} + ... + a_{n_a} q^{-n_a}$, $C(q) = 1 + c_1 q^{-1} + c_2 q^{-2} + ... + c_{n_c} q^{-n_c}$, n_a is the order of the model, n_c is the number of zeros of the system, and e_k is a standard white noise.

5.3.2 Model Parameter Estimation

Once a model structure is selected, the next step is to determine the model parameters. The main method is to use the measured data to choose model parameters optimally. In this paper model parameters were determined through the least-squares optimal fitting method [97]. To estimate the model parameters, a typical data set was chosen for system identification and parameter estimation. Figure 45 illustrates the recordings of one rat's firing rates in our experiments. In Figure 45, the firing rates (in the middle plot) increased dramatically in response to the inputstimuli of broadband noise, and then dissipated after the noise stimuli stopped.

For both figures, the top plot is the spike train of a single neuron recorded over a period of 45 seconds. The middle plot shows the firing rates to external (acoustic) stimulation. The vertical lines indicate the starting times of the noise stimuli. The stimuli were given in an interval of 10 second with duration of 50 ms, 80 dB broadband
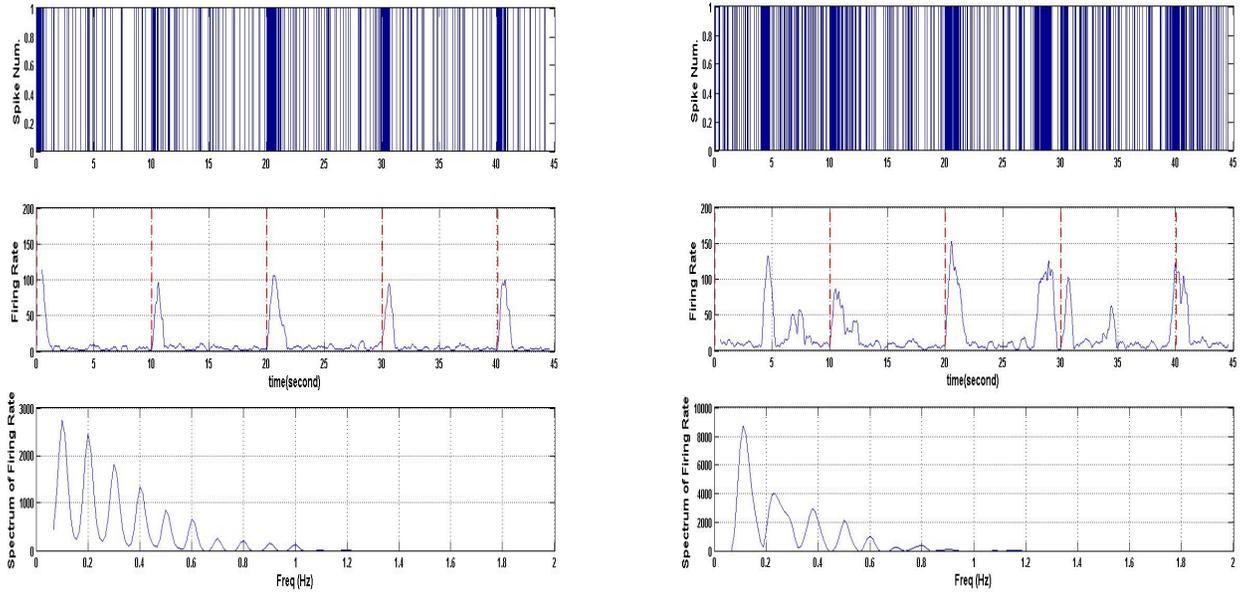
(a) Deep anesthesia

(b) Light Anesthesia

Figure 45: The spike train, firing rate and its power spectrum.

noise. The bottom plot is the power spectra of the firing rates. The primary frequency component of 0.1 Hz represents the impulses of the firing rates that occurred every 10 seconds (frequency 0.1 Hz) during the periodic stimuli of the same period.

When rats were under deep anesthesia with a high dose of isoflurane, the activities of primary auditory cortex neurons were significantly activated by acoustic stimulation with broadband noise. On the other hand, the spontaneous activities were largely suppressed, see Figure 45(a). Under light anesthesia, the spontaneous activities were more visible than those in deep anesthesia, see Figure 45(b). Although anesthesia impact on auditory neurons could be seen directly from the recorded time series, quantifying anesthesia effects on neurons activities required detailed analysis. Mod-

eling for the auditory system made it possible to analyze such effects systematically. The procedure of our method is detailed in next.

The inherent sampling interval of the original firing rates was 1 ms second. For system identification, this step size is too small to get an accurate model. As a result, the data set was re-sampled with a larger sampling interval $\tau = 18ms$. The re-sampled signals became $y_k = y(k\tau), u_k = u(k\tau), \tau = 0, 1, \ldots$. Due to randomness in neural activity and measured signals, signal averaging was conducted.

1. ARX Model Parameter Estimation

To attenuate noise effect, stimuli were applied periodically every 10 seconds. The data were then divided into segments of 10 seconds each. The firing rates over consecutive data segments were averaged. In this data processing, five segments of the data (a total of 50-second data) were averaged to generate a 10-second combined segment for model estimation. The model parameters were estimated using the function ARX in the Matlab *System Identification Toolbox*. The orders of the model were chosen as $n_a = 3$ and $n_b = 2$. The delay time was estimated with the function DELAYEST in *System Identification Toolbox*. Given a white noise with power 80 dB and duration 50 ms as the input signal, the transfer function of the ARX model structure with a delay of $n_k = 31$ was identified as:

$$H_{ARX}(z) = z^{-31} \frac{10^{-3}(-0.36z - 0.52)}{z^3 - 1.805z^2 + 1.084z - 0.2605} \tag{5.18}$$

2. ARMA Model Parameter Estimation

The averaged firing rates after $t = 2$ seconds in Figure 46 were used in estimation of the ARMA model. The model order was usually selected by an iterative process of increasing model orders and checking model fidelity as a tradeoff between model complexity and accuracy. Such a process led to the selected orders $n_a = 3$ and $n_c = 2$. The discrete-time transfer function of the ARMA model was identified, by applying the ARMA function in *System Identification Toolbox* of MATLAB, as:

$$H_{ARMA}(z) = \frac{z^2 + 0.03146z - 0.8969}{z^3 - 1.102z^2 - 0.6824z + 0.7996} \tag{5.19}$$

5.3.3   Model Fidelity Evaluation

1. ARX Model Fidelity

To evaluate the accuracy of the identified model and its prediction ability, the model was used to produce the output with an input as the actual stimuli. The model output was employed to predict the firing rates under a given white noise with the same SPL and duration in a 10-second interval which followed the data used to estimate the model parameters. Actual firing rates were compared with the model output in Figure 46. The model output fitted well with the data. In Figure 47, the firing rates in the next 10-second interval and model predictions were compared. In both cases, the model output captured the real data authentically.
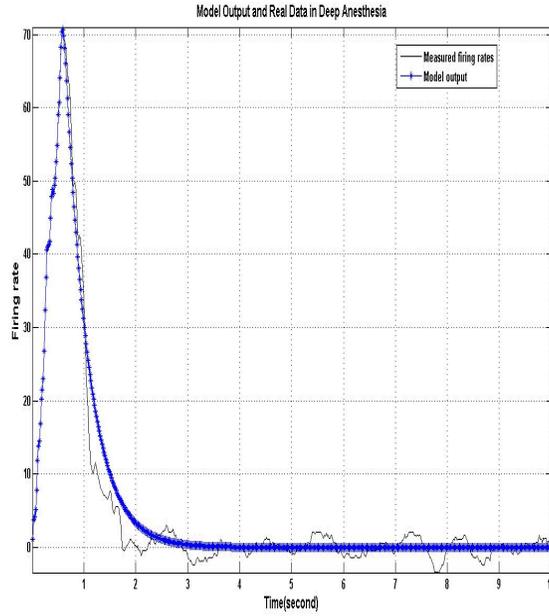
Figure 46: Model output and real firing rate

2. ARMA Model Fidelity

Performance of the identified ARMA model was evaluated by comparing the power spectrum of the model output and the real data in Figure 48. The spectrum of the model output captured the main frequency components of the real firing rates. So, the parameters obtained in the frequency domain could be used for analysis. In this paper, model accuracy was measured by $\beta = \sqrt{\frac{P_{Model}}{P_{realdata}}}$. Here P is the total power of firing rates during the time interval of interest.

In Table 6, the ARMA model β values were compared under different anesthesia levels and conditions of the auditory system. From Table 6, β was approximately equal to 1 for all cases. Hence the output of the ARMA model well represented the real firing rates.
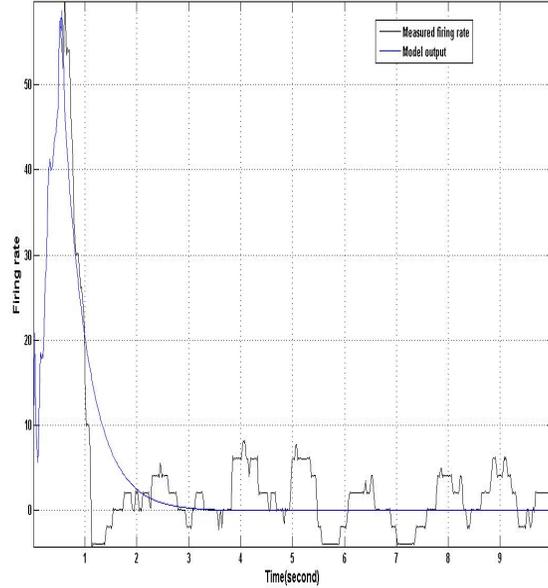
Figure 47: Predicted firing rate and measured data in 10 second interval

Table 6: β values of normal auditory system and auditory system after noise lesion

Rats No.	β_{deep}	β_{light}	$\beta_{light,noiseleison}$
Impl25	0.9337	0.9091	1.0625
Impl26	0.9353	1.0143	0.9043
Impl29	0.8339	0.9904	1.0065
Impl30	0.9266	0.9017	data not usable

5.4   Results

Anesthesia has a significant impact on auditory systems. In addition, hearing damage may cause changes in the auditory neural tuning curves [98]. To investigate the impact of anesthesia and hearing-damage-induced effects on the auditory system, the two subsystems of the proposed model structure, ARX model and ARMA model, were analyzed for the auditory system under different conditions. Although a model is completely determined by its structure and parameters, for its utility in this study,
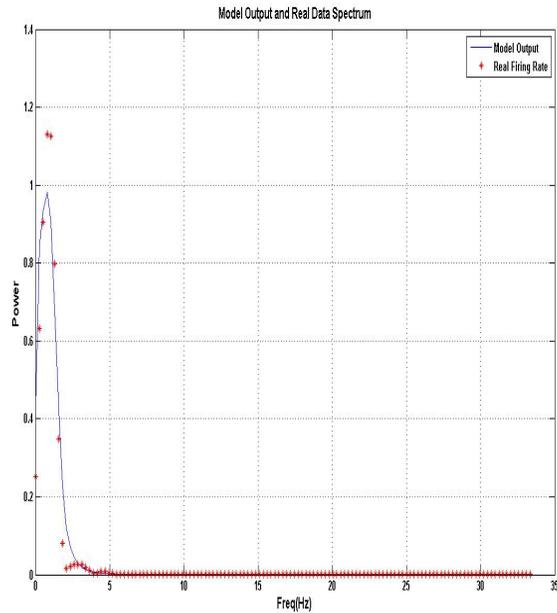
Figure 48: The power spectrums comparison between ARMA model output and the spontaneous firing rate.

we extract certain characterizing variables as indices to quantify neural activity. ARX and ARMA models carry certain physically meaningful variables that can be used to describe neural activity intensity in more details than signal energy or power density. As such, they can be potentially used to distinguish a patient's auditory system in terms of its response to stimuli or self-excited neural firing actions. In particular, we focus on the time constant, time delay, bandwidth, and power ratio. In the following sections, we will discuss those system characteristic variables in details. The results were first obtained from the data analysis of two levels anesthesia, then extended to more anesthesia levels

5.4.1 Light vs. Deep Anesthesia

We first studied the relationship between the model variables and the anesthesia levels, by using only two cases: Deep anesthesia with high dose (2.5%) of isoflurane and light anesthesia with a low dose (1.5%). In addition, it was observed that experiment conditions usually had an influence on collected signals that may affect the generality of the results. As a result, we also investigated the effect of stimulus intervals to see whether the same conclusions could be achieved. For this analysis, the broadband noise with same SPL and duration was applied periodically, first in the 5 second interval, and then the 10 second interval.

Time Constant   The time constant is defined as the time for the system step response reaching to the 63% of the steady value. Its meaning was illustrated in Figure 49.
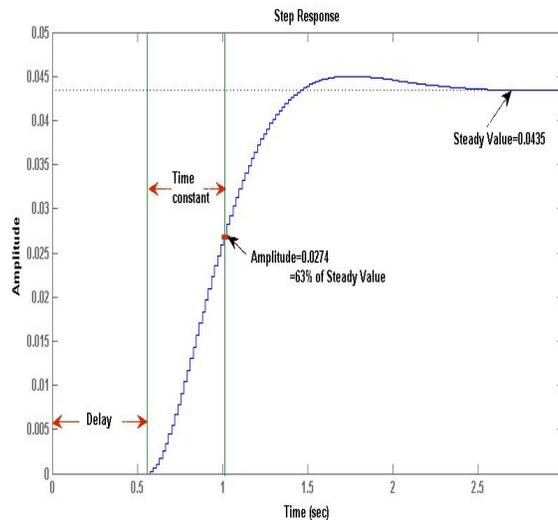
Figure 49: The step responses of the identified system.

Figure 50 displayed the time contants of ARX (Figure 50 (a) and (b)) and ARMA models (Figure 50 (c)). From Figure 50 (a) and (b), it could be seen that the system variables were affected by the level of anesthesia and hearing conditions. For a stable LTI system, its time constant determines its response speed to an outside stimulus. From Figure 50, we found that the mean response speed (the inverse of the time constant) was slower for the system in light anesthesia without hearing damage, than those after noise lesion or the normal system in deep anesthesia. In addition, no obvious effect could be seen from the trend of system variables when the stimuli were applied over different time intervals. Similar trends were observed for the ARMA model (Figure 50 (c))except for one case that the time contant kept at the same value while the drug dosage was changed.

For both ARX and ARMA models, the time constant changed with the anesthesia levels and hearing conditions. In Figure (a), the stimulus noise was presented every 10 second with 50 millisecond and 80 dB SPL. In Figure (b), the stimulus noise was presented every 5 second with 50 millisecond and 80 dB SPL.

Time Delay   The time delay is defined as the initial time interval before the system responds to the stimuli. Its meaning was illustrated in Figure 49.

Figure 51 illustrated time delays of the ARX model when stimulus were applied over different intervals. The system delay went down after the drug dosages were reduced and it decreased further after the noise lesion.

In plot (a), the stimulus noise was presented every 10 seconds with 50 millisecond
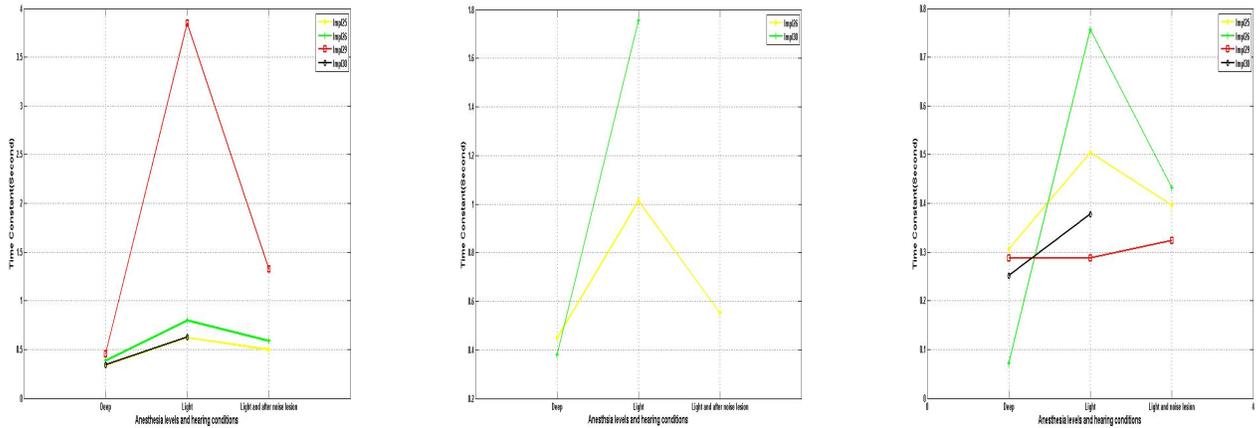
(a) Time constants of ARX models(Stimulus interval: 10sec)

(b) Time constants of ARX models(Stimulus interval: 5sec)

(c) Time constants of ARMA model

Figure 50: The variation of system time constant corresponding to the anesthesia levels and hearing conditions.

and 80 dB SPL. The system delay of all cases have the same variation trend. In plot (b), the stimulus noise was presented every 5 seconds with 50 millisecond and 80 dB SPL. The trend of one case is reversed comparing to that of other cases. Obiviously, when the noise stimuli interval was 5 seconds, the time delay of one case was reversed, comparing to other cases. This means the time delay was sensitive to the intervals of input stimuli. As a result, it was judged as a non-robust index for dectecting the anesthesia levels.

Bandwidth The bandwidth is defined in the frequency response of the model. Then, the bandwidth is the frequency when the magnitude of its frequency response reduces to -3 dB from its DC value.
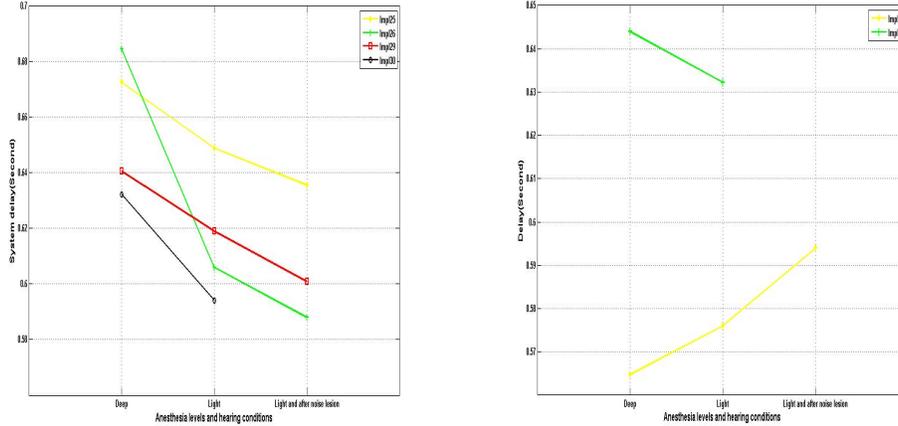
(a) Time delay of the ARX models(Stimulus interval: 10 seconds)

(b) Time delay of the ARX models(Stimulus interval: 5sec)

Figure 51: The variation of system delay corresponding to the anesthesia levels and hearing conditions.

The values of system bandwidth of ARX and ARMA models were displayed in Figure 52. From the figure, it was clear that the variation trend of system bandwidth was similar to that of time constant. For ARX model, all of the cases demonstrated the same trend for both noise intervals. However, for the ARMA model, one case was showing a different trend after the auditory system experienced the noise lesion.

In plot (a), the stimulus was presented every 10 seconds with 50 millisecond and 80 dB SPL. The bandwidth of all cases had the same variation trend. In plot (b), the stimuli was presented every 5 seconds with 50 millisecond and 80 dB SPL. The trend of one case was reversed comparing to other cases.
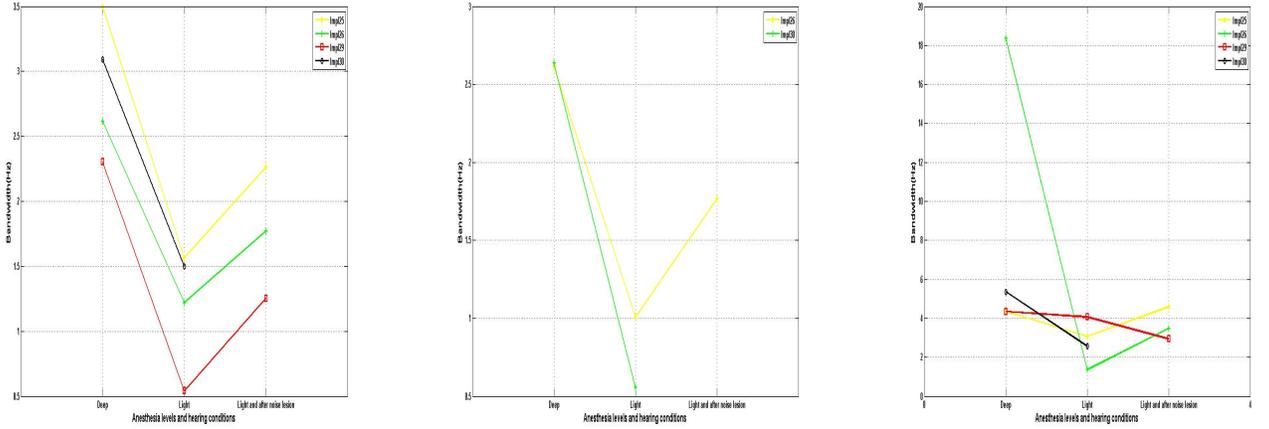
(a) Bandwidth of ARX model(Stimuli interval: 10sec)

(b) Bandwidth of ARX model(Stimuli interval: 5sec)

(c) Bandwidth of ARMA model

Figure 52: The variation of system bandwidth corresponding to the anesthesia level and hearing conditions.

Power Ratio In an ARMA model, the parameters derived from the signal spectrum were used for analysis. The power ratio μ was evaluated as a potential indicator of anesthesia levels. For two levels anesthesia, it is defined as

$$\mu = \sqrt{\frac{P_{light}}{P_{base}}}.$$

Where the $P_{base} = P_{DeepAnesthesia}$ is the power of firing rates when the animal was given a high dosage of drug which is supposed to induce deep anesthesia level. This is especially useful under the ARMA models to show the relative impact of anesthesia on spontaneous activity. Table 7 listed the μ values of the ARMA model when the noise stimulus was presented every 10 seconds. And the μ values of the ARMA model when the noise stimulus was presented every 5 seconds were listed in Table 8. The

ARMA model's μ values were compared under different conditions of the auditory system.

Table 7: μ values of normal auditory system and auditory system after noise lesion. The stimuli were applied every 10 seconds

Rats No.	μ_{normal}	$\mu_{light,noiseleison}$
Impl25	4.09 ± 1.18	6.3 ± 1.34
Impl26	4.42 ± 1.1	6.8 ± 1.4
Impl29	3.75 ± 0.86	2.3275 ± 0.68
Impl30	2.5 ± 0.74	$datanotusable$

Table 8: μ values of damaged and normal auditory system. The stimuli were applied every 5 seconds.

Rats No.	μ_{normal}	$\mu_{light,noiseleison}$
Impl26	2.25 ± 0.95	2.6 ± 1.17
Impl30	1.26 ± 0.74	$datanotusable$

Here, we define a parameter K to relate the μ and the drug dosages r: $K * \frac{r_{high}}{r_{low}} = \mu$. K increases as the anesthesia levels being from deep to light. All rats used in our experiments were undergoing the anesthesia with a high dose of 2.5% and low dose of 1.5%. Then the $K \approx \frac{\mu}{1.67}$. When the noise stimulus was presented every 10 seconds, the K was averaged among all rats and we got $K = 2.2$, while $K = 1.05$ when the stimulus presented every 5 seconds. Obviously, the K is proportioned to the stimulus intervals. For the systems after noise leison, the values of K are around 3.9 (noise was applied every 10 seconds) and 2.6 (noise was applied every 5 seconds), which were larger than those of the normal systems.

5.4.2 Extended Anesthesia Levels

In this section, our method will be investigated for the case of extended anesthesia levels. A long-Evans rat was firstly anesthetized with a high dose of isoflurane (3.0%), then multi-channel brainstem responses recording were started after around 30 min when the rat was supposed to be in a steady status. The recording continuous about 2 min, after that the isoflurane was turn down to a very low dose of (1.25%) which makes the rat recover gradually to awake status. The response signals (around 30min in length) were collected till the animal was fully awake. The 30 min data was separated into three time-continuous blocks with each representing the deep-light anesthesia, light anesthesia and light-awake status respectively in time order.

The stimulus with 80 dB SPL and 50ms duration was presented periodically in 5 seconds interval. The proposed model structure was applied and the identical system parameters were calculated for multi-level anesthesia problem. Results were summarized in Table 9 for comparing μ, time constant and bandwidth of the ARMA subsystem and system delay of ARX subsystem when the auditory system is under different anesthesia levels. In this case, the power ration is defined as:

$$\mu = \sqrt{\frac{P_L}{P_{base}}}$$

, where the P_L can be the signal power of one of the anestheisa levels: $P_{Deep-light}$, P_{light} and $P_{light-awake}$. $P_{base} = P_{DeepAnesthesia}$ is the power of firing rates when the animal was given a high dosage of drug which is supposed to induce deep anesthesia.

Figure 53 demonstrates the trend of the time constant and bandwidth of the ARX

Table 9: μ, time constant and bandwidth of ARMA model, as well as the system delay of the ARX model when the auditory system is under 4 anesthesia levels: deep, deep-light, light and light-awake status.

	Deep	Deep-light	Light	Light-awake
μ	1	0.997 ± 0.37	1.15 ± 0.38	1.5287 ± 0.53
Time constant(ARMA)	0.105	0.145	0.126	0.14
Bandwidth(ARMA)	17.4915	12.3797	14.3701	12.9027
Dealy(ARX)	0.16	0.1275	0.1585	0.1487

system when the auditory system is under 4 anesthesia levels. Obviously, the values of time constants are increasing and bandwidth are decreasing gradually as expected. That coincides wi
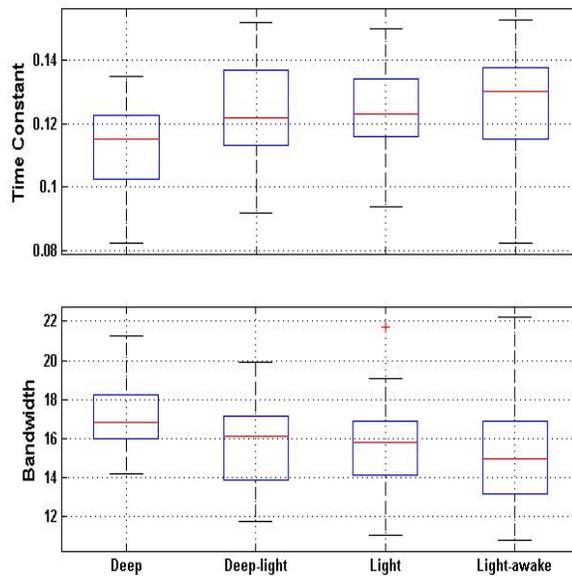
Figure 53: Box plots of the time constant and bandwidth of the ARX system in 4 levels anesthesia.

5.5 Discussion and Conclusions

In this paper, we investigated the problem of anesthesia impact on auditory neuron activities and characterized the noise lesion effect on auditory systems from a system viewpoint. A simple and application-oriented system structure was proposed and system identification methods were applied to estimate the system parameters, which indicated the changes of system conditions. Anesthesia is widely believed to affect the audio signal processing in auditory systems. Understanding the anesthesia effects is essential when for charaterizing how the information is processed in auditory systems. Our modeling method makes it possible to characterize the anesthesia impact at a system level. A distinct feature of our models is that those derived system parameters have physical meanings for easy understanding.

5.5.1 Impact of Anestheisa Levels on the Auditory System

We have studied the impact of anesthesia levels on the auditory system for the case of two levels anesthesia (deep anesthesia witha high dose of 2.5% and light anesthesia with low dose of 1.5%) and the case of extended anesthesia levels (4 levels anesthesia were considered). The system variables (time constant, bandwidth, system delay, and power ratio) of both models, ARX and ARMA, were calculated and compared to identify the anesthesia status. In Figures 50,51, 52 and 53 , we observed that the system parameters were affected by the levels of anesthesia and hearing conditions. From the results, several interesting findings were highlighted.

1. ARX Model: For the ARX model, the varibales of the time constant, delay and bandwidth were calculated. The time constant determines response speed to an outside stimulus. The mean response speed was slower for the system in light anesthesia without hearing damage when compared with an auditory system in deep anesthesia. Meantime, the bandwidth decreased when the drug was reduced to a lower dosage. In addition, the neuron responses to noise stimuli were delayed in the auditory system under deep anesthesia. In the case of multi-level anesthesia, the time contant increased and bandwidth decreased gradually as the animals recovered from deep anesthesia to awake, while the system delay fluctuates during the recovery procedure.

2. ARMA Model: In an ARMA model, both of the the time-domain and freuquency-domain parameters, the power ratio, time constant and bandwidth, were used for analysis. The power ratio μ parameters derived from model outputs and calculated from measured real firing rates were similar. On the other hand, the obvious difference of μ could be found from the auditory system in distinct anesthesia status (See Table 7,8 and 9). For most animals, the time constant was lower in deep anesthesia and higher in light anesthesia, the case was reversed for bandwidth. However, for the auditory system of one animal (Impl29), the time constant and bandwidth did change although the drug was reduced to a lower dosage. Furthermore, in the case of extended anesthesia levels, these variables derived from the ARMA model flucatuated in the recovery procedure

(See Table 9). In addition, the values of the time constant and bandwidth are different from those of ARX models implying that the auditory system was a nonlinear system in response to outside stimuli.

5.5.2 Impact of Noise Lesion

Except for anesthesia, we also considered the impact of noise leison on the auditory system. The same variables were extracted from the ARX model and ARMA model. From the results, we can see that:

1. ARX Model: For the ARX models of all animals, the time constant decreased a little bit after the animals experienced the noise leison, although the anesthesia was kept at the seam dosage (1.5%). Meanwhile, the bandwidth increased. The broader bandwidth may indicate the abnormal hearing conditions caused by the noise leison or anesthesia. From the results of all animals, the system response was delayed futher after the noise leison.

2. ARMA Model: In an ARMA model, the variables demonstrated the same trend as those of the ARX model, except for the system of one animal(Impl29). From Tables 7 and 8, μ parameters derived from model outputs and calculated from real firing rates were similar. On the other hand, the obvious difference of μ can be found from the auditory system before and after noise lesion. The parameter μ of the auditory system after noise lesion was much larger than that of a normal system, except for one animal(Impl29). When the stimulus interval was adjusted to 5 seconds, it could be seen from Table 8 that although

the μ values showed the same trend as the initial findings in the cases of 10 seconds stimulus interval (the μ increased when the drug dosage was reduced). For the same rat, the μ values were relatively small when the stimulus was presented every 5 seconds. Hence the μ was not only a function of anesthesia levels and noise leison, but also a function of stimulus intervals. But the μ did not detect the samll changes in the auditory system when extended anesthesia level were considered.

By comparing the system variables of the ARX and ARMA model, we concluded that it was essential to use acoustic stimuli to track the anesthesia levels and hearing conditions more precisly. However, the system time delay of ARX model was sensitive to the periodical stimulus intervals. In contrast, the time constant and bandwidth of were more robust variables in detecting the anesthesia status because these variables of all animals reflected trend variations as the anesthesia levels and hearing conditions. Obviously, both anethesia drugs and noise lesion had impact on the animals' auditory systems. From the results, we concluded that the effect of noise lesion was similar to an increase of the drug dosage. In other words, both anesthesia drugs and noise lesion affected similarly the fuctions of the auditory system in terms of response speeds to outside acoustic stimuli and the sound frequency selection.

5.5.3   Signal Processing and Modeling Issues

We calrify several points in the data analysis to avoid the ambiguity in explaining the results and reaching a conclusion.

1. The values of the system time constant and bandwidth:

They were relative values and maybe different among a group of animals. The size of the windows applied for neuron spike trains to get the firing rates determined those relative values as "large" or "small". Thus, it is important to keep an identical window size in calculating the time-dependent firing rates in each animal. The size of the windows was usually between 100-500 millisecond. How to choose the window size was determined by the noise-induced response durations which were different among the animals. If the response duration was short, a small window size should be chosen to derive a more accurate time-dependent firing rate.

2. The length of signals used for calculating averaged firing rates:

As long as the signals remained in the same conditions (identical anesthesia dosage, with or without noise lesion), the longer of the data segment used for calculating the averaged firing rate, the more accuracy would be achieved for the results.

3. Choice of the data segments used for analysis:

It is desirableto use as much data as possible for computing averaged firing rates. However, choice the proper data segments from original signals was essential. In this paper, those data segments in non-steady status, such as the data recorded at the time when the anesthesia dosage and the noise interval were changed, as well as those recordings immediately after several hours of the noise lesion,

were removed from analysis.

CHAPTER 6: PLAN OF FUTURE WORKS

Along these directions, there are some remained works need to be completed in the near future. In this chapter, several topics are proposed as the future research efforts to supplement the current works.

6.1 Clinlic Proof of Relative β_2/θ-Ratio

An EEG parameter β_2/θ-ratio was developed and compared with relative β-ratio which is one of main parameters used for producing the BIS index. Our results have reached a conclusion that the use of β_2/θ-ratio can potentially improve the monitor's perfromance in detecting the awareness of anestehsia patients during emergence stage. To prove the effectiveness of this parameter, it's performance needs to be verified through population based statistical analysis. This is a long term work and is up to the amount of patient data being availiable.

6.2 Hardware Implementation for MIMO Modeling and Diagnosis

In this work, a decision-oriented modeling method was introduced for real-time mornitoring, diagnosing, and predicting multiple outcomes of anesthesia patients. This model was used for outcomes prediction, drug impact prediction and observing all potiential outcome sets to assist anesthesiologists in making decisions during surgery. Simulation results proved that this model could represent the real patient

dynamics with minor accuracy loss.

Labview graphical programming software (National Instrument Inc.) can be used for model based design. Recently, NI is making effort to support developing medical device through Labview. We have sucessfully implemented the SISO real-time model for prediction in operation room. In the future work, we will update the device to the one that embeds the multivariable patient model and apply it in operation room for multi-outcome anesthesia diagnosis.

6.3   Signal Averaging in Nonlinear Systems

In this project, the problem of the impact of signal averaging on close-loop systems with applications on the wireless anesthesia control has been studied. With a simple linear anesthesia patient model, we derived the stablity margin against exponential windows and calculated the optimal window size to optimize the system performance. Actually, patient models show much nonlinearity. For simplicity, the anesthesia patient model was figured out as a special wiener model struture, which was composed of a linear dynamic model followed by a static nonlinear function. The future work will be focused on the performance analysis of nonlinear wiener system with feedback controller and averaging windows. In addition, in current proble framework, the noise was added to the transmitted signals, while the noise is not additional or not white, the results will be definitly different.

[7] O. Dressler, G. Schneider, G. Stockmanns and E.F. Kochs, Awareness and the EEG power spectrum: analysis of frequencies, British Journal of Anaesthesia 93(6):806-9, 2004.

[8] John C. Drummond, Monitoring depth of Anesthesia: with emphasis on the application of bispectral index and the middle latency auditory evoked response to the prevention of recall, Anesthesiology 2000; 93:876-82.

[9] Lalkman, Cor J., Drummond, John C., Monitors of depth of anesthesia, Qua Vadis?, Anesthesiology: Vol. 96(4) April 2002, pp 784-787.

[10] Thompson E, Varela F. Radical embodiment: Neural dynamics and consciousness. Trends Cogn 2001; 5: 418-425.

[11] Eger EI II, Saidman LJ, Brandstater B., Minimum alveolar anesthetic concentration: a standard of anesthetic potency. Anesthesiology 1965; 26:756-763.

[12] Jensen E, Litvan H, Struys M, Martinez-Vasquez P. Pitfalls and challenges when assessing the depth of hypnosis during general anaesthesia by clinical signs and electronic indices. Acta Anaesthesiol Scand 2004; 48: 1260-1267.

[13] Bruce J. Fisch, "Fisch and Spehlmann's EEG Primer: Basic Principles of Digital and Analog EEG", Third Revised and Enlarged Edition, Elsevier Science B.V. 1999.

[14] Guedel AInhalational anesthesia. A fundamental guide, New York:Macmillan Company,1937.

[15] Heir T, Steen PA, Awareness in anesthesia: incidence, consequences and prevention, Acta Anaesthesia Scand 1996; 40(9):1073-86.

[16] Schwilden H, Stoeckel H. Closed-loop feedback controlled administration of alfentanil during alfentanilnitrous oxide anaesthesia. Br J Anaesth 1993; 70: 389-393.

[17] Schwilden H, Stoeckel H. Quantitative EEG analysis during anaesthesia with isoflurane in nitrous oxide at 1.3 and 1.5 MAC. Br J Anaesth 1987; 59: 738-745.

[18] Rezek IA, Roberts SJ. Stochastic complexity measures for physiological signal analysis. IEEE Trans Biomed Eng 1998; 45:1186-91.

[19] Christian Jeleazcov, Gerhard Schneider, Michael Daunderer et al., The discriminant power of simultaneous monitoring of spontaneous electroencephalogram and evoked potentials as a predicator of different clinical states of general anesthesia, Anesth Analg 2006;103:894-901.

[20] Drummond JC, Brann CA, Perkins DE, Wolfe DE, A comparison of median frequency, spectral edge frequency, a frequency band power ratio, total power, and dominance shift in the determination of depth of anesthesia. Acta Anaesthesiol Scand. 1991 Nov;35(8):693-9.

[21] Lee A. Jr Kearse, Paul Manberg, Nassib Chamoun, Fred deBros, Alan Zaslavsky, Bispectral Analysis of the Electroencephalogram Correlates with Pa-

tient Movement to Skin Incision during Propofol/Nitrous Oxide Anesthesia. Anesthesiology. 81(6):1365-1370, December 1994.

[22] Stockard J, Bickford R The neurophysiology of anesthesia. In: Gordon E, ed., A basis and practice of neuroanesthesia. New York: Excerpta Medica, 1981: 3-50.

[23] Johansen JW, Sebel PS, Development and clinical application of electroencephalographic bispectrum monitoring. Anesthesiology. 2000 Nov;93(5):1336-44.

[24] Miika Koskine, et al., Monotonicity of approximate entropy during transition from awareness to unresponsiveness due to propofol anesthesia induction, IEEE Transactions on Biomedical Engineering, Vol. 53,No. 4, April 2006.

[25] Amod Kumar, Sneh Anand, A Depth of Anaesthesia Index from Linear Regression of Eeg Parameters, Journal of Clinical Monitoring and Computing, Volume 20, Number 2 / April, 2006.

[26] Eckert O, Werry C, Neulinger A, et al. Intraoperative EEG monitoring using a neural net work. Biomed Tech,1997, 42(4): 78.

[27] Leslie C. Jameson, Tod B. Sloan, Using EEG to Monitor anesthesia drug effects during surgery, Journal of clinical monitoring and computing (2006) 20:445-472.

[28] Rampil, Ira J. MS, A primer for EEG signal processing in anesthesia, Anesthesiology, Volume 89(4), October 1998 pp980-1002.

[29] Sally E. Rampersad, Michael F. Mulroy, A Case of Awareness Despite an "Adequate Depth of Anesthesia" as Indicated by a Bispectral Index Monitor, Anesth Analg 2005;100:1363-1364.

[30] Veselis RA, Reinsel R, Sommer S. et al. Use of neural network analysis to classify electroencephalographic patterns against depth of midazolam sedation in intensive care unit patients, J Clin Monit, 1991,7(3):259.

[31] Hudson RJ, Stanski DR, Saidman LJ, Meathe E. A model for studying depth of anesthesia and acute tolerance to thiopental. Anesthesiology 1983; 59: 301-308.

[32] Llinas RR, Leznik E, Urbano FJ. Temporal binding via cortical coincidence detection of specific and nonspecific thalamocortical inputs: a voltage-dependent dye-imaging study in mouse brain slices. Proc Natl Acad Sci USA 2002; 99: 449- 454.

[33] Johnson RW, Shore JE. Which is the better entropy expression for speech processing: $-SlogS$ or $logS$? IEEE Trans Acoust 1984; ASSP-32:192-37

[34] Gerhard Schneider, Regina Hollweck, Michael Ningler, Gudrun Stockmanns and Eberhard F. Kochs, Detection of consciousness by electroencephalogram and auditory evoked potentials, Anesthesiology, Vol.103, No. 5, Nov, 2005.

[35] Harbhej Singh, Bispectral index (BIS) monitoring during propofol-induced sedation and anaesthesia. European Journal of Anaesthesiology (1999), 16: 31-36.

[36] Mika Särkelä et al. Automatic analysis and monitoring of burst surpression in anesthesia, Journal of clinical monitoring and computing 17 :125-134, 2002.

[37] Inouye T, Shinosaki K, Sakamoto H et al. Quantification of EEG irregularity by use of the entropy of the power spectrum. Electroencephalogr Clin Neurophysiol 1991; 79: 204-10.

[38] Nitish V. Thakor and Shanbao Tong, Advances in quantitative electroencephalogram analysis methods, Annual Review of Biomedical Engineering. Vol. 6: 453-495, Aug, 2004

[39] HS Traast and CJ Kalkman, Electroencephalographic characteristics of emergence from propofol/sufentanil total intravenous anesthesia. Anesthesia & Analgesia, Vol 81, 366-371, 1995.

[40] P.H. Tonner, B.Bein, Classic electroencephalographic parameters: Median frequency, spectral edge frequency etc., Best practice & research clinical Anesthesiology, Vol. 20, No. 1, pp. 147-159, 2006.

[41] H. Viertio-Oja et al, Description of the EntropyTM algorithm as applied in the Datex-Ohmeda S/5TM Entropy Module, Acta Anaesthesiol Scand 2004, 48:154-161.

[42] Zhang, X., Roy, R. J. Jensen, E.W. et al, EEG complexity as a measure of depth of anesthesia for patients, IEEE Transactions on Biomedical Engineering, Dec 2001, Vol.: 48, Issue: 12, pp:1424-1433

[43] P. D. Welch, The use of fast Fourier transforms for the estimation of power spectra: A method based on time averaging over short modified periodograms. IEEE Transactions on Audio and Electroacoustics, vol. 15, pp. 70-73, 1967

[44] Peter T. Walling, Kenneth, Nonlinear changes in brain Dynamics during emergence from sevoflurane anesthesia, Anesthesiology, Vol.105, No. 5, Nov, 2006.

[45] Tatjana Zikov, Stephane Bibian, Guy A. Dumont, Mihai Huzmezan and Craig R. Ries, Quantifying cortical activity during general anesthesia using wavelet analysis, IEEE Transactions on Biomedical Engineering, Vol. 53, No. 4, April 2006.

[46] Schüttler J., Ihmsen H. Population pharmacokinetics of propofol: a multicenter study. Anesthesiology 2000; vol. 92, pp. 727-738

[47] Stadler K. Modeling and control in anesthesia from design to validation. Ph.D. Thesis, ETH Zyrich, Institutfur Automatik Publikation NO. 23, 2003.

[48] V. Sartori, P.M. Schumacher, and M. Morari et al, "On-line estimation of propofol pharmacodynamic parameters", in 27th Annual International Conference of the Engineering in Medicine and Biology Society, 2005, pp. 74-77.

[49] A. Gentilini, M. Rossoni-Gerosa, and M. Morari et al, "Modeling and closed-loop control of hypnosis by means of bispectral index (BIS) with isoflurane", *IEEE Trans. on biomedical engineering*, vol. 48, pp. 874-889, 2001.

[50] E. Furutani, Y. Sawaquchi, and G. Shiralami et al, "A hypnosis control system using a model predictive controller with online identification of individual parameters", in 2005 IEEE control application conference, 2005, pp. 154-159.

[51] C. Dong, J. Kehoe, and J. Henry et al., "Closed-loop Computer Controlled Sedation with Propofol", in Procceeding of the Anaesthetic Research Society, 1999.

[52] J.C. Eisenach, "Reports of Scientific Meetings - Workshop on Safe Feedback Control of Anesthetic Drug Delivery", *Anesthesilogy*, vol. 91, pp. 600-601, 1999.

[53] C. Nunes, M. Mahfouf, and D. Linkens, "Modeling and multivariable control in anesthesia using neural-fuzzy paradigms Part I. Classification of depth of anesthesia and development of a patient model", *Artificial Intelligence in Medicine*, vol. 35, pp. 195-206, 2005.

[54] M. Mahfouf, C. Nunes, and D. Linkens et al., "Modeling and multivariable control in anesthesia using neural-fuzzy paradigms Part II. Close-loop control of simultaneous administration of propofol and remifentanil", *Artificial Intelligence in Medicine*, vol. 35, pp. 207-213, 2005.

[55] H. H. Lin, C.L. Beck, and M. J. Bloom, "On the use of multivariable piecewise-linear models for predicting human response to anes-thesia" *IEEE Trans on Bio. Eng.*, vol. 51, pp. 1876-1887, 2004.

[56] T. J. Gan, F. FRCA, and P. S. Glass et al., "Bispectral Index Monitoring Allows Faster Emergence and Improved Recovery from Propofol, Alfentanil, and Nitrous Oxide Anesthesia", *Anesthesiology*, vol. 87, pp. 808-815, 1997.

[57] D.A. Linkens, "Adaptive and Intelligent Control in Anesthesia", *IEEE Control Systems Magazine*, vol. 12, pp. 6-11, December 1992.

[58] L. Ljung and T. Söderström, Theory and Practice of Recursive Identification, MIT Press, 1983.

[59] C. Rosow and P.J. Manberg, "Bispectral Index Monitoring", *Annual of Anesthetic Pharmacology*, vol. 2, pp. 1084-2098, 1998.

[60] L.Y. Wang and H. Wang, "Control-oriented modeling of BIS-based patient response to anesthesia infusion", in 2002 International Conference on Mathematical Engineering, 2002.

[61] L.Y. Wang and H. Wang, Feedback and predictive control of anesthesia infusion using control-oriented patient models, in 2002 International Conference on Mathematical Engineering, 2002.

[62] L.Y. Wang, H. Wang, and G. Yin, "Anesthesia infusion models: Knowledge-based real-time identification via stochastic approximation", in 41st IEEE Conference on Decision and Control, 2002, pp. 2512-2517.

[63] L.Y. Wang, H. Wang, and G. Yin, "Reliable nonlinear identification in medical applications", in 13th IFAC Symposium on System Identification, 2003.

[64] X.-S. Zhang, R.J. Roy, and J.W. Huang, "Closed-loop System for Total Intravenous Anesthesia by Simultaneously Administering Two Anesthetic Drugs", in the 20th Annual International Conference of the IEEE Engineering in Medicine and Biology, 1998 pp. 3052-3055.

[65] M. Nakayama, H. Ichinose, and S. Yamamoto et al. "The effect of Fentanyl on hemodynamics and bispectral index changes during anesthesia induction with propofol", Journal of Clinical Anesthesia, vol. 14, pp. 146-149, 2002.

[66] J. S. Shieh, M. F. Abbod, and C. Y. Hsu et al., "Monitoring and Control of Anesthesia Using Multivariable Self-Organizing Fuzzy Logic Structure" Fuzzy Systems in Bioinformatics and Computational Biology, vol. 242, pp. 273-295, 2009.

[67] Y. Sreenivas, S. Lakshminarayanan, and G. P. Rangaiah, "Automatic regulation of anesthesia by simultaneous administration of two anesthetic drugs using model predictive control". in World Congress on Medical Physics and Biomedical Engineering 2006, 2007, pp: 82-86.

[68] S. L. Talbot,B. F. Boroujeny, Spectral Method of Blind Carrier Tracking for OFDM, IEEE Transactions on Signal Processing, Vol. 56, NO. 7, Jul. 2008

[69] E. Bataillou, E. Thierry, H. Rix, and 0. Meste, Weighted averaging using adaptive estimation of the weights, Signal Processing, 44 (1995) 5l-66.

[70] Richard W. Jones, Andrew Lowe, and Micheal J. Harrison, A framework for intelligent medical diagnosis using the theory of evidence, Knowledge-Based Systems, vol 15, pp. 77-84, 2002.

[71] O. Simanski, M. Janda, A. Schubert, J. Bajorat, R. Hofmockel, and B. Lampe, Progress of automatic drug delivery in anaesthesia-The 'Rostock assistant system for anaesthesia conrol(RAN)', Internatinal Journal of Adaptive Control and Signal Processing, vol. 23, pp. 504-521, 2009.

[72] Schwilden H., Stoecjle H., Sch$\ddot{u}$ttler J., Closed-loop feedback control of propofol anaesthesia by quantitative EEG analysis in humans. British Journal of Anaesthesia, vol.62, pp. 290-296, 1989.

[73] Mahfouf M., Linken D.A., Generalised predictive control an bioengineering. Taylor and Francis: London, 1998.

[74] C.S. Nunes, T. Mendonca, J. M. Lemos, and P.Amorim, Predictive adaptive control of the bispectral index of the EEG(BIS): Exploring Electromyography as an accessible disturbance, Mediterranean Conference on Control and Automation, July 27-29, Athens-Greece, 2007

[75] A. Gentilini1, C. W. Frei1, and A. H. Glattfedler1 et al., Multitasked closed-loop control in anesthesia, IEEE ENGINEERING IN MEDICINE AND BIOLOGY, Jan. 2001.

[76] A.M.H.J. Aertsen and P.I.M. Johannesma. "The spectro-temporal receptive field," *Biological Cybernetics*, vol. 42, no.2,pp.133-143,1981.

[77] J.J. Eggermont, A.M.H.J. Aertsen, and P.I.M. Johannesma, "Quantitative characterization procedure for auditory neurons based on the spectro-temporal receptive field," *Hearing Research*,vol.10,pp.167-190,1983.

[78] F.E. Theunissen, K. Sen, and A.J. Doupe, "Spectral-temporal receptive fields of nonlinear auditory neurons obtained using natural sounds," *Journal of Neuroscience*, vol.20,pp.2315-2331,2000.

[79] C.K. Wu, S. V. David, and J. L. Gallant, 2006. "Complete functional characterization of sensory neurons by system identification," *Annual Review of Neuroscience*,vol.29,pp.477-505,2006.

[80] M. Borst, A. Knoblauch, and G. Palm, "Modeling the auditory system: preprocessing and associative memories using spiking neurons," *Neurocomputing*, vol.58-60,pp.1013-1018,2004.

[81] M.G. Heinz,*Computational models of the auditory system*, Springer Handbook of Auditory Research, Vol. 35, pp.177-202,2010.

[82] C. Curto, S. Sakata, S. Marguet, V. Itskov, and K.D. Harris(2009), "A Simple Model of Cortical Dynamics Explains Variability and State Dependence of Sensory Responses in Urethane-Anesthetized Auditory Cortex," *The Journal of Neuroscience*, vol.29,pp:10600-10612, Aug. 2009.

[83] I. J. Rampil, "A primer for EEG signal processing in anesthesia," *Anesthesiology*, vol.98, pp:980-1002,1998

[84] Z. Tan, L.Y. Wang, G. McKelvey, A. Pustavoitau, G.X. Yu, H.M. Marsh, and H. Wang, "Evaluation of EEG β_2/θ-ratio and channel locations in measuring anesthesia depth," *J. Biomedical Science and Engineering*, vol.3, pp.39-46,2010.

[85] Z. Tan, R. Kaddoum, L.Y. Wang, and H. Wang,"Decision-Oriented Multi-Outcome Modeling for Anesthesia Patients," *The Open Biomedical Engineering Journal*, vol.4, pp.99-108,2010.

[86] A. Gentilini, M. Rossoni-Gerosa, C.W. Frei, R. Wymann, M. Morari, A.M. Zbinden, and T.W. Schnider, "Modeling and closedloop control of hypnosis by means of bispectral index (BIS) with isoflurane," *IEEE Transactions on Biomedical Engineering*, vol. 48, no. 8, pp. 874-889, 2001.

[87] L.Y. Wang and H. Wang, "Control-oriented modeling of BISbased patient response to anesthesia infusion," in Internat. Conf. Math. Eng. Techniques in Medicine and Bio. Sci.,2002.

[88] S.Schraag, U. Bothner, R. Gajraj, G. N. C. Kenny, and M.ichael Georgieff,"The Performance of Electroencephalogram Bispectral Index and Auditory Evoked Potential Index to Predict Loss of Consciousness During Propofol Infusion," *Anesthesia and Analgesia*, vol.89,pp.1333-1315, 1999.

[89] B.A. Porter, T. R. Rosenthal, K. G. Ranasinghe and M. P. Kilgard, "Discrimination of brief speech sounds is impaired in rats with auditory cortex lesions," *Behavioural Brain Research*,vol. 219, Issue 1, pp.68-74, May 2011.

[90] O. R. Floody, , L. Ouda, B. A. Porter and M. P. Kilgard, "Effects of damage to auditory cortex on the discrimination of speech sounds by rats," *Physiology and Behavior*, vol.101, Issue 2, pp.260-268,Sep. 2010.

[91] M.A.J. Looij, S.S. Liema, H. Burgb, J. Weesc, C.I. Zeeuwb and B.G.A. Zanten,"Impact of conventional anesthesia on auditory brainstem responses in mice," *Hearing Research*, vol.193,pp.75-82,2004.

[92] M.H. Dueck, F. Petzke, H.J. Gerbershagen,M. Paul, V. Heβelmann, R. Girnus, Krug, B. Sorger, R. Goebel, R. Lehrke, V. Sturm, and U. Boerner,"Propofol attenuates responses of the auditory cortex to acoustic stimulation in a dose-dependent manner: A FMRI study," *Acta Aaesthesiologica Scandinavica*, vol. 49, Issue 6, pp. 784-791,2005.

[93] J. Sykaa, D. Suta, and J. Popelàr, "Responses to species-specific vocalizations in the auditory cortex of awake and anesthetized guinea pigs," *Hearing Research*, vol. 206, Issues 1-2,pp.177-184,2005.

[94] W. Schaffartzik, J. Hirsch,F. Frickmann, P. Kuhly, and A. Ernst,"Hearing Loss after Spinal and General Anesthesia: A Comparative Study," *Anesthesia and Analgesic*, vol.91,pp.1466-1472,2000.

[95] A. Hutt and A. Longtin,"Effects of the anesthetic agent propofol on neural populations," *Cogn. Neurodyn.*, vol.4, pp.37-59, 2010.

[96] P. Dayan and L.F. Abbott, *Theoretical Neuroscience: Computational and Mathematical Modeling of Neural systems.* MIT press, Cambridge, 2001.

[97] L. Ljung and T. Söderström T, *Theory and Practice of Recursive Identification*, MIT Press, Cambridge,1983.

[98] "Pure tone audiometry", http://en.wikipedia.org/wiki/Pure_tone_audiometry.

ABSTRACT

MONITORING, DIAGNOSIS AND CONTROL
FOR ADVANCED ANESTHESIA MANAGEMENT

by

ZHIBIN TAN

August 2011

Advisor: Dr. Le Yi Wang

Major: Electrical Engineering

Degree: Doctor of Philosophy

Modern anesthesia management is a comprehensive and the most critical issue in medical care. During the past dacades, a large amount of research works have been focused on the problems of monitoring anesthesia depth, modeling the dynamics of anesthesia patient for the purpose of control, prediction, and diagnosis.

Monitoring the anesthesia depth is not only for keeping the patient in adquate anesthesia level but also for preventing the patient from overdosing. Several EEG based indexes have been developed such as the BIS, and Entropy etc. for measuring depth. However, reports mentioned that those indexes in some cases fail in detecting the awareness of the the patient. In this research work, a new EEG based parameter,β_2/θ-ratio, was introduced as a potential enhancement in measuring anesthesia depth. It was compared to the relative β-ratio which had been commercially used in the BIS monitor and proved that the β_2/θ-ratio has improved reliability and sensitivity in detecting the awareness than the β-ratio does.

Traditional modeling, diagnosis and control in anesthesia focus on a one-drug one-outcome scenario. In fact, Anesthesia drugs have impact on multiple outcomes of an anesthesia patient. Due to limited real-time data, real-time modeling in multi-

outcome modeling requires low complexity model structures. A method of decision-oriented modeling which employs simplified and combined model functions in a Wiener structure to reduce model complexity was introduced. This model structure was implemented in device level and tested in operation room for real-time anesthesia monitoring, diagnosis, and prediction.

Furthermore, the impact of wireless channels on patient control in anesthesia applications was also investigated. Such a system involves communication channels which introduce noises due to quantization, channel noises, and have limited communication bandwidth resources. Usually signal averaging can be used effectively in reducing the noise effects. However, when feedback was intended, we showed that signal averaging will lose its utility substantially. To explain this phenomenon, we analyzed stability margins under signal averaging and derived some optimal strategies for selecting window sizes.

Finally, a mathematical model for the auditory system was introduced to characterize the impact of anesthesia on auditory systems, and analyze and diagnose hearing damage. The auditory system was represented by a black-box input-output system with external sound stimuli as the input and the neuron firing rates as the output. Two parallel subsystem models were developed for modeling the auditory system dynamics: an ARX (Auto-Regression with External Input) model for the auditory system under external stimuli and an ARMA (Auto-Regression and Moving Average) model for the spontaneous activities of the neurons on primary auditory cortex. These models provide a quantitative characterization of anesthesia's impacts and diagnosis of hearing loss on auditory transmission channels.

AUTOBIOGRAPHICAL STATEMENT

ZHIBIN TAN

Education

- Ph.D. in Electrical Engineering, August 2011
  Wayne State University, Detroit, Michigan
- M.S. in Electrical Engineering, April 2007
  Wayne State University, Detroit, Michigan
- M.S. in Electrical Engineering, August 2004
  University of Science and Technology of China, Hefei, China
- B.S. in Comunication Engineering, July 2001
  Anhui University, Hefei, China

Awards

- Summer Dissertation Fellowship, Wayne State University, 2010.
- Olbert Travel Award for excellence in graduate student research, College of Engineering, Wayne State University, 2010.
- Graduate Teaching Assistantship, Department of Electrical and Computer Engineering, Wayne State University, 2009-2011.
- Thomas C. Rumble University Graduate Fellowship,
  Department of Electrical and Computer Science, Wayne State University, 2008.9-2009.5.
- Graduate Research Assistantship, Department of Electrical and Computer Engineering, Wayne State University, 2006-2008.

Selected Publications

1. Zhibin Tan, Le Yi Wang, Hong Wang, Xueguo Zhang, Jinsheng Zhang, "Modeling for the Impact of Anesthesia and Noise lesion on Neural Activity in the Auditory System", IEEE Tran. On Biomedical Engineering (In submission).

2. Zhibin Tan, Le Yi Wang, George McKelvey, Guangxiang Yu, and Hong Wang, "Evaluation of EEG β_2/θ-Ratio and Channel Locations in Measuring Anesthesia Depth", Journal of Biomedical Science and Engineering, Vol.3, pp. 39-46, 2010.

3. Zhibin Tan, Romeo Kaddoum, Le Yi Wang, Hong Wang, "Decision-Oriented Multi-Outcome Modeling for Anesthesia Patients" The Open Biomedical Engineering Journal, http://www.bentham.org/open/, Vol. 4, pp: 99-108, 2010.

4. Zhibin Tan, Le Yi Wang, Hong Wang, "Signal Averaging for Noise Reduction in Anesthesia Monitoring and Control with Communication Channels", Journal of Biomedical Science and Engineering, Vol. 2, pp: 564-573, 2009.